**Master Thesis, Department of Geosciences**

# Feasibility Study on Heavy Metal Adsorption by Weathered Dunites with Emphasis on the Minerals Pyroaurite and Dypingite

**Muhammad Uzair Naqvi**

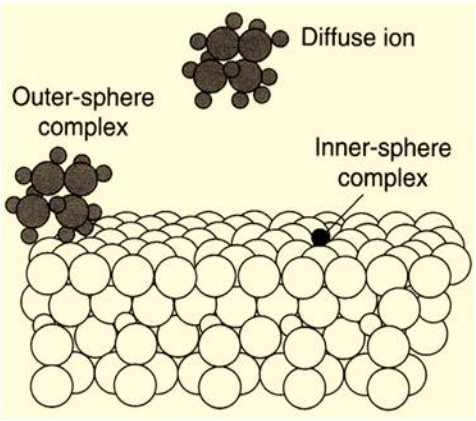


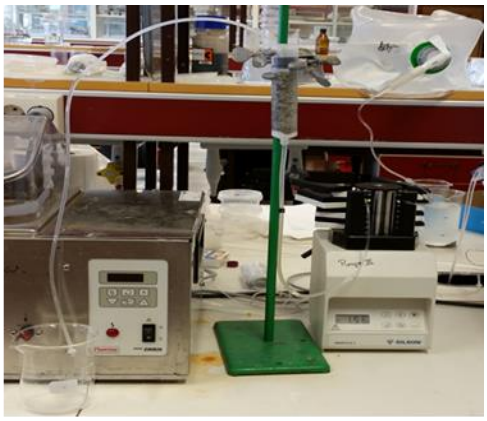

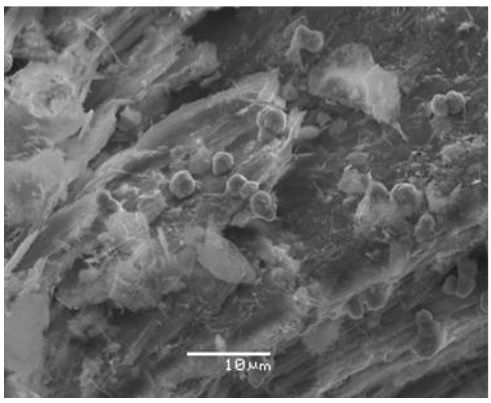


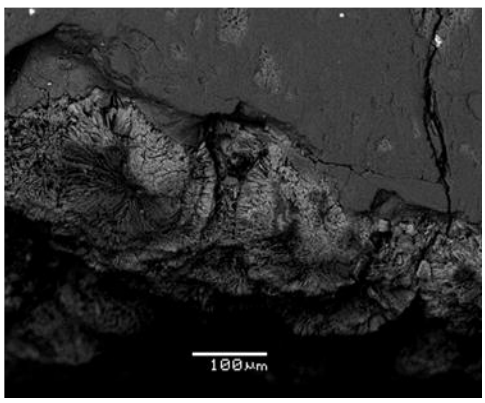


UNIVERSITY OF OSLO
FACULTY OF MATHEMATICS AND NATURAL SCIENCES

# Feasibility Study on Heavy Metal Adsorption by Weathered Dunites with Emphasis on the Minerals Pyroaurite and Dypingite

**Muhammad Uzair Naqvi**

Master Thesis in Geosciences

Discipline: Environmental Geology and Geohazards

Department of Geosciences

Faculty of Mathematics and Natural Sciences

University of Oslo

**June 02, 2014**

**Tutors: Prof. Håkon O. Austrheim, Per Aagaard, and Helge Hellavang**

This work is published digitally through DUO – Digitale Utgivelser ved UiO

http://www.duo.uio.no

It is also catalogued in BIBSYS (http://www.bibsys.no/english)

# Acknowledgement

In the name of Allah, the most Compassionate, the Most Merciful.

I would like to express my heartfelt gratitude to my supervisor Professor Håkon Austrheim for his affection, support and guidance that kept me on track throughout the tenure of my research. I'm really thankful to him for offering me this wonderful innovatory project and continued confidence in me. I'm truly thankful to him for all of his time and efforts for this research. I'm really impressed with the affection and devotion he has shown for this research.

I would extend my deepest gratitude to my supervisors Per Aagaard and Dr. Helge Hellavang. I'm delighted by their personal interest, time and devotion for this project. I would like to thank them for giving me the key knowledge of Geochemistry.

I would like to express my deep gratitude to all academic staff at Department of Geosciences, University of Oslo. My deepest gratitude to Muriel Erambert, Berit løken, and Siri lene Simonsen for helping me with EMP, SEM and ICPMS. I would like to say thanks to Fernando Corfu and Gunborg Bye Fjeld for helping me with mineral separation. I express my cordial thanks to Mufak for helping me with IC. A sincere thanks to Maarten Aaerts for always being there for helping me with XRD. I would like to say thanks to Salahalldin Akhavan for helping me preparing the samples. I highly appreciate the Norwegian Government policy of providing free education to international students which enabled me to study here at University of Oslo.

I want to say Thank's to my parents and siblings for all the love and support they have given me. I want to tell you that I love you guys. I would like to say thank's to my maternal Dr. Javed ahmed kazmi without his love, encouragement and support it would have never been possible for me to achieve my goal. Finally, the continuous support of my cousin Dr. Najaf, mymaternal aunts Kauser Kazmi and Beenish Kazmi. Thank's for always been there guys when I needed you the most, trust me it really means alot to me.

I'm also greatly thankful to my friends who encouraged and supported me throughout my stay in Norway. Especially, my seniors and colleagues including Muhammad Jamil, Tauqeer ahmed saadi, Arif butt Junaid Riaz, Umar, Waqas, Asad, Oystein, Beyene Gima Haile, Issak Habtemical, Grahm Gilbert, Mohsin, Naqi, Nasib, Basit, Qamar, Anum Irfan and Maria Forsgård. I would like to tell you guys without your love, support and prayers this task could have been very hard to accomplish and this means a lot to me.
I wish and pray that my research may help in the future for reducing the water contamination from the world.

P.S
Department of Geology, UIO my love! You were like a home to me, I will miss you ☺.

# Abstract

The discharge of contaminated industrial and mining wastes may contain heavy metals. Water contamination by these heavy metals can cause significant environmental and medical issues. Over the years researchers have tried to develop synthetic adsorbents for the remediation of heavy metals from drinking water but their usage is very limited due to the extensive costs. Thus, to develop low cost methods which can be used on a larger scale for the removal of heavy metals from drinking water has become a challenge for us in this era. In this work we have investigated the efficiency of weathered mine tailings containing mineral dypingite and pyroaurite for the removal of heavy metals from contaminated water. This was done by reacting the samples with heavy metals and performing column experiments using the samples from mine tailings. The samples from the mine tailings were cut to $1cm^3$ chip and subsequently reacted with different heavy metals including Cu, Pb, Cd and Cr. The areas in chips with mineral pyroaurite and dypingite were first characterized to see the changes after the experiments using SEM-BSE imaging and XRD characterization. The column was filled with selected material from mine tailings and $CdCl_2$+NaCl solution was passed through it. The fluid samples from the column experiments were characterized by using ICPMS and IC and the reacted column material was characterized using SEM and XRD. The SEM-BSE images from the chip experiments showed that Cd, Pb and Cr were preferentially sorbed/precipitated on dypingite whereas Cu was sorbed on pyroaurite. Pb and Cd precipitated in the form of cerrusite ($PbCO_3$) and Otavite ($CdCO_3$) on the surface of dypingite respectively. However, the SEM-BSE along with EDS images from reacted column material revealed different results. Cd in this case was precipitated on both pyroaurite and dypingite and formed otavite. XRD results suggest constant mineralogy before and after the experiment. The results from column experiments showed that $Cl^-$ is not working as an ideal conservative tracer. The concentration of Cd in the column was accommodated up till after 1.2 pore volume when the concentration of Cd reached a peak with more than ten times of the inlet concentration. This sudden increase in the concentration of Cd was most likely due to the fine grained otavite precipitates that got through the column.

# Table of Contents

# List of Abbreviations

| | |
|---|---|
| WHO | World health organization |
| Pyr | Pyroaurite |
| Dyp | Dypingite |
| Srp | Serpentine |
| Cd | Cadmium |
| Pb | Lead |
| Cu | Copper |
| Cr | Chromium |
| ICPMS | Inductive coupled plasma spectroscopy |
| IC | Ion chromatography |
| SEM | Scanning electron microscope |
| EMP | Electron microprobe |
| BSEI | Backscattered Electron Image |
| SEI | Secondary Electron Image |
| EDS | Energy-dispersive X-ray Spectroscopy |

# 1. Introduction

The rapid increase in industrialization and urbanization over the past few decades have caused substantial environmental problems worldwide. The discharge of heavy metals from mining and industrialization can cause intense damage to human life. According to a report by WHO, water contamination causes more than 3.5 million deaths every year worldwide and heavy metals due to their high toxicity level and non-biodegradability makes the situation even worse (Pronczuk et al., 2011; Jayakumar et al., 2010 cited in Setshedi, 2011).

The sources of heavy metals in water may be divided into two groups: natural sources and anthropgenic sources. The natural sources inculde heavy metals released from erosion of minerals and rocks, leaching of ore deposits and volcanc materials. The antrhopgenic sources include solid waste disposal, wharf channel dredging and industrial or muncipal effluents (Vodela, 1997 cited in Pirsaheb, 2013). The heavy metals found in industrial waste water include Cd, Pb, Cu, Zn, Ni and Cr that are result of lead battery manufacturing, metal plating facilities, ceramic production, glass industries, paints and pigments (Argun, 2007 cited in Salama, 2011) . The human exposure to heavy metals is mostly linked to contaminated drinking water and consumption of sea food that can cause several fatal diseases like renal failure, breakdown of central nervous system, liver cirrhosis, chronic anaemia etc. (Hanaa, 2000).

Therefore, to develop effective and cheap methods to control the presence of heavy metals in soil and groundwater has become biggest challenge for society in our era.There have been many studies done that suggest several methods for the romoval of heavy metals from contaminated water that may include membrane filtration, chemical precipitation, coagulation, reverse osmosis, electrolysis, Ion exchange and adsorption . Among all these mehods which are listed above, adsorption method is recognized as an effective, simple and easy process for the removal of heavy metals from contaminated water. (Bhatnagar, 2005). Despite the effectiveness of various adsorbents for heavy metals like activated carbons it is difficult to use them due to their extensive costs. Therefore, a lot of studies have been carried out lately to find cheap and locally available natural adsorbents like chitosan, zeolites, clay,

or certain waste products from industrial operations such as fly ash, coal and oxides (Babel, 2003).

## 1.1 Background of study

The study focuses on the observation of the sorption behavior of different heavy metals (Cu, Cr, Pb, Cd) by using weathered dunites collected from mine tailings. The samples were collected from mine tailing of a chromite mine named as " Stensgruva" feragen (figure 1.1). The mines lie in the area of Feragen ultramafic body which is situated NS-Norway close to the norwegian swedish border at 62º32.9´N 11º 48.4´E (Beinlich, 2012). The area is dominated by partly serpentinized dunite and peridotite with hazburgite and chromite layers (Moore, 1980 cited in Beinlich, 2012). The area was mined for chromite until 1927 when the minning was stopped and have about 100-200 chromite mines with a mass of about 32,000 metric tons of ore was extracted (Beinlich, 2012) (mindat.org). The remnants of the mines are present in the form of mine tailings in the area.

The mine tailings in the area contain variably weathered serpentinized dunite rocks that contain carbonate minerals belonging to the hydrotalcite group ($Mg_6R^{3+}_2(OH)_{16}CO_3 \cdot 4H_2O$). The minerals of the hydrotalcite group are the natural phases of layered double hydroxide (Mills et al. 2012). Previous studies have suggested that the synthetic forms of minerals from hydrotalcite group can be used as efficient adsorbents for heavy metals. However, the purpose of this study is to test if the natural form of mineral pyroaurite from hydrotalcite group and mineral dypingite can be used as an efficient adsorbent for heavy metals. This is a novel approach since there is not much literature on natural varieties of these two minerals and they may be cheaper to produce than the synthetic ones.

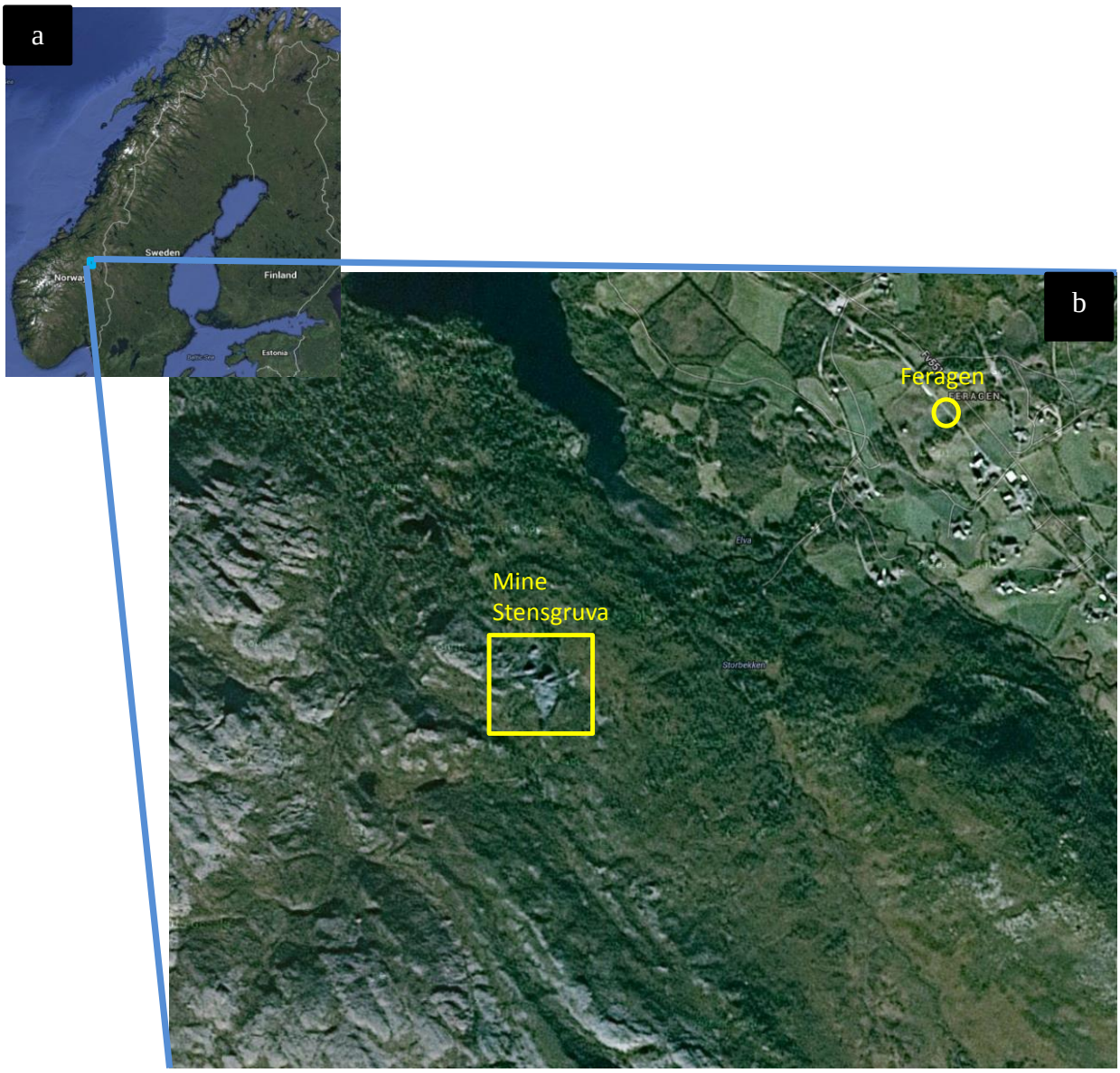


**Figure 1.1 A) Location of Feragen in Norway is shown by blue box B) Zoomed in image of the Feragen area showing the location of mine stensgruva.**

## 1.2 Objective of the study

The objective of this study was to evaluate the efficiency of weathered dunites from mine Stensgruva as adsorbents for a selected group of heavy metals. This was done by:

1. Reacting weathered material containing mineral dypingite and pyroaurite with different heavy metals including Pb, Cu, Cd and Cr by chip and column experiments.

2. Characterizing and analyzing the reactant and product by SEM, EMP , XRD and ICPMS in order to assess the efficiency of mineral dypingite and pyroaurite if they could be used to remove heavy metals from the contaminated water.

# 2. Theoretical background of Sorption Theory

Sorption is a general term comprising different processes which include adsorption, absorption and Ion exchange. The term adsorption defines a process of a chemical sticking on the solid surface, absorption process is defined as the intrusion of chemical substance into the solid and Ion exchange is defined as the replacement of one from the solid surface by other ion (figure 2.1) (Appelo, 2006). The main thing that differentiates the sorption processes from precipitation and dissolution of solids is that sorption is dependent on the preexistence of a solid surface as compared to for e.g. precipitation (Sposito, 1989 cited in Appelo, 2006). The prime focus of this study is adsorption which will be illustrated in detail in the following section.

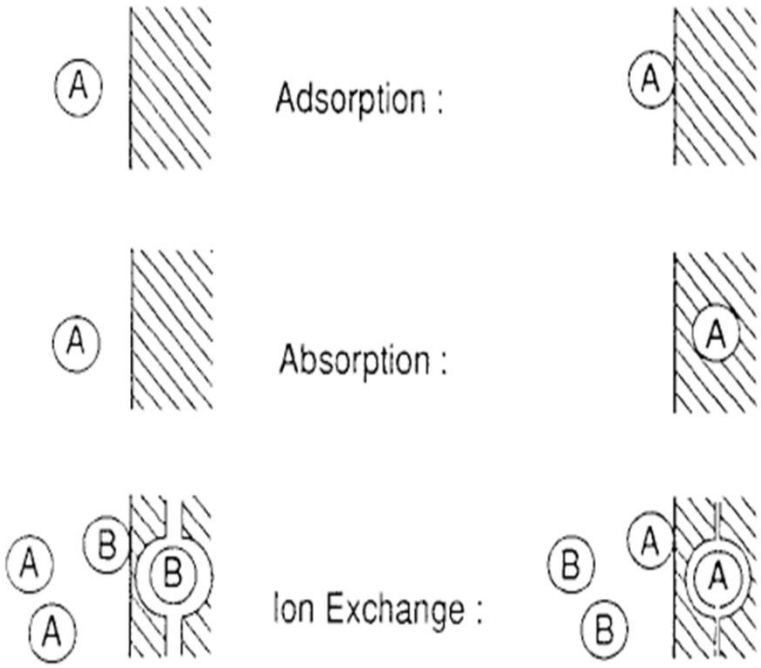


**Figure 2.1: Pictorial demonstration of the three sorption processes (Appelo, 2006).**

## 2.1.1 Adsorption Theory

Adsorption is defined as the process through which chemical substance is attached to the surface of a solid. The surface on which the chemical substance attaches itself is termed as an adsorbent and the chemical substance that accumulates at the adsorbent is called adsorbate. The chemical specie in the liquid phase that can be potentially adsorbed is termed

as an adsorptive. The attachment of the adsorbate on the adsorbent can be result of either physical or chemical adsorption (Sposito, 1989). Physical adsorption is the result of universal Van der Waals interaction that are very weak bonds and easily separable. It is not site specific and doesn't include the sharing of electrons and easily reversible. Chemical adsorption on the other hand is due to the reaction between adsorbate and adsorbent which results in forming chemical bonds. Chemically adsorbed adsorbents are attached to the specific sites on the surface of adsorbents which may result from sharing or transferring of electrons and unlike physical adsorption this process is irreversible (Adamson, 1990 cited in Dabrowski, 2001). There may be various processes that control the metal retention in soil. The removal of the metal ions from the aqueous solutions may involves the concentration of the solute on solid surface, which is regulated by precipitation, adsorption, solid formation which are differentiated on the base of interaction between the metal and host mineral (Sposito, 1989). The fate of contaminants in the groundwater is very much dependent on these sorption processes as they retard their movement. The retardation is defined by the following equation

$$R = 1 + kd$$

Here, $kd$ is the distribution coefficient which shows the relative tendency of two elements to become adsorbed and defined as

$$kd = \frac{dq}{dc}$$

Where dq is the the concentration of solute adsorbed on solid and dc is the concentration of solute in solution. If the concentration of solute adsorbed on solid is equal to the concentration of solute in the solution the will Kd be equal to 1 and the system will be at equilibrium. At equilibrium condtions the system will be dependent on temperature, solute, solvent, adsorbent and pH among others (Faust and Aly, 1987). As the adsorption continues the metal ions will keep filling the adsorbent sites, a stage will come when all the sites are filled at that point the solution will be saturated with respect to the metal ions. The adsorption of a metal ion that is bound to the surface of solid can forms three types of complexes which include Interlayer complex, Outer layer complex and interlayer complex (figure 2.2). Interlayer complex and outerlayer complex are localized on an adsorbent. The

diffuse ion is the solvated complex that means they are surrounded by a hydration shell of water molecules which does not form a direct complex with the charged surface (Koretsky, 2000). The diffuse-ion and the outer sphere complex are bound due to the surface by the electrostatic bonding and are characterized as nonspecific adsorption. The term non-specific adsorption refers to the weak binding of the the ions with the surface. In case of Innersphere complex, the metal ions make a strong bond with the surface of solid by covalent bonding and is characterized as specific adsorption. The term specific adsorption refers to the covalent bonding of metal ions with the surface which is dependent on the particular electron configurations of both surface group and complex ion (Sposito, 1989). The figure 2.2a is showing a model that was proposed by Sposito (1989) to show the three different modes of metal ion adsorption at the mineral surface and figure 2.2b is illustrating how ion distributes at the charged surface (Appelo, 2006, Sposito, 1989). The alkali metals Na+ and the acid anion Cl are solvated or they are surrounded by a shell of hydration water and are bounded through the outersphere complexes to the surface which is the example of non-specific adsorption while the protons, heavy metal Cu ion and most oxyanions are found strongly bonded with the surface oxygens which is an example of specific adsorption (Koretsky, 2000, Appelo, 2006, Sposito, 1989).

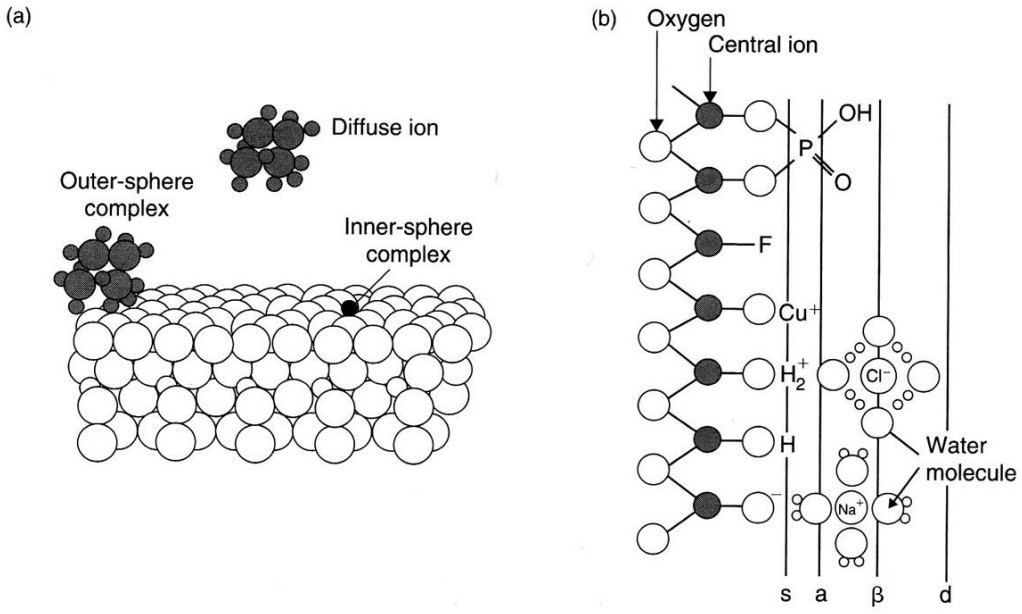


**Figure2.2: (a) The three modes of ion adsorption b) Planes associated with different kind of bonding: "s" for surface hydroxyl groups, "a" for inner sphere complexes, "β" for outer-sphere complexes and "d" for ions in the diffuse layer (Appelo, 2006).**

## 2.1.2 Mineral pyroaurite and Mineral dypingite as an adsorbent

Although the potential of the natural mineral pyroaurite ($Mg_6Fe^{3+}_2(CO_3)(OH)_{16}•4(H_2O)$) and mineral dypingite ($Mg_5(CO_3)_4(OH)_2•5(H_2O)$) as adsorbents for heavy metals was not studied by anyone before yet we find some literature where the synthetic pyroaurite like compound was studied for the removal of heavy metal from aqueous solution. Seida., 2001 suggested that synthetic pyroaurite like compounds have the characteristic to buffer the pH which could be effective for the removal of dilute heavy metals from the water. The dissolution of the compound creates a weak alkali solution by releasing metal cations and hydroxides which work as coagulants or precipitants (Seida., 2001). The mineral pyroaurite is a clay-type anion exchanger and belongs to the hydrotalcite group ($Mg_6Al_2(CO_3)(OH)_{16}·4(H_2O)$) which is subgroup of hydrotalcite supergroup. Hydrotalcite belongs to the natural phase of layered double hydroxides. Layered double hydroxides (LDH) are compounds (natural and synthetic) whose layered structure is very similar to brucite $Mg(OH)_2$ structure (Mills et al. 2012). Brucite consists of a sheet of octahedrally packed divalent cations such as $Mg^{2+}$ with the intercalation of hexagonally close-packed anions (Kao, 1984). The structure of natural LDHs also comprises of anions which are intercalated between the cation layers (figure 2.3) (Mills, 2012). The anions which are intercalated between the layers have very weak bonding which makes them favorable for the exchange reactions (Meyn et al., 1990; Amphlett, 1958; as sited in Mills et al.2012).

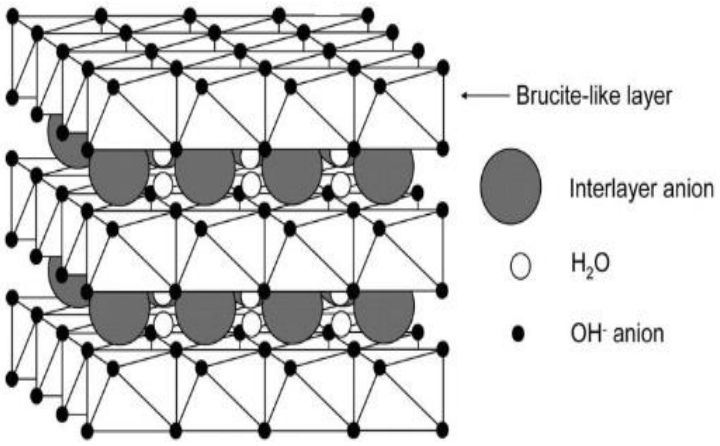


**Figure 2.3: Structure of layered double hydroxide (Source: Zhaoyi, 2008)**

Mineral pyroaurite is composed of Mg (36.55 %), Fe (24.13%), H (32.67%) and C (6.65% $CO_2$). The crystal structure of pyroaurite consists of a positively charged brucite like layer ($Mg_6Fe_2^{+3}OH_{16)}$ with intercalated negatively charged interlayers $(CO_3.4H_2O)^{2(}$figure 2.4).

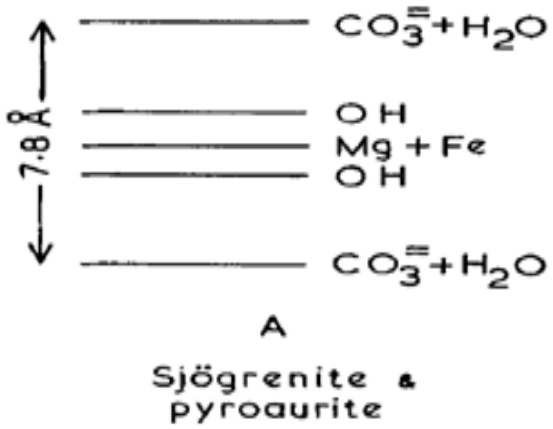


**Figure 2.4: Layered sequence of mineral pyroaurite (Modified from Taylor, 1969)**

These Interlayers have a weak bond with the brucite like layers, it can be best thought as a$H_2O$ and $CO_3$ changing their positions result in forming new hydrogen bonds and disconnecting the old ones that is same like the water molecules do in the liquid state. These hydrogen bonds exist within the interlayers and the weak ones connect the hydroxyl groups of brucite layer to the interlayer (Allman, 1968).

# 3. Analytical Techniques

The analysis of the samples collected from the mine tailings was carried out at Department of Geosciences, University of Oslo. The following methods were used for the petrography and mineral compositional analysis in the samples collected from mine tailings.

1) Scanning electron microscope (SEM)
2) Electron Microprobe (EMP)
3) X-ray Diffraction (XRD)
4) Inductive coupled plasma spectroscopy(ICPMS)
5) Ion Chromatography (IC)

## 3.1 Scanning Electron microscope Analysis

### 3.1.1 Introduction

Scanning electron microscopy is a method used for the detailed imaging of solid objects including rocks and minerals as well as for microfossils. The samples were analyzed using JEOL JSM_6460LV scanning electron microscope at department of geosciences, University of Oslo. The microscope has detectors for Secondary electrons: SEI, Back-scattered electron detector: BEI, Back-scattered electron detector, Cathodoluminescent: CL and Energy dispersive x-ray detector: EDX-Analyzer.

### 3.1.2 Set up of Scanning electron microscope

In scanning electron microscope, images are produced by scanning the beam while displaying the signal from an electron detector on a computer screen. In order to do so, selection of suitable detection mode (composition or topography), contrast can be obtained.
The general set-up of SEM, with different parts is shown is shown by figure 3.1. SEM consists of an electron gun which is the source of electrons. Electron gun is usually made up of a tungsten filament with negative potential which upon heating accelerates electrons towards the sample.

Electron condensing lenses are present, which helps to focus the beam on the specimen, both lenses and electron gun combines to form the 'column'. The electron beam travels down the column and the size of the diameter of the beam is demagnified by the condenser-lenses. The beam is focused by the objective lenses in order to get a sharp image of the sample. An EDS system is attached to this microscope, which helps to separate characterististic X-rays of the selected element and thus form an image. Beam-deflection coils and electron detectors enable scanning images to be produced. (Reed, 2005)

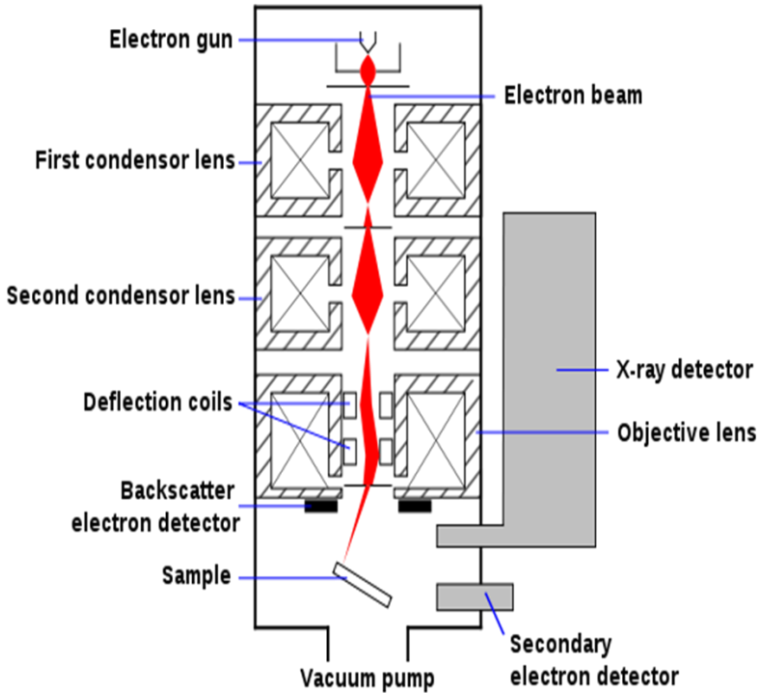


**Figure 3.1: The general setup of SEM (Reed, 2005).**

### 3.1.3 Electron interaction with the Specimen

The electron interaction with an atom in the specimen as shown by the figure 3.2. When high beam energy electrons hit the sample, they enter into the surface of atom layers and are scattered either in-elastically or elastically. In-elastically scattered electrons lose significant energy during collisions and therefore have low energy when they escape from the sample surface. These electrons are then known as secondary electrons**.** The secondary electrons are used for taking secondary electron (SE) images. The inelastic interaction of the electron with

specimen may also generate x-rays which could be of two types characteristic x-rays and continuum x-rays. The characteristic x-rays are generated when the incident electron hits the atom in the specimen kicks the electron out of the valence shell while the shell is loaded again with the electron it releases a packet of energy of specific wave length in the form of characteristic x-rays. These characteristic x-rays are used for the element mapping. Elastically scattered electrons lose very less or no energy during their collision. They escape with high energy and they get back into the direction where they came from i.e. electron gun. These types of electrons are known as backscattered electrons. Back scattering is defined by the backscattering coefficient equation 3.1 which is described by the following equation.

$$\eta = n_{BSE}/n_B$$

where $\eta$ is the backscattering coefficient $n_{BSE}$ is the number of backscattered electrons and $n_B$ is the number of electrons in the beam. So, the above equation can be written as

$$\eta = f(z)$$

which shows that back scattered coefficient is the function of atomic number, so higher the atomic number higher will be the electrons bouncing back to the detector. Back scattered electron images thus provide information on the relative composition of minerals (Reed, 2005).

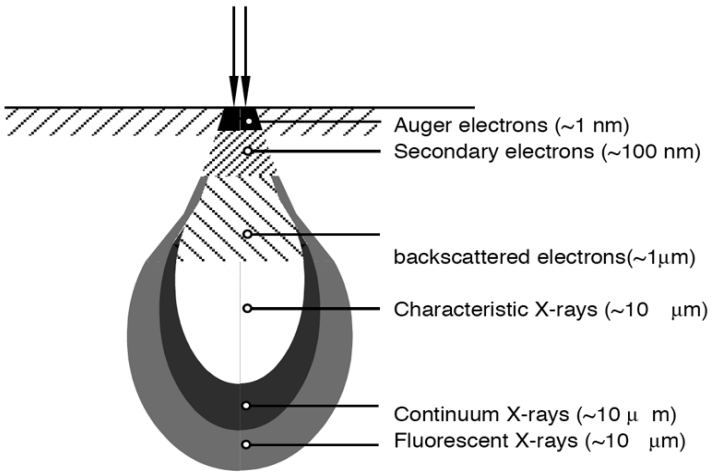


**Figure3.2: The interaction volume of electrons in crystalline sample (Reed. 2005).**

## 3.2 Electron Microprobe Analysis

### 3.2.1 Introduction

The electron microprobe is used for in-situ quantitative microanalysis of minerals, glasses, metals and other solids. Electron microprobe is very similar to the Scanning electron microscope (SEM) but SEM is good for taking images while electron microprobe is good for the chemical analysis (Reed, 2005). The sample was analyzed using Cameca SX100 electron microprobe at Department of geosciences, University of Oslo. The sample Fer_312B was chosen for the element mapping after the experiment to see the effect of $CrNO_3$ solution on the sample.

### 3.2.2 Setup of the electron microprobe

In case of Electron microprobe the system is set up similarly to Scanning electron Microscope. The main difference is that EMP has the optical microscope to maintain proper focus at the sample surface and it has Wave Dispersive Spectrometer (WDS) with a crystal that is aligned in a Rowland circle to diffract the X-rays to coming out of the specimen to the detector while SEM has a Electron dispersive spectrometer. Electron gun consists of the tungsten filament, wehnelt cylinder and an anode plate. The electrons start to escape when the tungsten filament is heated; the wehnelt cylinder helps the electrons not to disperse in all directions the anode plate that is placed right after the wehnelt cylinder attracts the electrons towards itself. Beam centering coils focuses the electrons and condenser lenses are used to to control the diameter of the beam.

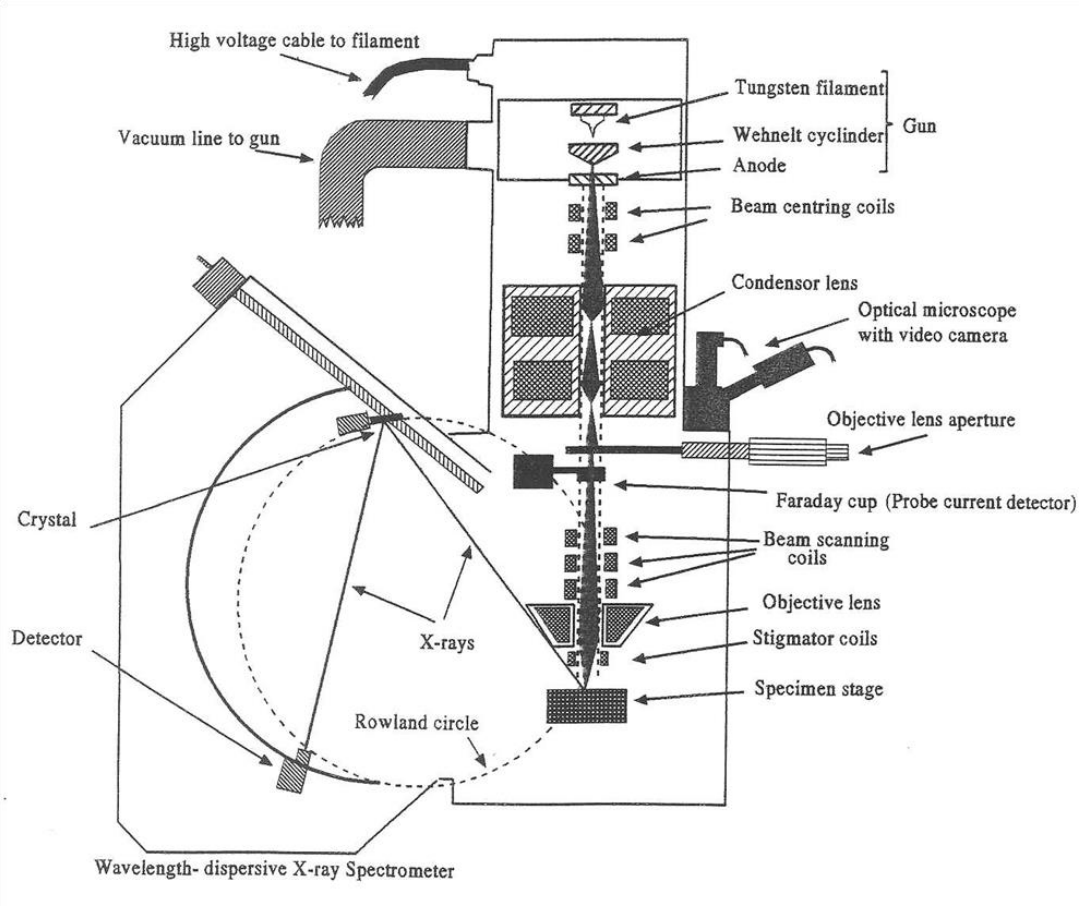


**Figure: 3.3: Schematic cross section of EMP (Reed, 2005).**

### 3.2.3 Electron-specimen Interaction

When the electron beam hits the specimen, the electrons present in the inner shells of an atom will be removed and the atom reaches an excited state. To bring the atom into more stable state electrons from the outer shell will jump to fill the vacant position in the inner shell leading to the release of energy (photons) of specific wave lengths which are known as characteristic x-rays. These characteristic x-rays of specific wavelengths may be diffracted from the crystal that is positioned at the correct angle relative to the sample surface in Rowland circle (figure 3.4). To change theta both crystal and detector move along the Rowland circle so the Sample, crystal and detector lie on the periphery of the Rowland circle (Reed, 2005). Wave dispersive spectroscopy is based on the principle of Bragg's Law which is defined in section 3 .3.

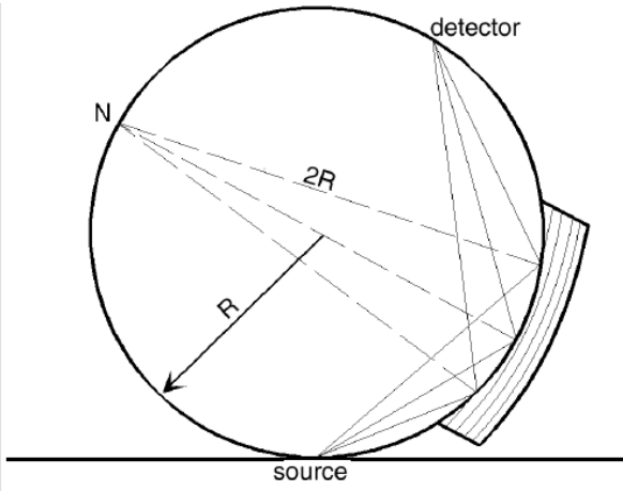


**Figure 3.4: Description of the rowland circle (Reed, 2005).**

## 3.3 X-Ray Diffraction Analysis

### 3.3.1 Introduction

X-ray diffraction technique is used to identify the speciation of the mineral based on their crystal structures. It also determines structural properties such as; defect structures, epitaxy, grain size, phase composition and preferred orientation. The samples were analyzed using Bruker D8 advance which is equipped with lynxeye linear psd detector, at department of geosciences, University of Oslo.

### 3.3.2 Principle

XRD is based on the principle of Bragg's Law which is defined by the following equation

$$n\lambda = 2dsin\theta$$

Where n is an integer, $\lambda$ is the wavelength of incident radiation, d is distance between the planes in the atomic lattice, and $\theta$ is the angle between the incoming x-rays and the scattering planes. The equation illustrates that we will have constructive interference when the two incident parallel beams of save wavelength interfere by the plane. The d value of the crystals is calculated by the modification following equation

$$d = \frac{n\lambda}{2sin\theta}$$

The equation shows that if we know the wavelength $\lambda$ and the angle $\theta$ we can calculate the d-spacing of the mineral which is distinctive for different minerals (figure 3.5).

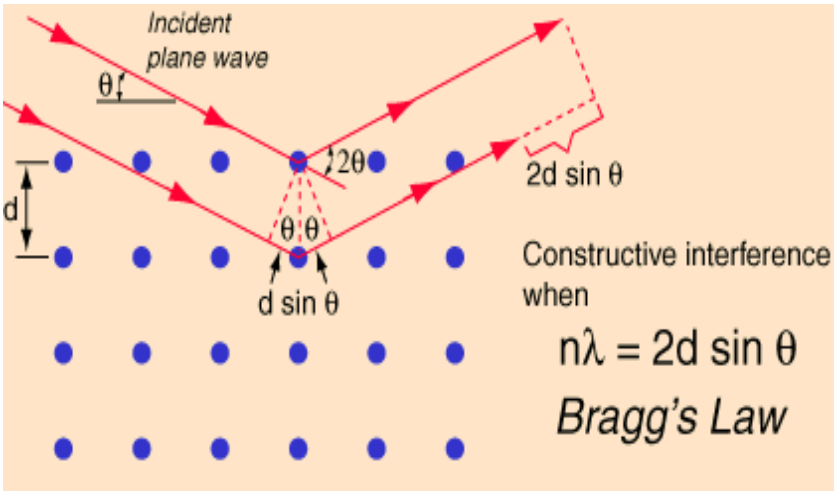


**Figure 3.5: Description of Bragg's Law. (source: http://hyperphysics.phy-astr.gsu.edu/hbase/quantum/bragg.html)**

## 3.4 Inductive coupled plasma spectroscopy(ICPMS)

The technique utilizes the mass of atoms in order to do qualitative and quantitative analysis on the trace level. In this study ICPMS was used to do find the heavy metal (Cd) content in our water samples. The samples were analyzed using Q ICP-MS Bruker aurora at department of geosciences, University of Oslo. The liquid sample is pumped into base of plasma by a pump, as it passes through the different heating zones of plasma torch it will be dried, vaporized, atmomized and ionized. During this process the sample which is in liquid form will change into solid form. As it reaches to the final analytical zone of the plasma it is excited to atoms and ions due to high temperature. The ions that are generated in this plasma zone travel are directed to the electrostatic analyzer which stabilizes the energies of the ions as homogeneous as possible by stabling their kinetic energy. The ions are then directed to the mass analyzer which separates the ions on the basis of their mass to charge ratio and send them to the detector (figure 3.6) (Thomas, 2001)

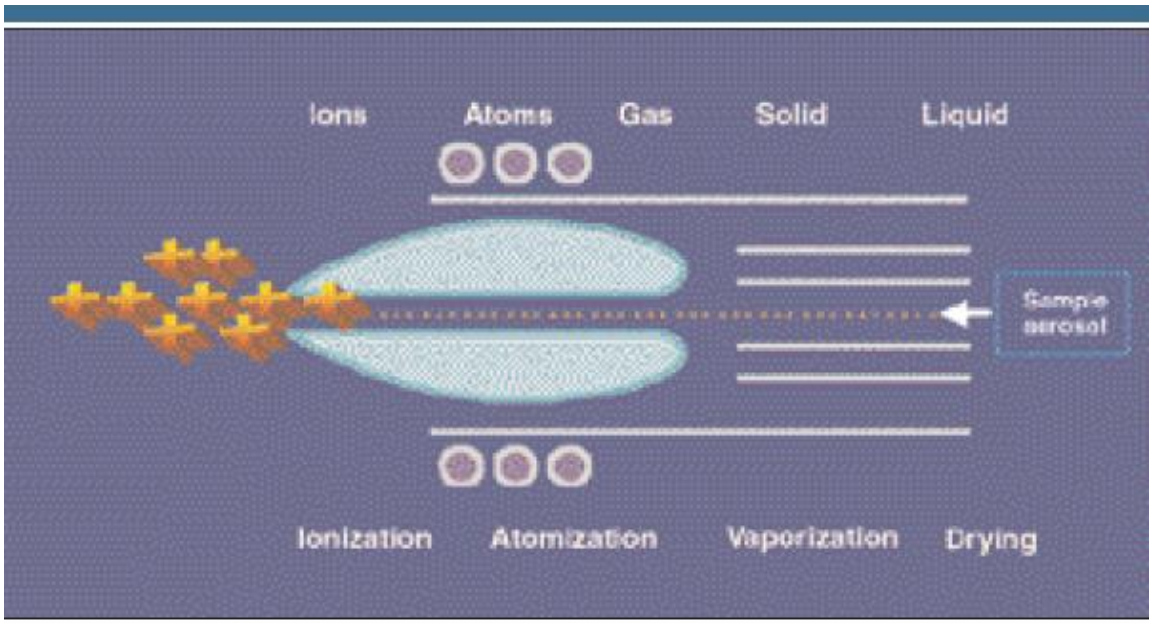


**Figure 3.6: Shows the generation of positively charged ions in the plasma (Thomas, 2001).**

## 3.5 Ion chromatography

Ion chromatography is an ideal method for determining the concentration of ions in the aqueous solutions. In this study the Dionex Ion chromatography system (ICS-2000) was used for the detection of ions (Cl) in the samples. The ICS consist of the following components: a liquid eluent, a high-pressure, pump, a sample injector, a guard and separator column, a chemical suppressor, a conductivity cell, and a data collection system. The system is calibrated to a standard solution before running the sample. The ICS is calibrated by a standard solution prior to running the samples. The results are from the obtained by comparing them with a calibrated standard solution. The data is collected on the computer running chromatography software which produces a chromatogram (Dionex Cor., 2005).

# 4. Methodology

## 4.1 Outline of the study

The outline of the study is shown by figure 4.1. The study includes the following procedures:

1. Mineral Identification and characterization
    - Petrography of Fer_312 A and B using SEM
    - Characterization of Fer_312 A and B using XRD
2. Chip Experiments with Heavy Metals and NaCl
    - Experimental Setup
3. Column experiments
    - Loading of Column with $CdCl_2$+ NaCl solution
    - Loading of Column with NaCl
    - Characterization of the Column Material by SEM and XRD

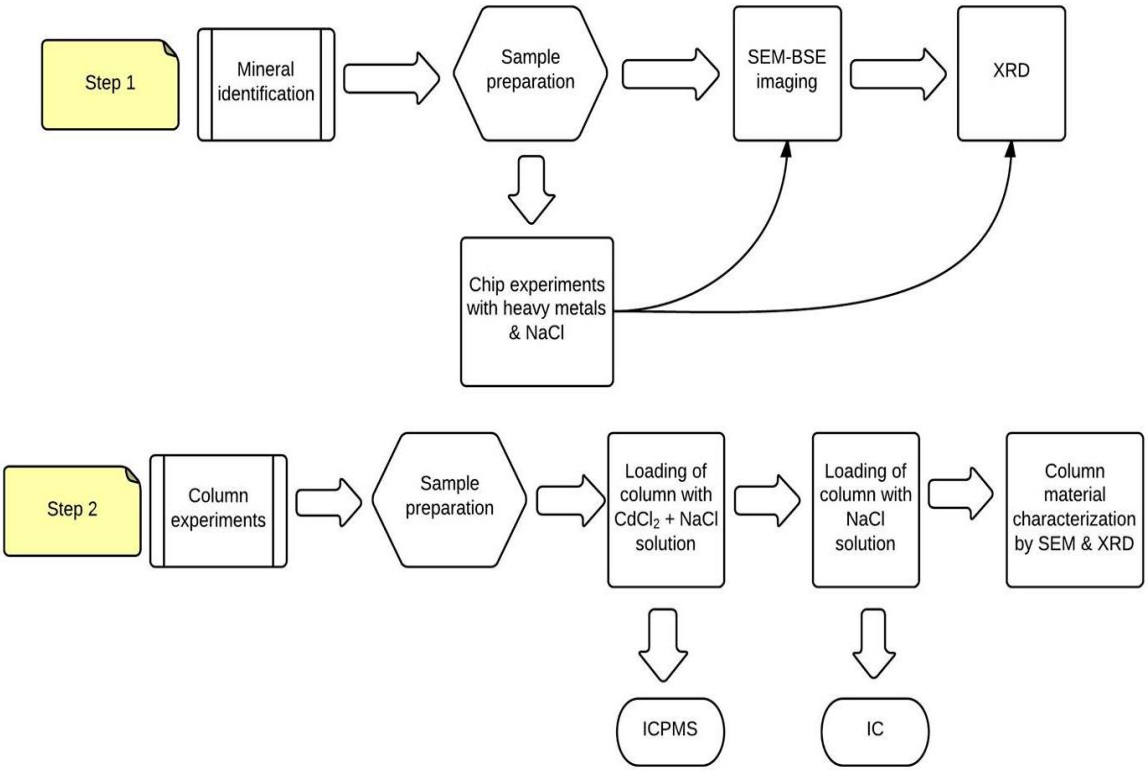


**Figure 4.1: The flow chart illustrating the overview of methodology.**

## 4.2 Mineral Identification and characterization

### 4.2.1 Petrography of Sample Fer_312(A) using SEM

**Sample description**

The scanned image of the sample Fer_312 (A) with the areas chosen for investigation is shown in appendix 1. This sample is the first chip named as Fer_312 (A) that was cut from the main sample Fer3_12. The sample is partially serpentinized, greenish, strongly weathered rock with brown vein of about 200 µm cutting through it. The sample was cut with a diamond saw to about 1 $cm^3$ and polished for the detailed observation in SEM. The original areas of interest were the two large brown veins which are running parallel to each other. The brown color of the veins suggests that they may carry the mineral pyroaurite.

**Area A**

Close up images of Area A are shown in the figure 4.2 below.

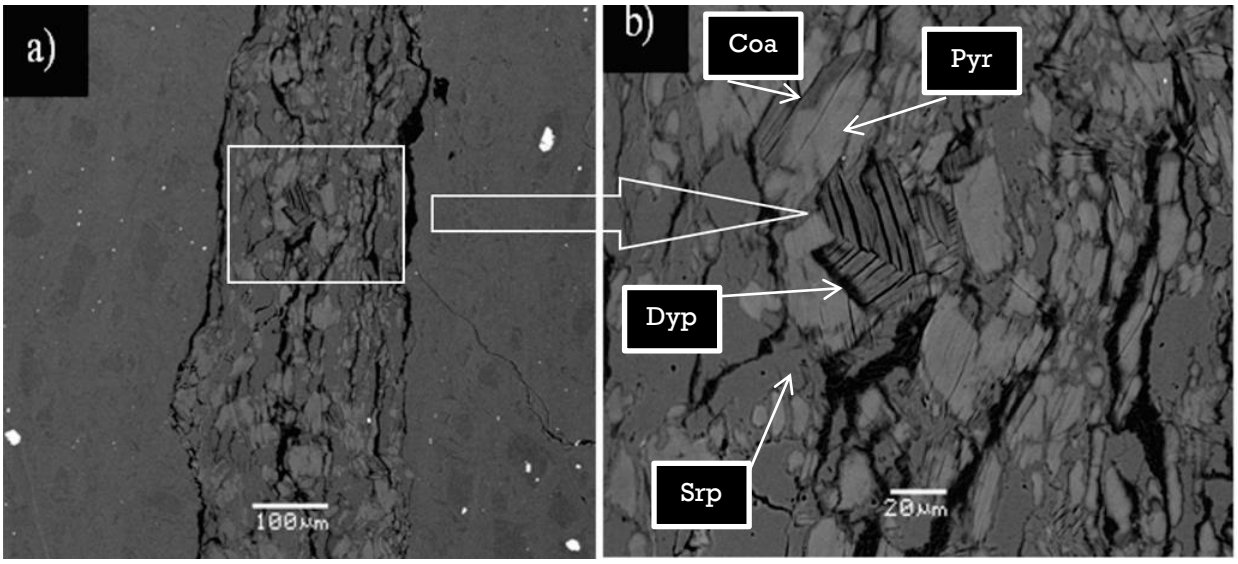


**Figure 4.2: BSE Images of Area A. Mineral abbreviations after Whitney and Evans. 2010. a). 200 µm wide vein running vertically across the image. b) BSE close up image of an area in the vein pointed out by the rectangle in image a showing minerals coalingite (Coa), pyroaurite (Pyr), dypingite (Dyp) and serpentine (Srp).**

The figure 4.2 is showing BSE image of a relatively wide vein of about 200 µm running across the image, dark brown parts of the vein correspond to most bright parts in the BSE image. These brown parts in the vein correspond to mineral pyroaurite. The figure 4.2 b is the zoomed in BSE image of the area in vein pointed by the white rectangle in figure 4.2a,

the bright or light greyish color grains are covered by a rim that seems slightly darker than this greyish part. The greyish part and slightly darker parts are most likely to be serpentine and mineral coalingite respectively. Mineral coalingite is a carbonate mineral which contains Magnesium and iron with the composition of $Mg_{10}Fe_2^{3+}(OH)_{24}[CO_3].2H_2O$. The crystal structure of mineral coalingite is very similar to mineral pyroaurite and sjogrenite. They can only be differentiated by XRD. The main difference between these minerals is that mineral pyroaurite has one brucite-like layer between each carbonate and water layer whereas mineral coalingite has two brucite layers between each carbonate and water layer (Taylor, 1971). The darkest parts surrounding the pyroaurite grains are most likely to be mineral dypingite.

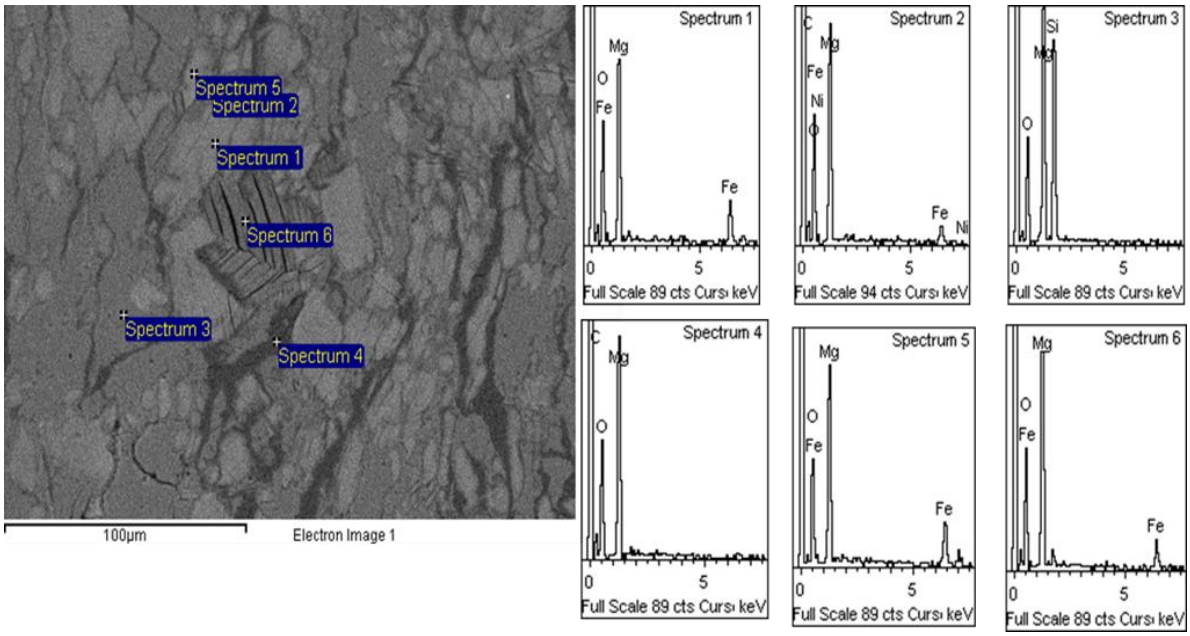


**Figure 4.3: BSE image with EDS spectra of same location as shown in figure 4.2b.**

Figure 4.3 is the close up BSE image taken from Area A with EDS spectra displayed next to it. Spectrum 1 is showing Mg, Fe and O with C which is most likely to be mineral pyroaurite. Spectrum 2 is from the rim covering the grain of mineral pyroaurite showing same composition as in spectrum 1 but with a slightly lower peak of Fe which corresponds to mineral coalingite. Spectrum 3 is showing Mg, Si and O which indicates presence of serpentine. Spectrum 4 is from the dark part showing Mg, O and C which is mostly mineral dypingite. Spectrum 5 is showing Mg, Fe and O same as spectrum 1 that depicts pyroaurite. Spectrum 6 is showing Mg, O with little peak of Fe that could be mineral coalingite.

**Area B**

Close up image of Area B is shown below in figure 4.4 below.

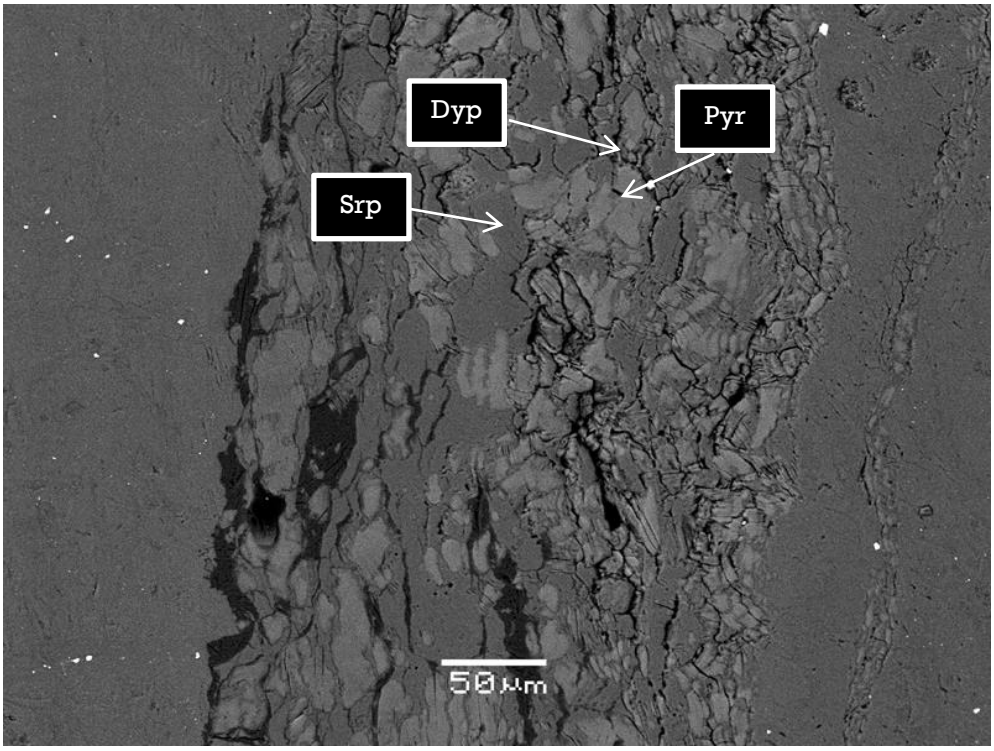


**Figure 4.4: BSE image of Area B showing minerals pyroaurite (Pyr), dypingite (Dyp) and serpentine (Srp).**

The figure 4.4 shows the BSE image of the Area B in the sample. The amount of mineral pyroaurite in this area is estimated to constitute 30-40% of the vein. The other areas in the vein are mostly covered by mineral dypingite (20-30%) and serpentine (40-50%). This area was also chosen for the elemental mapping.

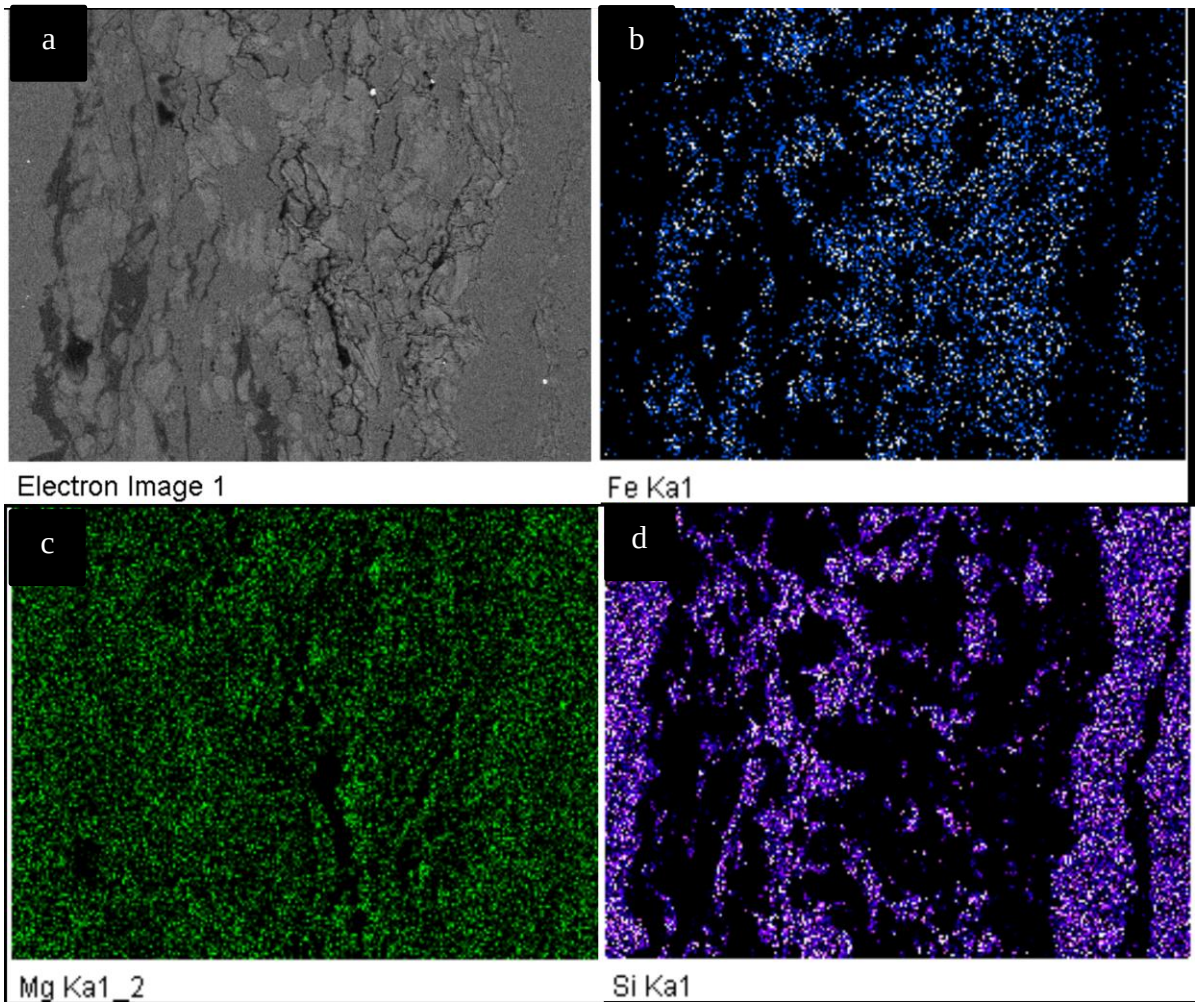


**Figure 4.5: Element maps of Area B from SEM. a) BSE image of the mapped area. b) Map of iron. c) Map of magnesium. d) Map of silica.**

The figure 4.5 is showing BSE image (figure 4.5a) and the element maps (b-d) of the area B. Image 4.5a is a BSE image of the area which was chosen for the element mapping. The highest concentration of the Fe in image 4.5b is found in the middle of the vein and marks presence of pyroaurite. The areas inside the vein that devoid of Fe most likely indicate the presence of dypingite. The concentration of magnesium in image 4.5c seems to be present at most of the parts in the area except the parts that are most likely to be holes in the area. The concentration of silica in image 4.5d is highest in the wall rock and reflects the relative high concentration of Si in serpentine. The areas of high Si inside the vein is also serpentine.

### 4.2.2 Petrography of Fer_312 B using SEM

**Sample Description**

The scanned image of the sample Fer_312 (A) with the areas chosen for investigation is shown in appendix 1. This sample is the second chip named as Fer_312 (B) which was from the main sample Fer3_12. The sample is cut with a diamond saw to about 1 cm and polished to be observed in SEM. The sample is observed by using low vacuum mode of the SEM and it is not carbon coated. The sample was not carbon coated with an intention to see if carbon coating make any change during the experiment. The sample is partially serpentinized, greenish, strongly weathered rock with large dark brown veins and light brown veins cutting through it. The main investigated areas are located on the big vein which is cutting through the center of the sample making a V shape.

**Area A**

Close up image of the vein running in Area A is shown in figure 4.6 on next page.

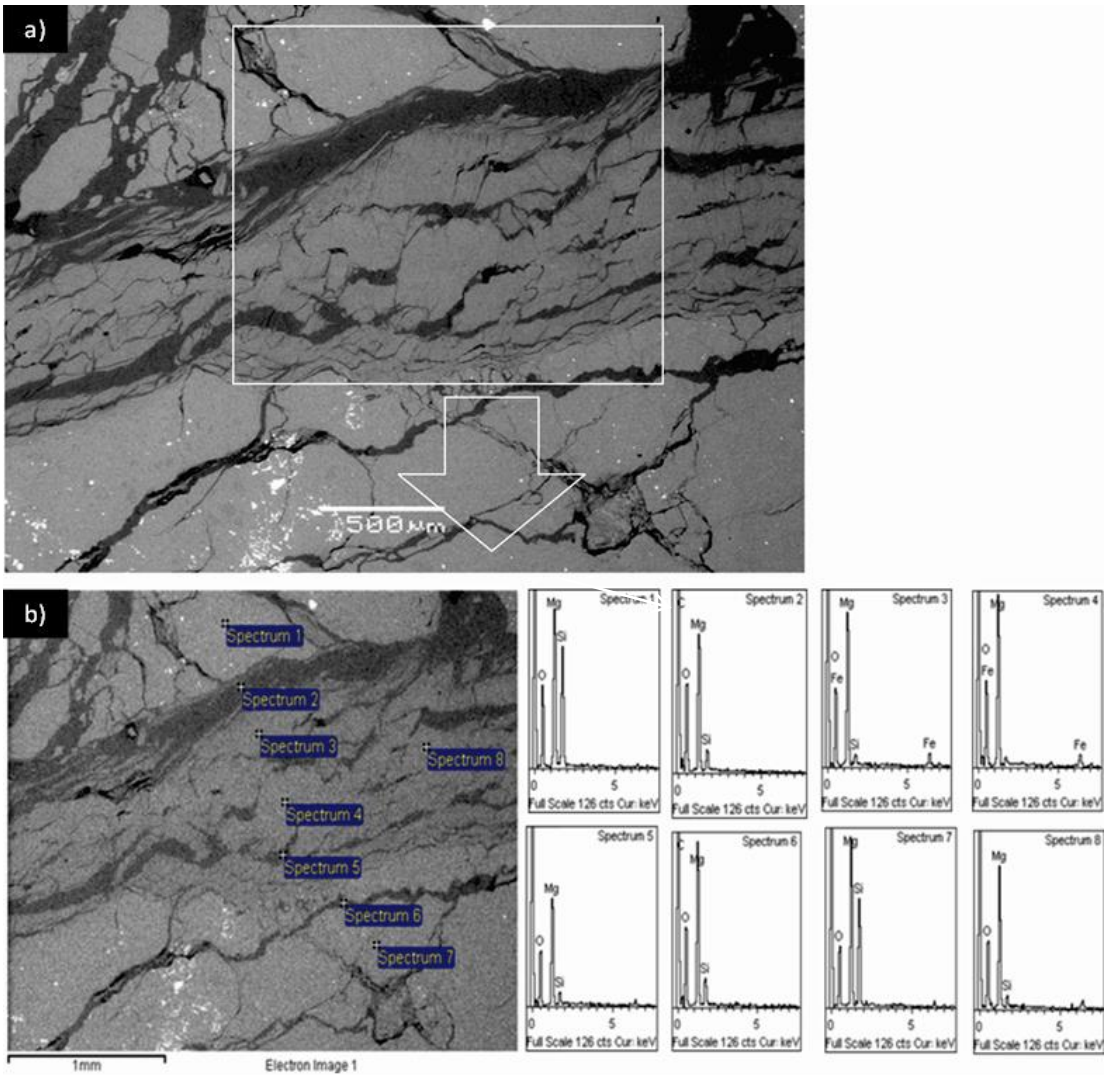


**Figure 4.6: BSE image with EDS spectra taken from Area A. a) Showing the area in the vein chosen for EDS analysis. B) The locations of the spectra with EDS spectra.**

Figure 4.6 b shows a BSE image with EDS spectra of selected points from Area A. Spectrum 1 is taken from the light greyish part showing C, O, Mg and Si documenting serpentine. Spectrum 2 is taken from the dark part of the vein showing C, O, Mg and little peak of Si which may represent the alteration of serpentine or a mixture of serpentine and dypingite. Spectra 3 and 4 are taken from the more greyish part of the sample. Both spectra 3 and 4 show that the elements O, Fe, Mg and Si are present in the pointing and the relative high Fe content indicate that this is altered pyroaurite. Spectra 5, 6, and 8 have same compositions showing C, Mg, and O with varying amount of Si which seems to be mixture of different phases. Spectrum 7 is showing Mg, O and Si which is serpentine.

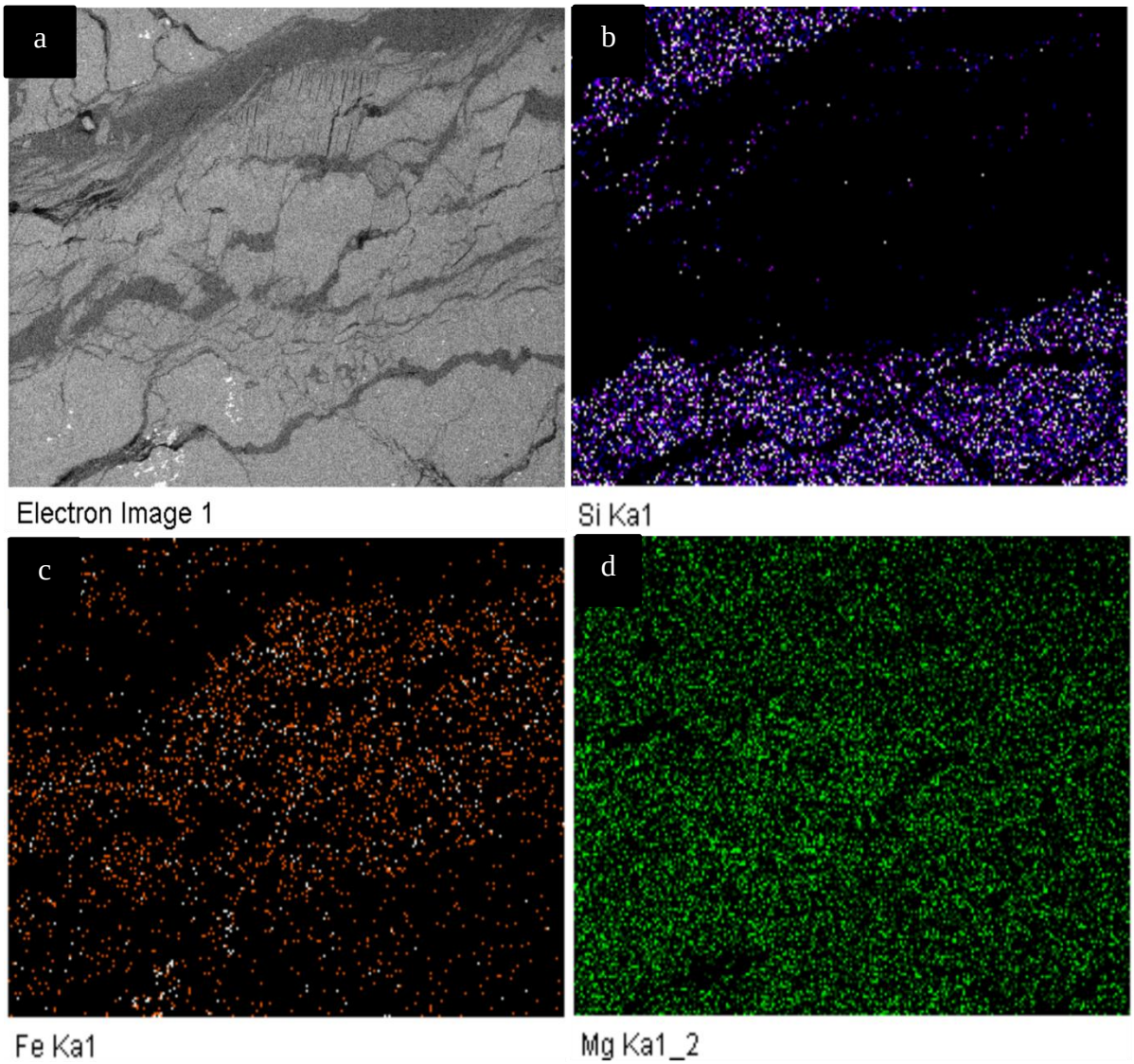


**Figure 4.7: Element maps of Area A from SEM. a) BSE image of the mapped area. b) Map of silica. c) Map of iron. d) Map of magnesium.**

The figure 4.7 is showing BSE image (figure 4.7a) and the element maps (b-d) of the area A. Image 4.7a is showing the area which was chosen for element mapping. The concentration of silica in image 4.7b is highest in the wall rock serpentine. The concentration of Fe in Image 4c is highest in the middle of the vein which may corresponds to the presence of mineral pyroaurite but in some areas it is absent which is most likely due to the presence of mineral dypingite. The concentration of magnesium in figure 4.7d seems to be present in most of the areas but there are some areas that completely devoid of Mg that are most likely to be holes in the areas.

**Area B**

Area B is located in the middle of the sample and is characterized by the V shape with a vein cutting into it.

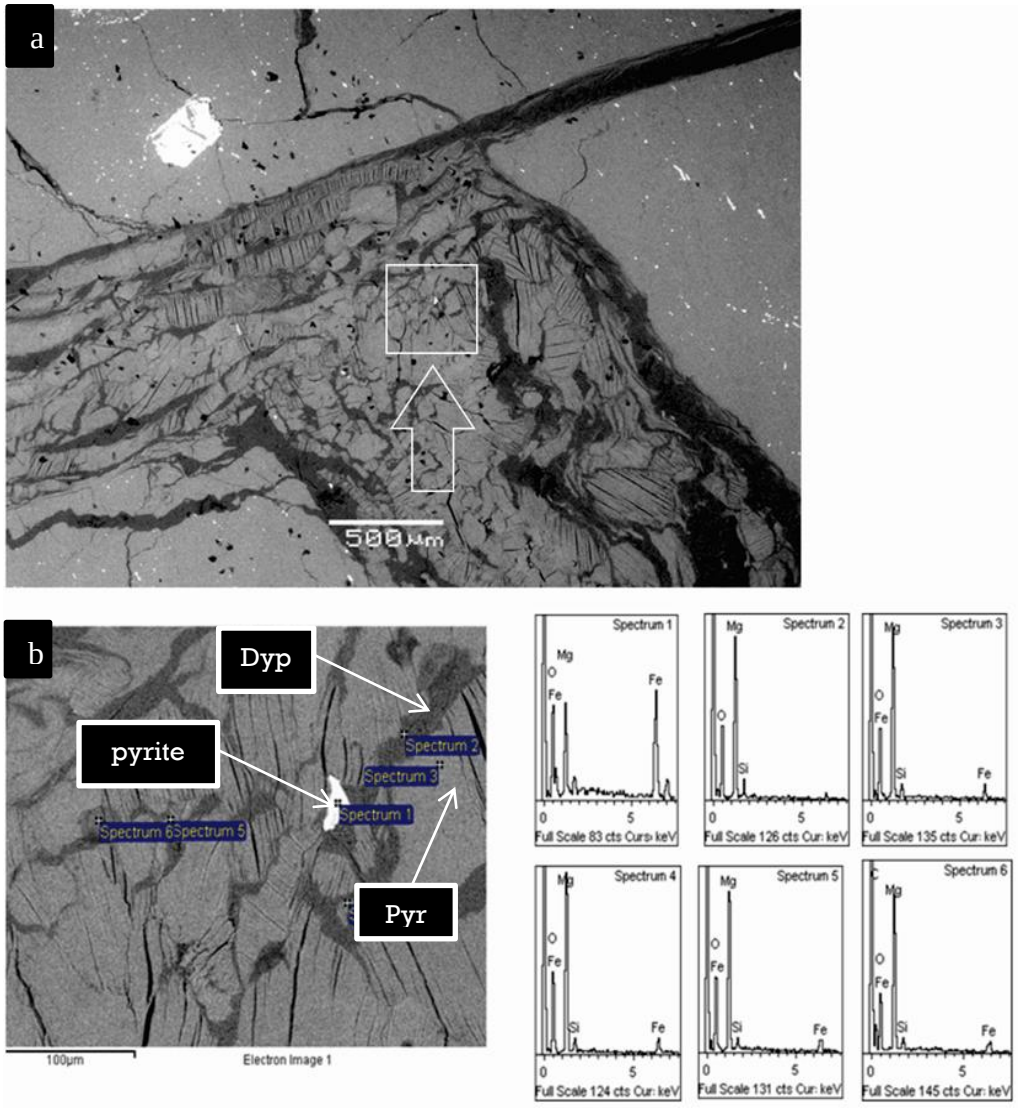


**Figure 4.8: BSE image of the Area B in the sample Fer 3/12 B a). This area shown by the square in the BSE image is chosen for EDS analysis. B) BSE image with EDS spectra of the Area B.**

Figure 4.8b is the close up BSE image taken from Area B with EDS spectra displayed next to it. Spectrum 1 is from the white part in the area c showing Mg, Fe, O which depicts pyrite the higher peak of Mg is most likely from the surroundings. Spectrum 2 is showing Mg, O, and Si which is most likely serpentine. Spectrum 3, 4 and 5 and 6 are showing the good peaks of Mg, Fe with small peaks of Si which is most likely pyroaurite. The small peak of Si is most likely from the serpentine in the surroundings.

### 4.2.3 Characterization of Initial material from chip by XRD

**Sample Preparation using Chip Fer_312A**

The sample for XRD was prepared by carefully scrapping off the powder from the veins in the sample Fer_312 A and B by using knife. The small red colored and cylindrical shaped grains were handpicked from the powder under Leica MZ16 stereo microscope at department of geosciences, University of Oslo.

**XRD Analysis**

The XRD pattern of the initial material that was scratched from the veins is showing the peaks of mineral pyroaurite, sjogrenite, coalingite and mineral dypingite (figure 4.9).

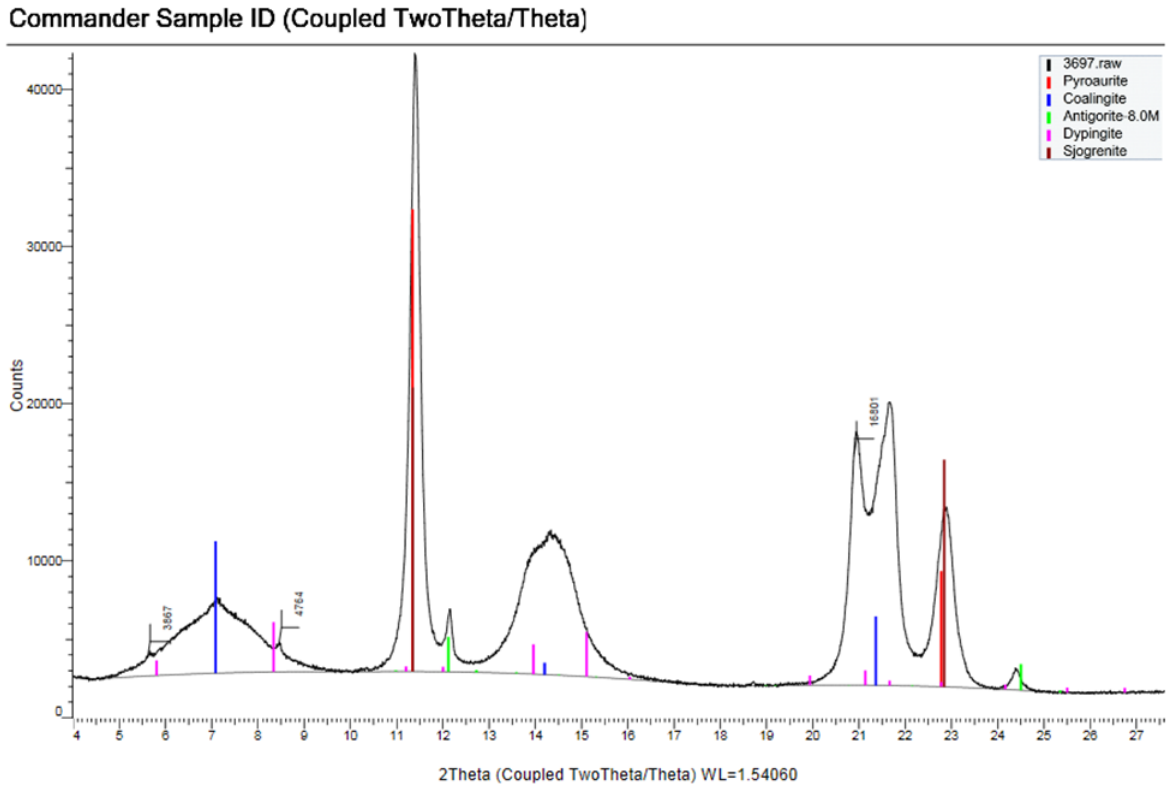


**Figure 4.9: XRD pattern of the initial material from the veins in the sample Fer_312A.**

## 4.3 Chip Experiments with heavy metals and NaCl solution

### 4.3.1 Experimental Setup

**Sample Preparation**

The samples Fer_312 and Fer_412 were taken from a carbonated boulder at the mine tailings of a chromite mine named as "Stensgruva'' located at Area C2 in Feragen (figure 1.1). The sample Fer_312 was cut into 4 small chips of 1 $cm^3$ named as Fer_312 A, B, C, D while sample Fer_412 was cut into 2 small chips of 1 $cm^3$ named as Fer_412A and B using diamond saw. The two chips Fer_312 A and B were studied in detail for the mineral identification purpose using SEM-BSE imaging. One of the chips Fer_312 (A) was carbon coated while the other chip Fer_312 (B) was analyzed in low vacuum without carbon coating as discussed earlier in sections 4.2.1 and 4.2.2). The main objective of doing this was to observe the effect of carbon coating on the chip Fer3_12 (B) after reaction with the reactants. It was found that the carbon coatings did not influence the experiment.

**Reaction of chips with Heavy metals and NaCl solution**

Chips Fer_312A and Fer_312B that were used to identify the minerals in the samples while with the remaining 4 chips named as Fer_312D, and Fer_412A and B were set to react with different heavy metals. However, one of the chips Fer_312C was set to react with NaCl solution following the results from the column experiments (see section 5.2). The chips were polished and carbon coated prior to the experiment. Afterwards, the chips were uncoated and reacted with reactant solutions. The chips were again carbon coated and analyzed in detail by SEM-BSE imaging to see changes after the experiment. The reactant solutions were prepared by dissolving different amounts of salts with varying amount of Ultra high pure deionized water (see table 4.1). The chips were set to react with the solution for 1 hour; afterwards they were washed 3 times with the Ultra high pure deionized water to make sure there is no salt left on the chips.

**Table 4.1: Metal solution preparation data.**

| Reactants | Salt Concentration | Amount of water | Molarity | Sample Name |
|---|---|---|---|---|
| Chromium Nitrate $(CrNO_3)_3$ | 1.9986g | 50 ml | 0.1 Mol | Fer_312A and Fer_312B |
| Cadmium Chloride $(CdCl_2)$ | 0.45668g | 20 ml | 0.1 Mol | Fer_412 B |
| Lead Nitrate $(PbNO_3)_2$ | 0.66242 g | 20 ml | 0.1 Mol | Fer_412 A |
| Copper Sulphate $(CuSO_4)$ | 0.3192g | 20 ml | 0.1 Mol | Fer_312 D |
| Sodium Chloride (NaCl) | 2.975g | 20 ml | 2.5 Mol | Fer_312 C |

## 4.4 Column Experiments

The column experiments were conducted to investigate the sorption potential of the weathered dunites. The column experiments comprise of two experiments, first experiment was performed to study the adsorption behavior of Cd and the second experiment was performed to check if $Cl^-$ could work as a conservative tracer with the material used for studying the sorption behavior of Cd following results from first batch experiment.

### 4.4.1 Experimental Setup

**Overview of column experiments**

The column was saturated with ultrahigh pure deionized water for 2 hours to check to make sure that there is no leakage or backflow and the system is stable. The column was then eluted with $CdCl_2$ and NaCl solution and the samples were taken with different time intervals for 120 minutes. The column was eluted with deionized water for 1 day prior to the elution of column with 1 molar NaCl solution. At the end of the column experiments, the material from the column was carefully taken out for XRD and SEM characterization (figure 4.10).

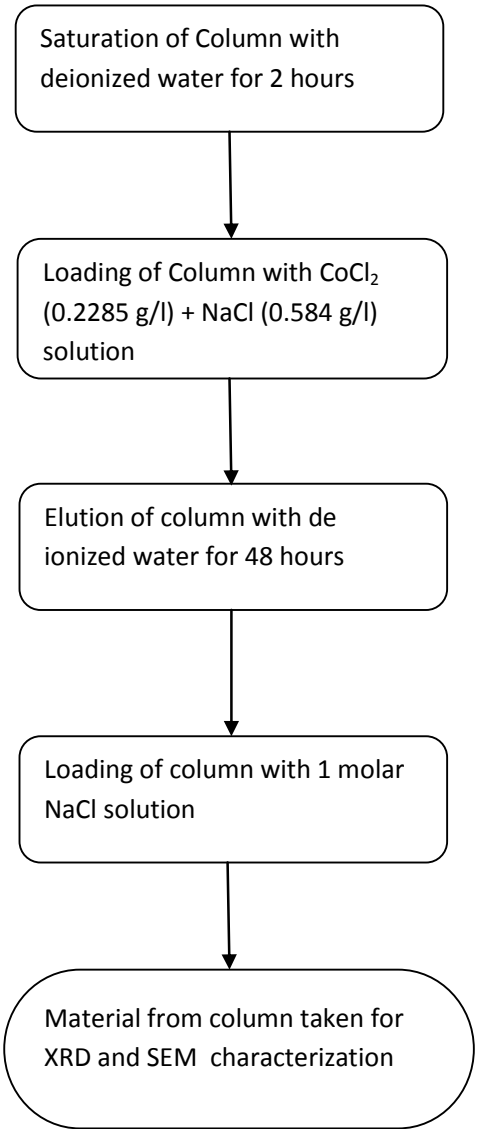


**Figure 4.10: Flow chart illustrating the overview of column experiments.**

### Sample Preparation

The sample was prepared by crushing different samples that were collected from the mine tailings of "Stensgruva" (figure 1.1). The areas with the veins and white spherical grains were separated from the samples by cutting the samples. Afterwards the column was mostly filled with the red grains and white spherical grains which were confirmed by SEM to be as mineral pyroaurite and mineral dypingite respectively (see section 4.2.2 and 4.2.3).

### Column Specifications

The experiments were carried out in a polypropylene column (13.5 cm high, 2.67 cm internal diameter). The column was filled with 50ml of the crushed material that covered 9cm

portion of the column. The cotton plugs along two filters of 45 microns that were cut according to the size of column openings were fitted at the two filter areas. The outlet of the column was sealed with non-reactive silicon rubber to avoid evaporation and leakage. The Teflon tubes were connected at the inlet and outlet of the column to pass the solution. A Gilson peristaltic pump was used to pump the water through the column and flow rate of the water was calculated to check if the flow is stable (figure 4.11).

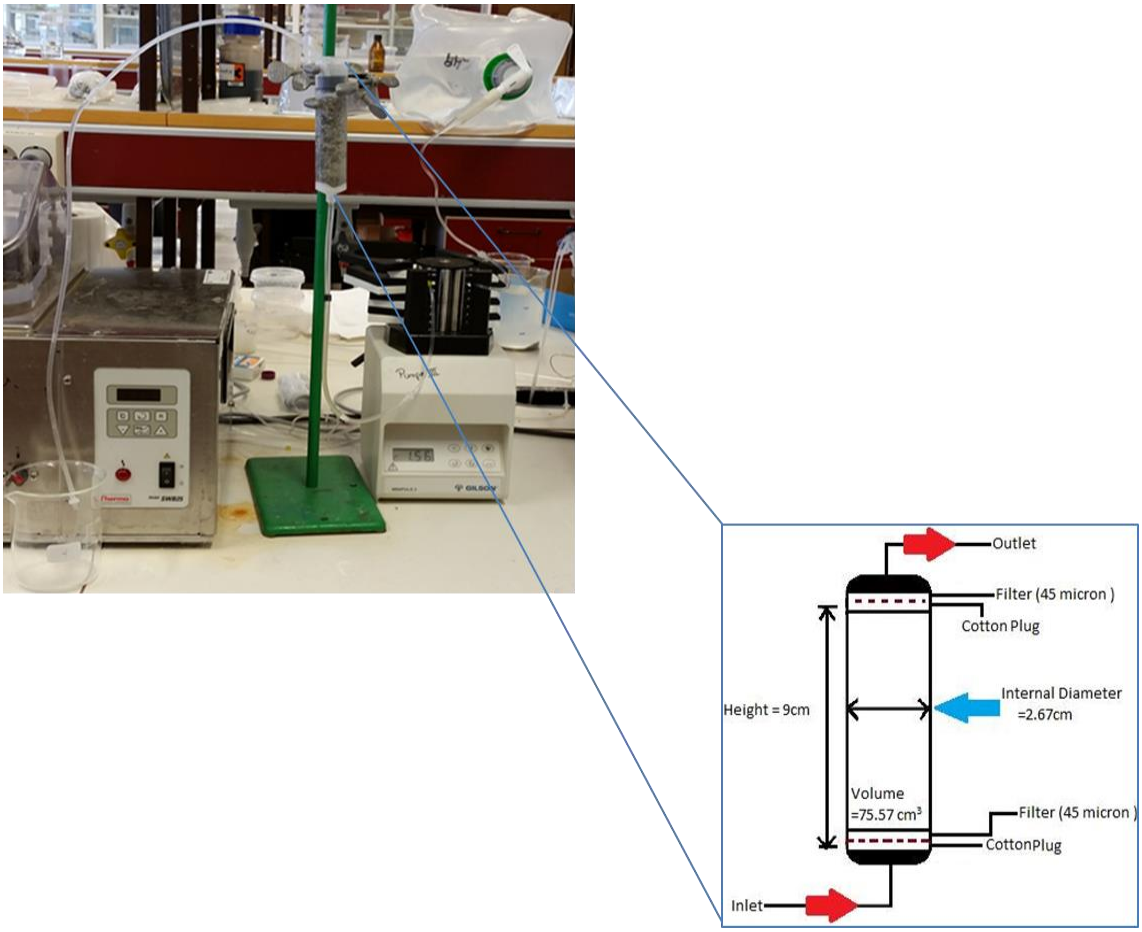


**Figure 4.11: Setup of column experiments. The small sketch at the bottom is showing the column specifications.**

## 4.4.2 Loading of Column with $CdCl_2$ and NaCl solution

An inlet solution was prepared by adding 0.0584 mg/l of NaCl and 0.2285 mg/l of $CdCl_2$ into 1 liter of Ultra high pure deionized water. The column was then eluted with the prepared solution ($CdCl_2$ and NaCl) at controlled flow rate of 0.47ml/min. The NaCl was added into

the solution to use $Cl^-$ as a conservative tracer. The effluent samples were collected at time intervals of 0, 10, 25, 30, 35, 40, 50, 60, 70, 80, 90, 100, 110, 120 minutes. The effluent samples were then diluted by using 1%$HNO_3$ prior to ICPMS analysis.

### 4.4.3 Loading of the Column with NaCl Solution

The second column experiment was performed by using the same material in the column. The column was eluted with 1 M NaCl solution at a controlled flow rate of 0.26 ml/min. The effluent samples were collected with the time interval of 10 minutes for 2 hours and 40 minutes. The effluent samples collected were diluted 10 times prior to the IC analysis. Afterwards, the samples were analyzed for chloride concentration measurement by using IC.

### 4.4.4 Porosity calculation

Porosity was calculated by filling a graduated cylinder with 45 ml of column material. Water was introduced into the cylinder slowly until it reached at the top of the material. The amount of water was noted when the material in the column was saturated. The total amount of water which was used to saturate the material was then divided by the total amount of the material which in our case was 47 %.

### 4.4.5 Characterization of Initial material from column by XRD

**Sample preparation**

The material in the column was crushed by using hand mortar. Afterwards crushed material was grinded to fine powder by using micronizer. The crushed material was shifted to a sample holder and powder was smeared properly by using a glass to make sure that the sample is flat and there is no irregularity along the corners of the sample holder.

**XRD Analysis**

The XRD pattern of the initial material used in column is shown below in the figure 4.12.

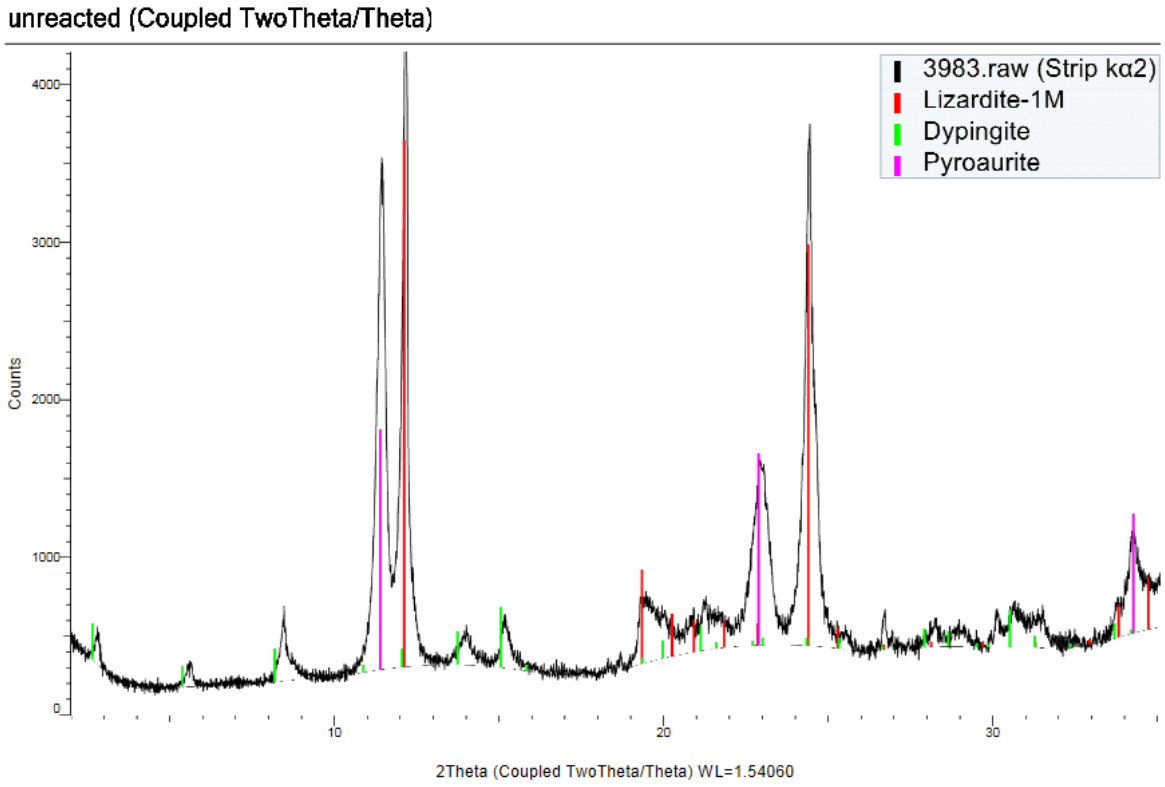


**Figure 4.12: XRD pattern of the initial material used in column.**

### 4.4.6 Characterization of the reacted column material by SEM

The material from the column after the experiments was taken out in a jar and two samples were analyzed using SEM-BSE imaging. The two samples were identified as mineral pyroaurite and mineral dypingite under Leica MZ16 stereo microscope at department of geosciences, University of Oslo.

# 5. Results and Discussion

## 5.1 Experiments with Heavy Metals

### 5.1.1 Reaction of Chromium Nitrate($CrNO_3)_3$ with Fer_312A

The scanned image of the areas chosen for detailed investigation by SEM is shown in appendix 1.

**Area A**

Close up BSE images of Area A before and after the experiment are given below.

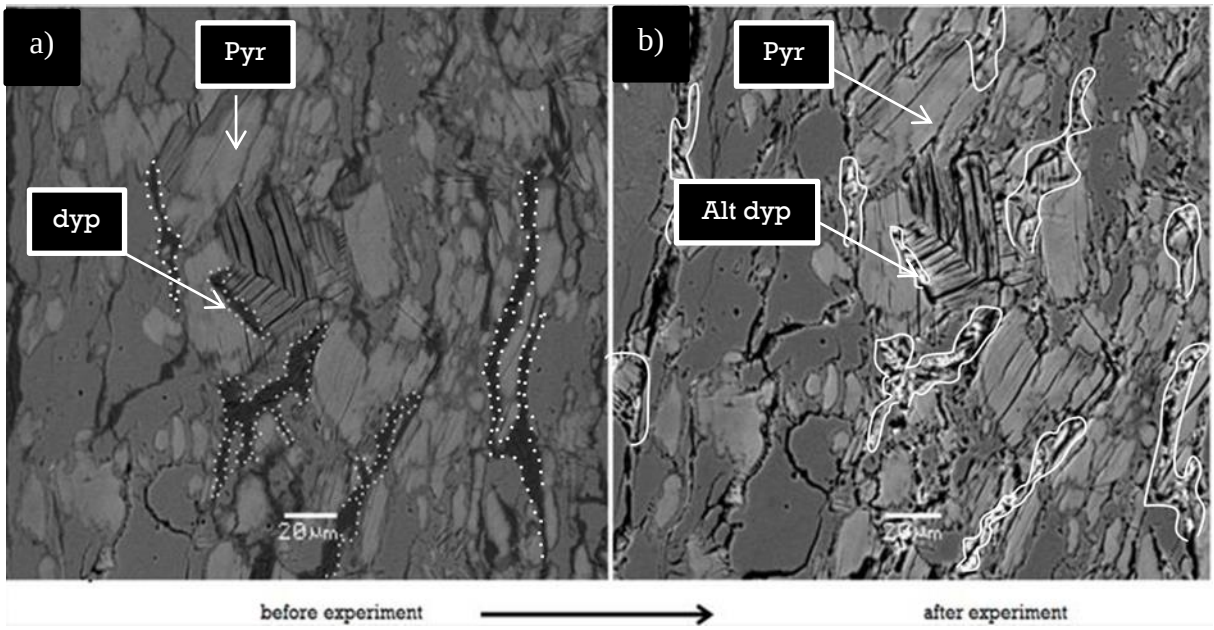


**Figure 5.1: Successive BSE images of the Area A in Chip Fer_312A: (a) before experiment. b) after experiment.**

The prominent changes can be seen by comparison of same areas before and after the experiment (figure 5.1). It can be observed that all the dark parts that were identified as dypingite before the experiment are shown by white dotted lines in image 5.1a took part in the reaction during the experiment which is now shown by the white boundary lines covering these areas in image 5.1b. This alteration on the surface of dypingite depicts the sorption of Cr. However, the slightly greyish parts in the area that were identified as mineral pyroaurite before the experiment did not take part in the reaction and were preserved during the experiment.

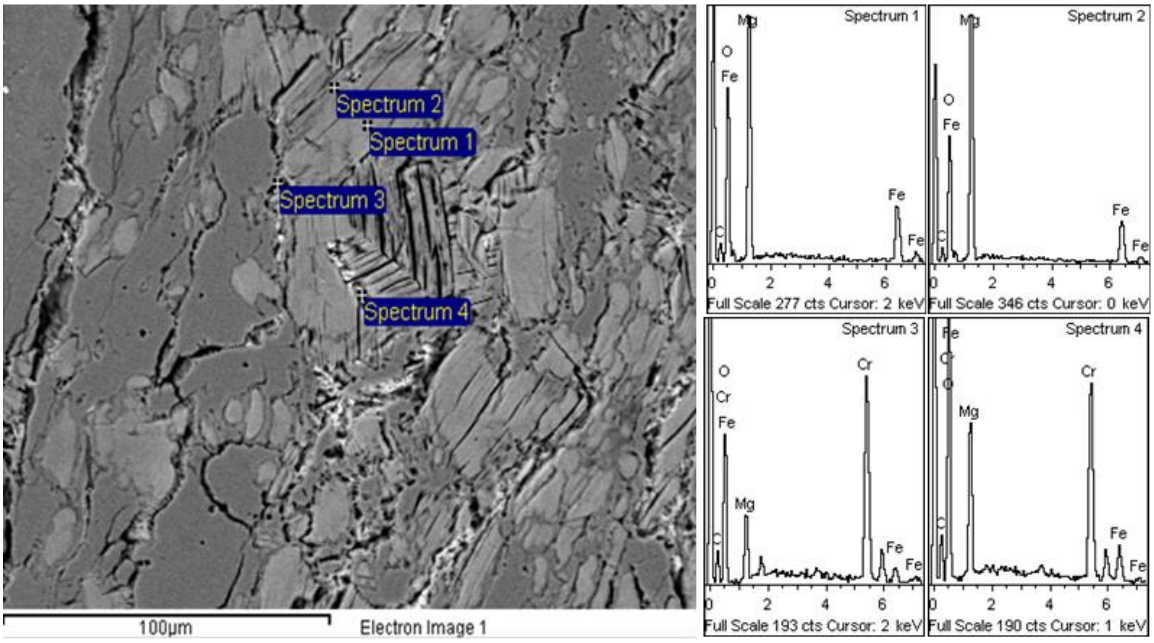


**Figure 5.2: BSE image with EDS spectra of same location after experiment shown in figure 5.1.**

The BSE image with EDS spectra (figure 5.2) shows the same location which was shown in the figure 5.1. Spectrum 1 show peaks of Mg, Fe with minor C which corresponds to pyroaurite. Spectrum 2 is from the rim covering the grain of mineral pyroaurite showing the same composition as spectrum 1 with peaks of Mg, O and small peaks of Fe and C which is most likely to be mineral coalingite. It can be observed that there is no difference in the composition of pyroaurite and coalingite and it is the same as it was before the experiment. Spectra 3 and 4 are taken from the dypingite areas, which show Mg, C, Fe and high Cr. This demonstrates that Cr was sorbed on the areas with dypingite. The lower concentration of Mg is an indication of Cr dissolving Mg and the small peak of Fe is due to the presence of mineral pyroaurite grain in the surrounding.

**Area B**

Close up images of Area B before and after the experiment are given below.

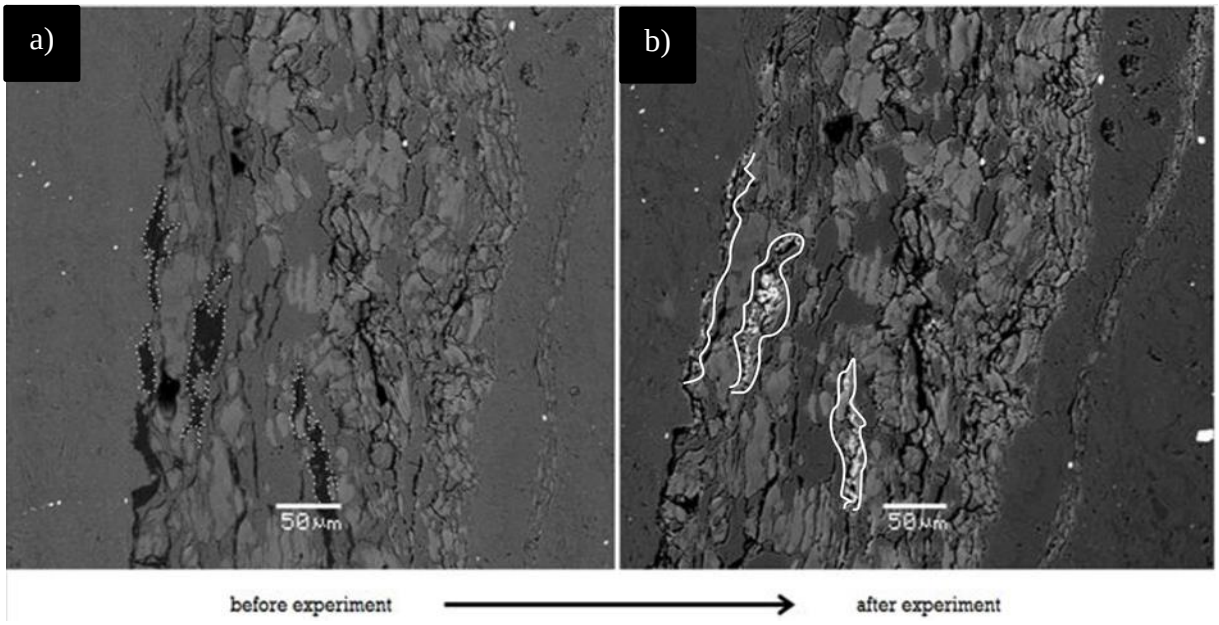


**Figure 5.3: Successive BSE images of the Area B in Chip Fer_312 A : (a) before experiment .b) after experiment.**

The prominent changes during the experiment can be seen by the successive BSE images of the Area B before and after experiment (figure 5.3). It can be observed that the darkest areas in the vein which were identified as mineral dypingite before the experiment are appearing as brightest parts in the vein after the experiment which indicates the sorption of Cr on mineral dypingite during the experiment. However, the slightly greyish parts in the areas which were identified as pyroaurite before the experiment did not take part in the reaction and were preserved during the experiment.

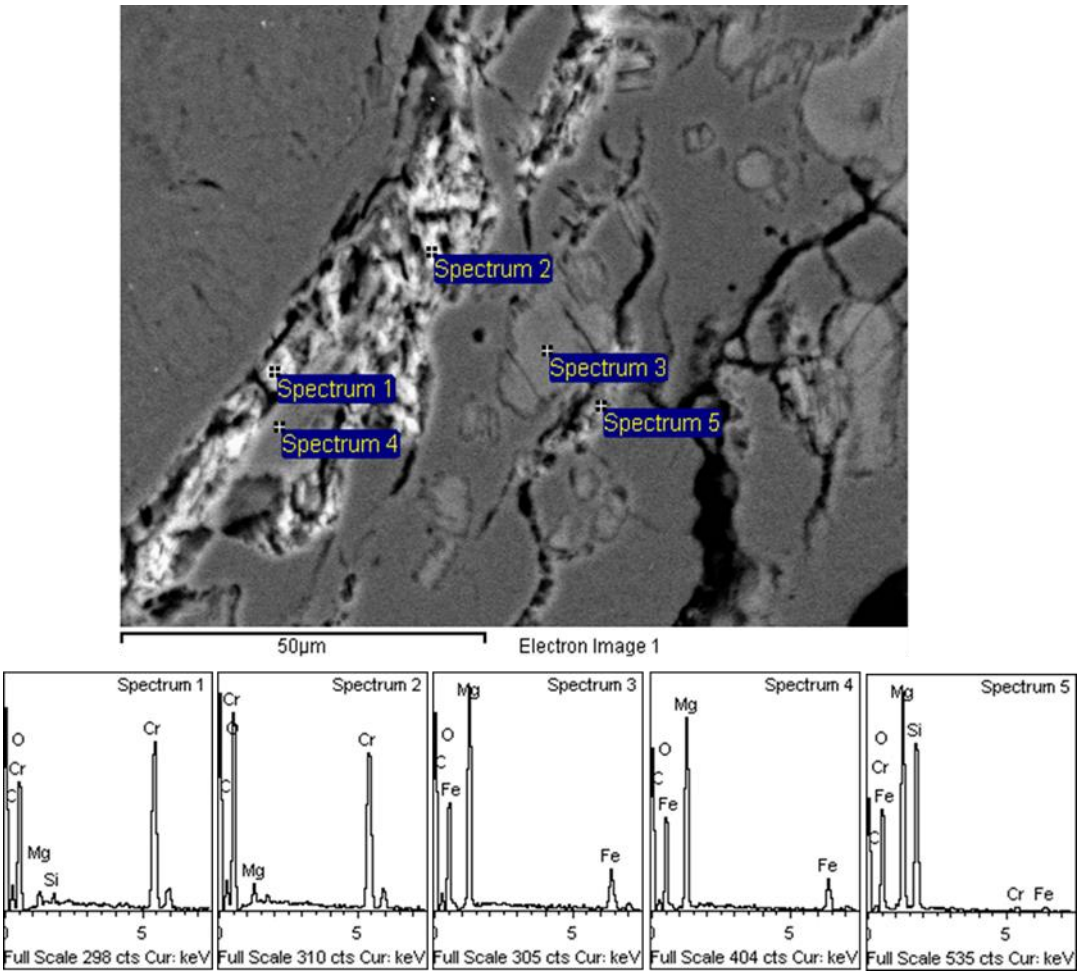


**Figure 5.4: Close up BSE image of an area b with EDS spectra of the same area shown in the figure 5.3.**

The BSE image with EDS spectra which are displayed at the bottom of it (figure 5.4), shows the close up of the same area which was shown in the figure 5.3. Spectrum 1 is taken from the brighter parts of the area those were dissolved during the experiment, showing high concentration of Cr, with small peak of Mg, O, C and Si. The small peak of Si, is from the presence of serpentine in the surroundings. Spectrum 2 is also from the brightest part in the area, shows a high peak of Cr, with small peaks of Mg and C which shows that Cr has more or less completely dissolved Mg and coated the dypingite with Cr phase. Spectra 3 and 4 reflect pyroaurite as indicated by the high Fe peak. Spectrum 5 is showing high peak of Mg, Si, O with small peak of Fe and Cr which most likely depicts serpentine. The small peaks of Fe and Cr are most likely due to the presence of mineral pyroaurite and altered mineral dypingite grains sitting in the surroundings.

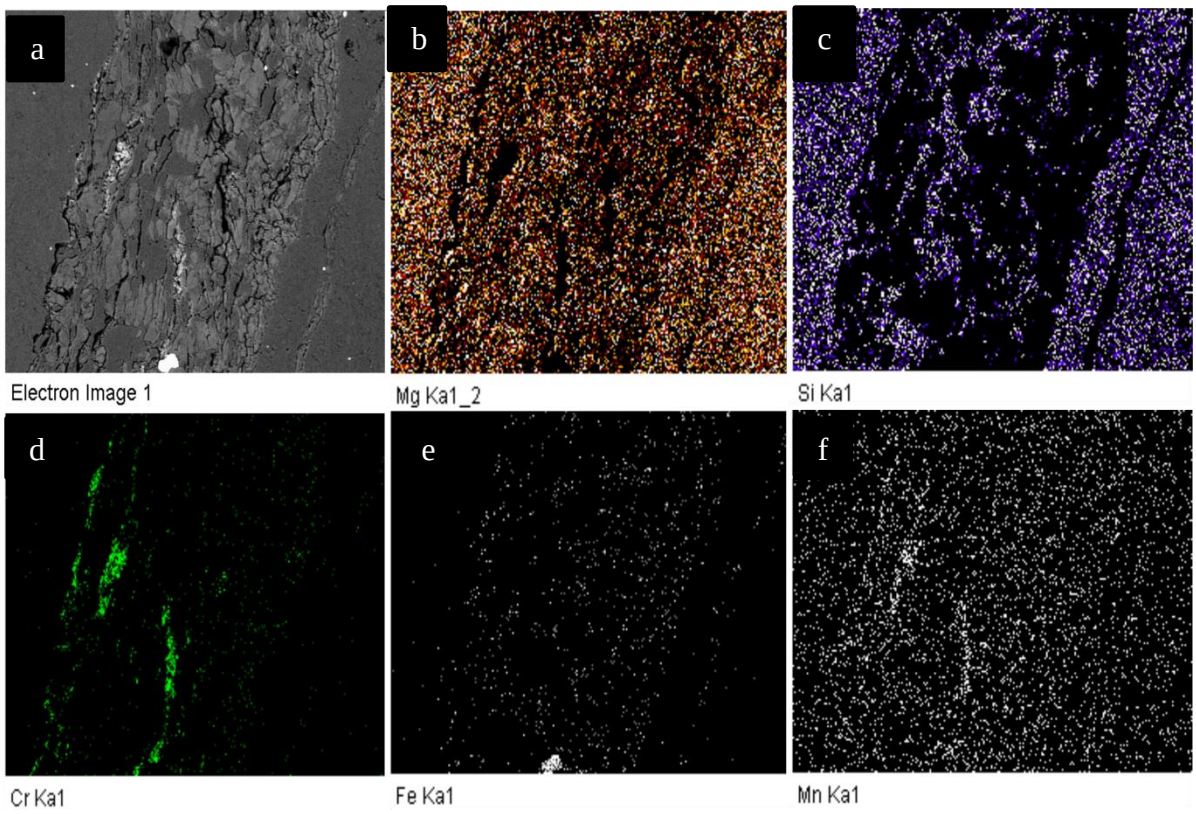


**Figure 5.5: Element maps of Area B by using SEM. a) BSE image of the mapped area. b) Map of magnesium. c) Map of silica. d) Map of chromium. f) Map of manganese.**

The figure 5.5 is displaying the element maps (b-f) over the area shown by BSE image (a) of the same area that was also used for element mapping before the experiment (see figure 4.5, chapter 4). The concentration of magnesium in image 5.5d seems very low or nil in the areas where Cr is sitting, which is most likely due to the dissolution/replacement of Mg by Cr during the experiment (see also figure 5.5 f). The higher concentration of Si in image 4.5c shows that serpentine is mostly present outside the vein. The concentration of Iron in Image 5.5e, shows the presence of Fe mostly in the vein which is due to the presence of mineral pyroaurite in these areas. The concentration of manganese in image 5.5f, shows the abundance of Mn in the areas where the Cr is sitting.

**Area E**

The close up image of area E is shown by figure 5.6. The area was also chosen for Element mapping by EMP.

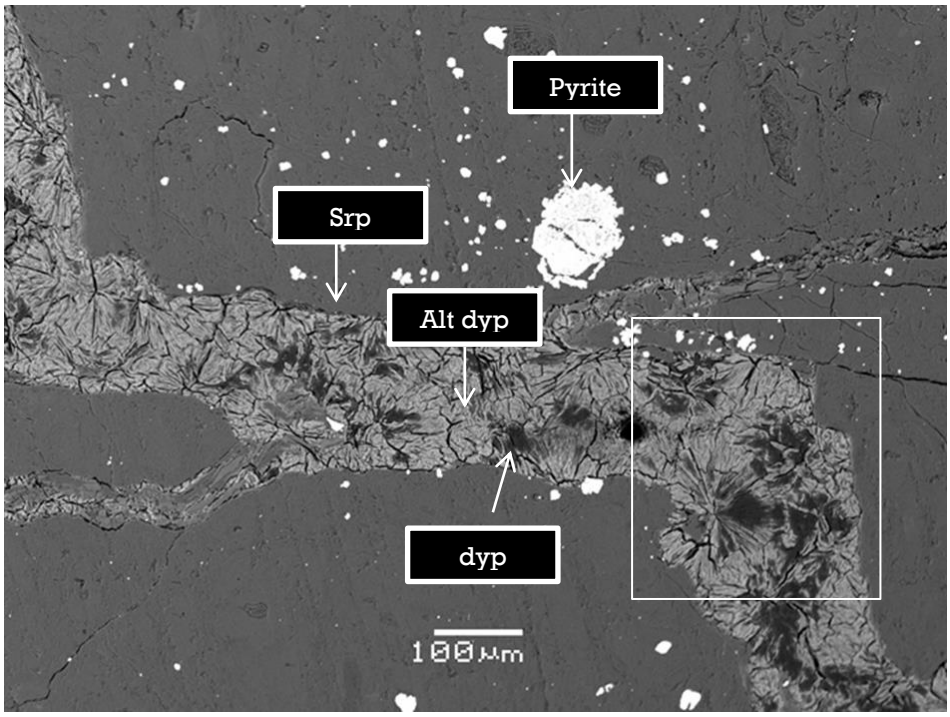


**Figure 5.6: Close up image of Area E showing the big vein with rosette structures. The rectangle is pointing out the area used for element mapping. The white bright spot in the area depicts pyrite ($FeS_2$).**

Area E is showing a 200um wide vein with spherical rose like structures which preserved their shape during the experiment. Some of the rose like structures have a slightly darker parts suggesting that the reaction was not complete. It seems like that Cr is dissolving these rose like structures. The areas outside the vein are serpentine which was completely unaltered during the experiment. The white spot in the area depicts pyrite.

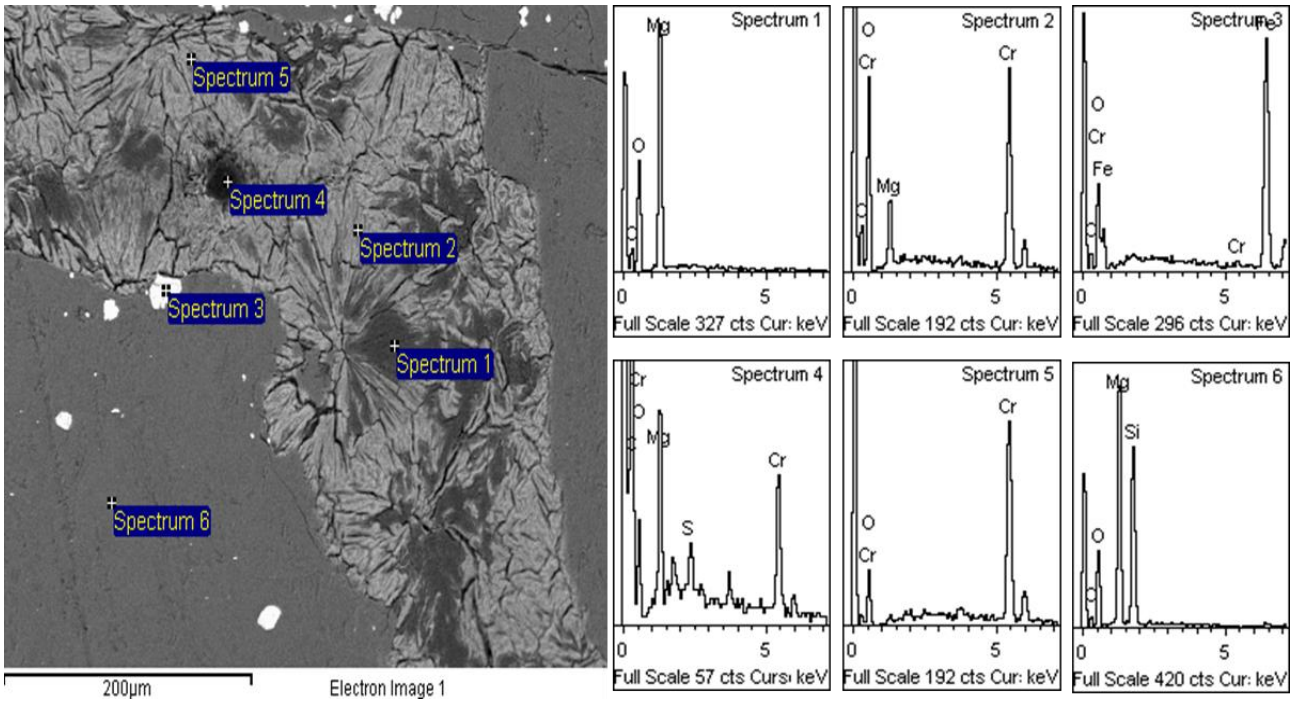


**Figure 5.7: Close up BSE Image of Area E with EDS spectra displayed next to it.**

The figure 5.7 is showing BSE close up image with EDS spectra of the area which is pointed out by the rectangle in figure 5.6. Spectrum 1 is taken from the rose type structure containing Mg, O with little bit of C which is most likely to be unaltered part of dypingite which was preserved during the experiment. Spectrum 2 is taken from the bright part just outside the rose like structure showing high peaks of Cr with quite a bit of Mg, O and C which most likely showing that Cr is exchanging magnesium from mineral dypingite or simply coating it. Spectrum 3 is from the white part of the area showing a lot of Fe, O with little bit of C and Cr which is most likely to be iron oxide. Spectrum 4 is taken from the darkest part of the area, showing a high peak of Mg, Cr, C, O with little bit of S, which is most likely from the hole in the sample. Spectrum 5 is showing only peaks of Cr and O which is most likely showing the complete replacement/dissolution of Mg by Cr in mineral dypingite. Spectrum 6 is showing Mg, Si and O that depicts the presence of serpentine.

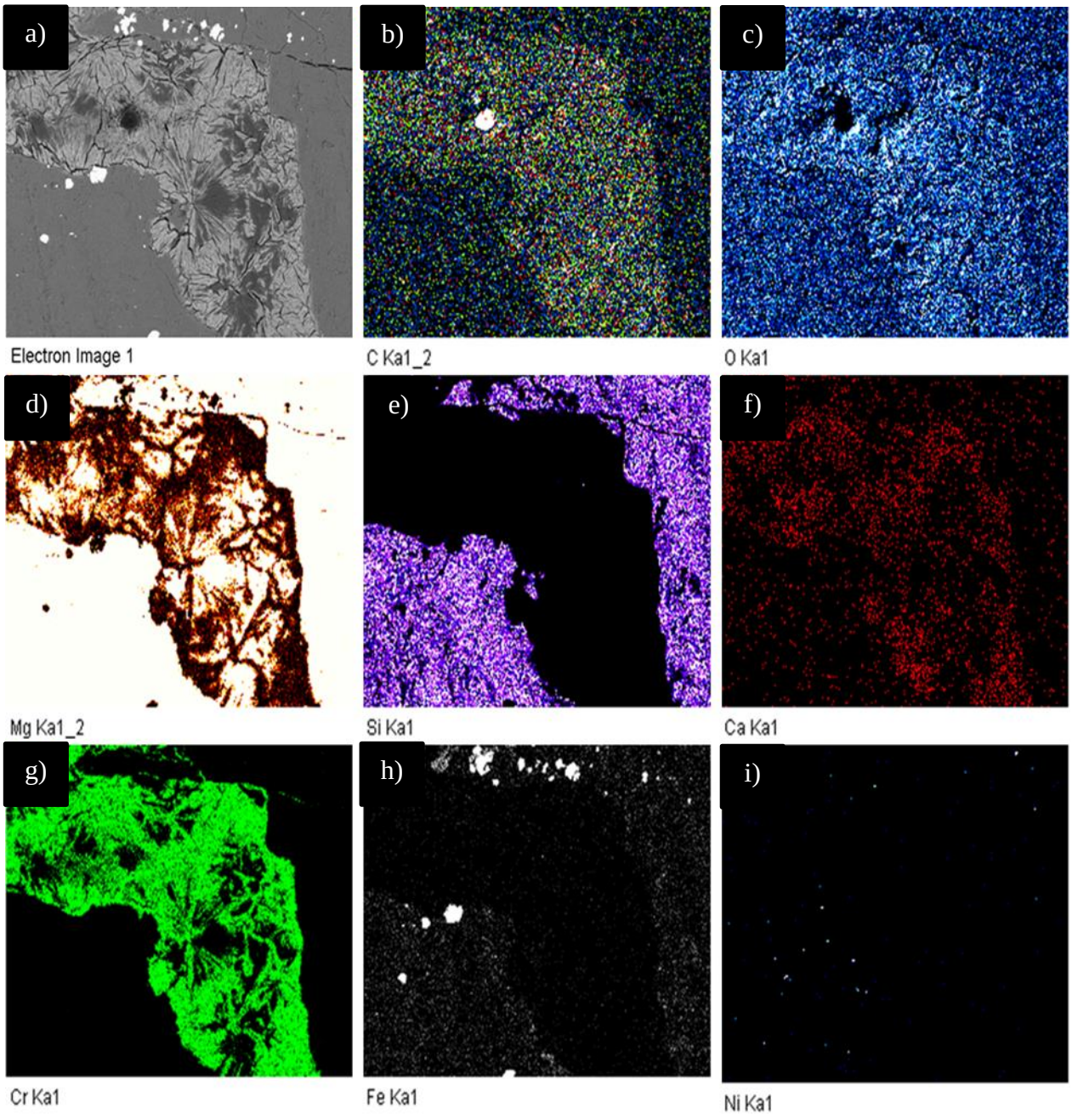


**Figure 5.8: Element Maps of Area E by using EMP. a) BSE image of the mapped area. b) Map of carbon. c) Map of oxygen. d) Map of magnesium. e) Map of silica. f) Map of calcium. g) Map of chromium h) Map of Iron. I) Map of nickel.**

The figure 5.8 is showing the element maps of the area E. Image 5.8a is BSE image showing the area which was chosen for the element mapping. The concentration of carbon in image 5.8b, is showing the abundance of the carbon at the place that is most likely to be a hole in the area. The vein displays a carbon level that appears to be above the detection limit represented by the serpentine in the wall rock. The concentration of the oxygen in image

5.8c is showing most of the oxygen in the inner part of the vein. The concentration of the magnesium in image 5.8d is highest in the preserved core of the rose like structure that is most likely representing mineral dypingite. The concentration of silica in image 5.8e is highest in the wall rock in accordance with the presence of serpentine outside the vein. The concentration of calcium, which can be seen from image 5.8f, shows quite a bit of calcium in the vein. The concentration of chromium in image 5.8g, shows the presence of Cr mostly outside the rim of rose like structures. The concentration of iron in image 5.8f seems to be more abundant outside the vein. The small grains of Ni-phase in image 5.8g may be mineral awaruite.

**Area F**

Close up image of Area F is shown by the figure given below. Area F lies at the bottom of the sample shown by the spherulites in the area (see appendix 1).

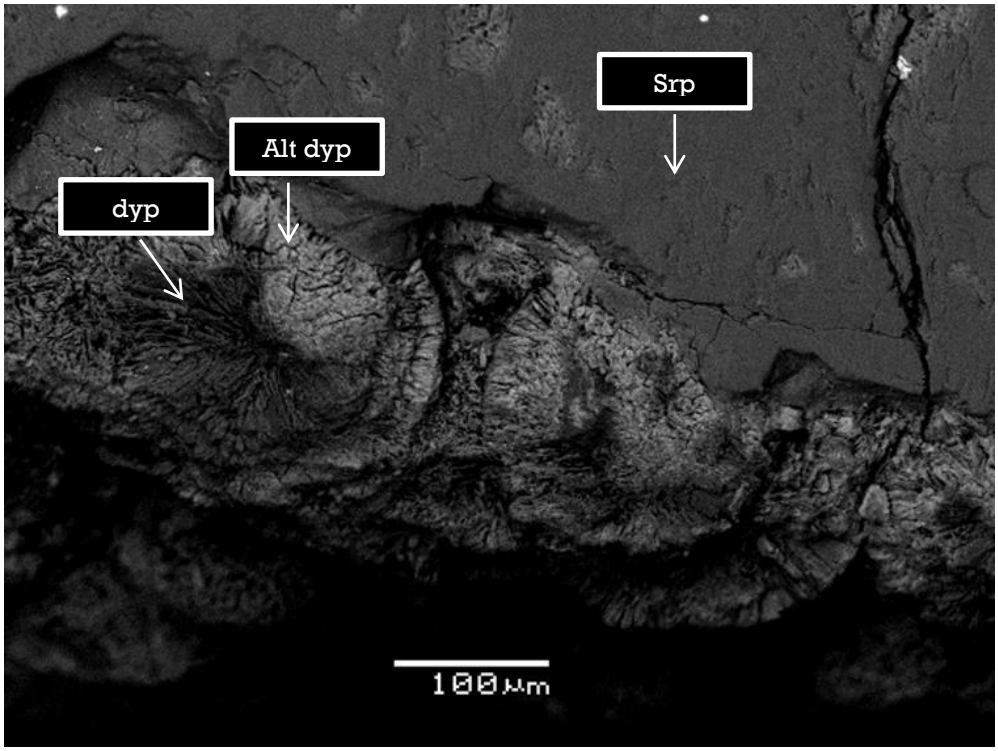


**Figure 5.9: Close up BSE image of Area F, showing spherulites or rose like structures.**

The figure 5.9 is showing Area F lies at the bottom of the sample shown by the rose like spherulites in the area. The dark color of outside these spherulites is may be due to the topographic effect.

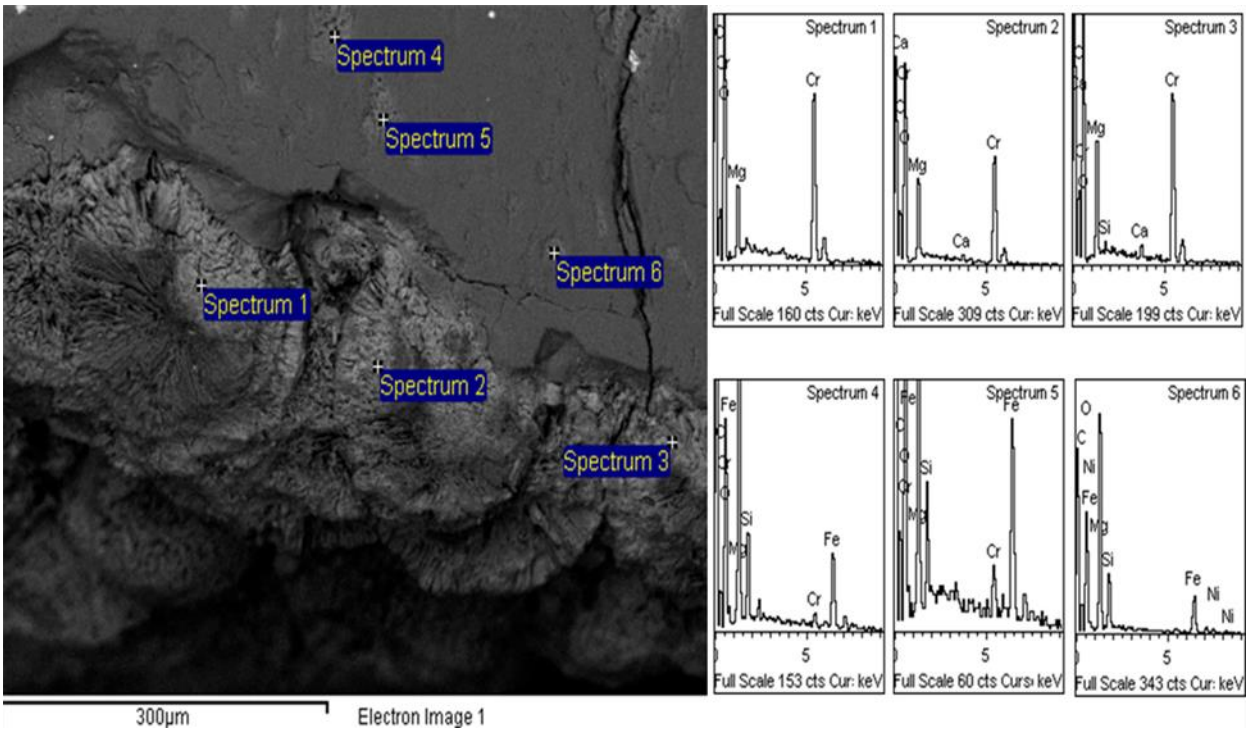


**Figure 5.10: BSE image of Area f with EDS spectra displayed next to it.**

The BSE image shows the location of the spectra, which are displayed next to it (figure 5.10). Spectra 1, 2 and 3 are taken from the brighter parts of the spherulites or rose like structures showing high concentration of Cr with changing concentrations of Mg, O, C and Ca. Spectrum 4 and 5 are taken from the slightly less brighter spots shows Mg, Si, Fe, O and a bit of Cr which is most likely to be altered serpentine. Spectrum 6 is also from slightly brighter spot showing peaks of Mg, Si, O, Fe and little bit of Ni that is most likely to be altered serpentine.

## 5.1.2 Reaction of $Cr(NO3)_3$ with Fer_312 B

The scanned image of the areas chosen for detailed investigation by SEM is shown in appendix 1. The sample was not carbon coated to see the effect of reaction between a carbon coated and uncoated sample after experiment.

**Area A**

Close up BSE image of the Area A is shown by figure given below. The Area was also chosen for the element mapping by SEM.

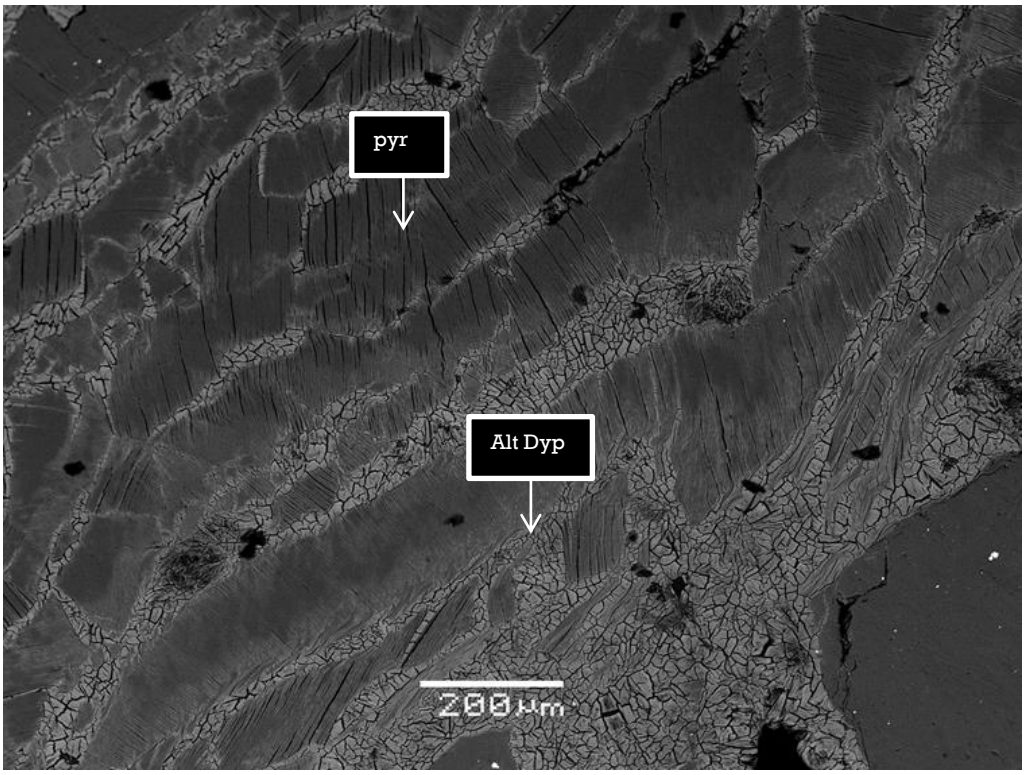


**Figure 5.11: Close up image of Area A showing the lamellae formed in the vein during the experiment.**

The close up BSE image of Area A is showing the change in the area during the experiment (figure 5.11). It could be observed that the lamellae have formed in the area in the vein during the experiment that was characterized with dypingite before experiment. However, pyroaurite did not take part in the reaction and remained completely unaltered during the experiment.

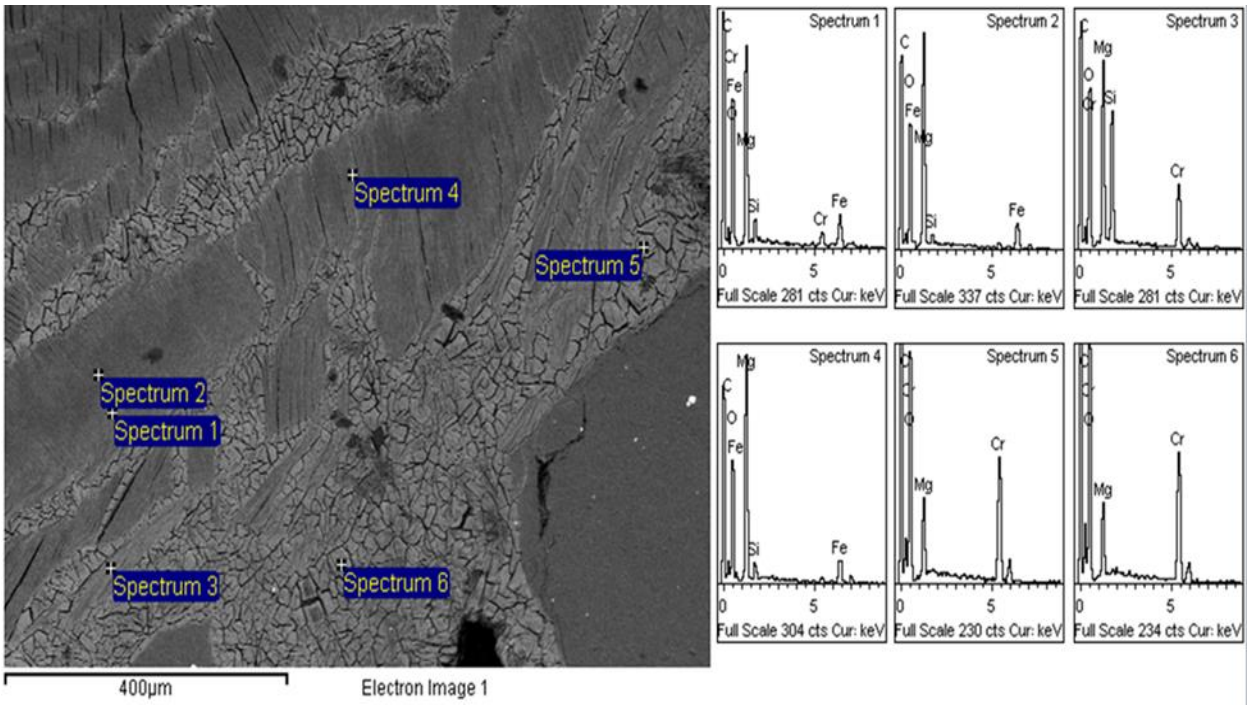


**Figure 5.12: BSE close up image of area A with EDS spectra displayed next to it.**

The close up BSE image of Area A with EDS spectra shown next to it (figure 5.12). Spectrum 1 is showing a pyroaurite like spectra with small additional peaks of Cr and Si. Spectrum 2 is similar to spectrum 1 but Cr and Si peaks are smaller. Spectrum 3 is showing Mg, O with a high peaks of Si and Cr which also seems to be altered serpentine. Spectrum 4 is showing peaks of Mg, Fe, and bit of silica that is most likely to altered pyroaurite. Spectrum 5 and 6 taken from the cleavage that are showing a high concentration of Mg, O and Cr which is most likely to altered dypingite.

**Area B**

Close up BSE images of Area B before and after the experiment is shown below.

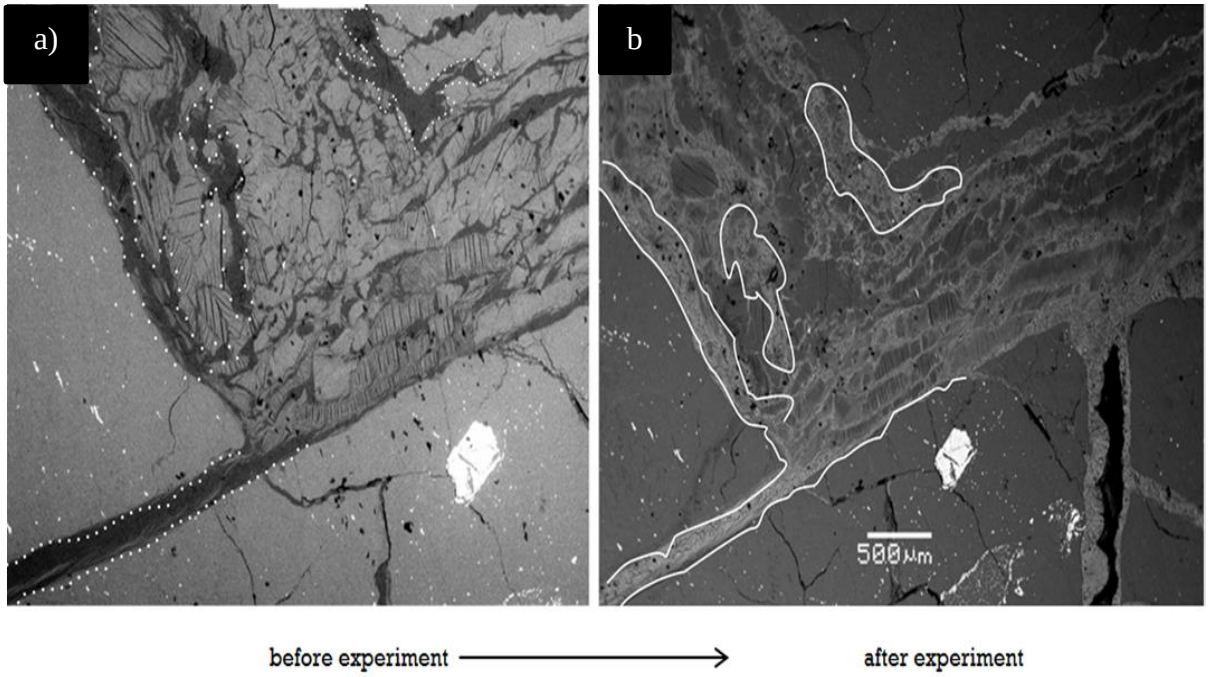


**Figure 5.13: Successive BSE images of the Area B in Chip Fer_312 B: (a) before experiment .b) after experiment.**

The prominent changes can be seen from the successive BSE images (figure 5.13). It can be observed that the darker areas which were identified as mineral dypingite before the experiment have been completely altered after the experiment. However, the areas with mineral pyroaurite and serpentine were preserved during the experiment.

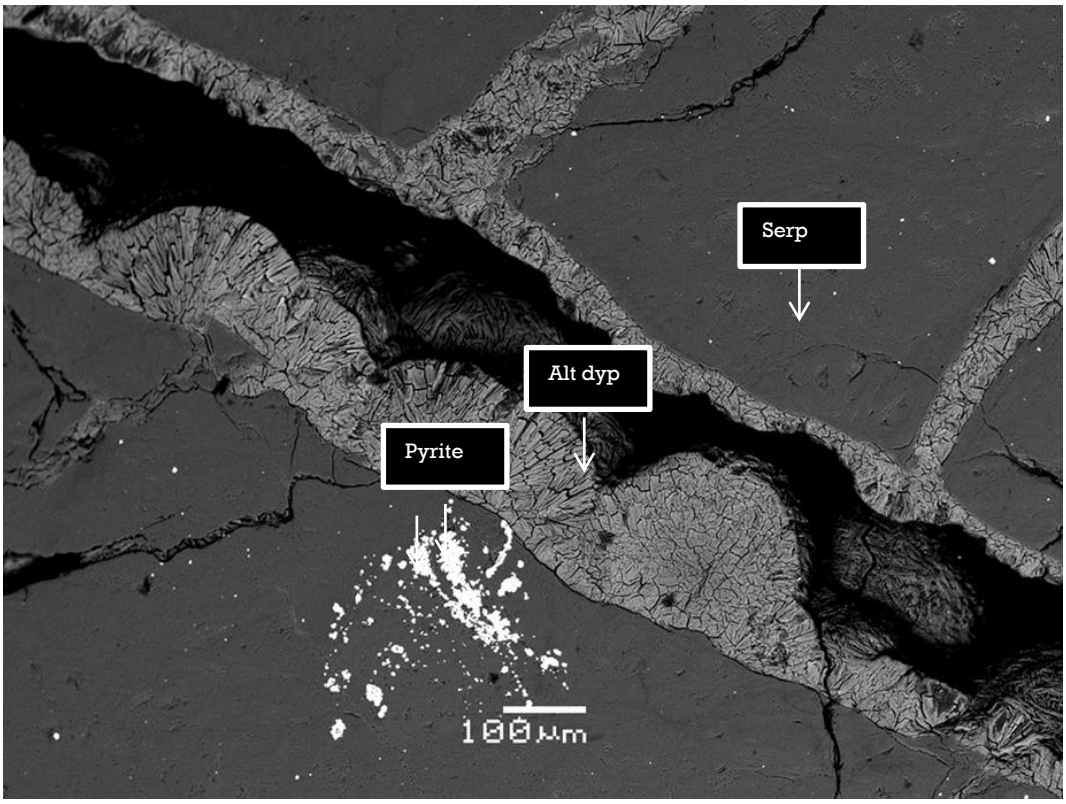


**Figure 5.14: Close up BSE image of a small vein in Area B.**

The close up BSE image of the Area B is showing a small vein which is dominated with rose like spherulites.. These rose like spherulites were having charac as mineral dypingite before the experiment. It could be observed that the parts in the vein with mineral dypingite are heavily fractured which is most likely due to their alteration during the experiment. The white part in the area depicts the presence of mineral pyrite ($FeS_2$) (figure 5.14).

### 5.1.3 Reaction of Fer_412A with Lead Nitrate$(PbNO_3)_2$

The scanned image of the area that was chosen for detailed investigation by SEM is shown in appendix1.

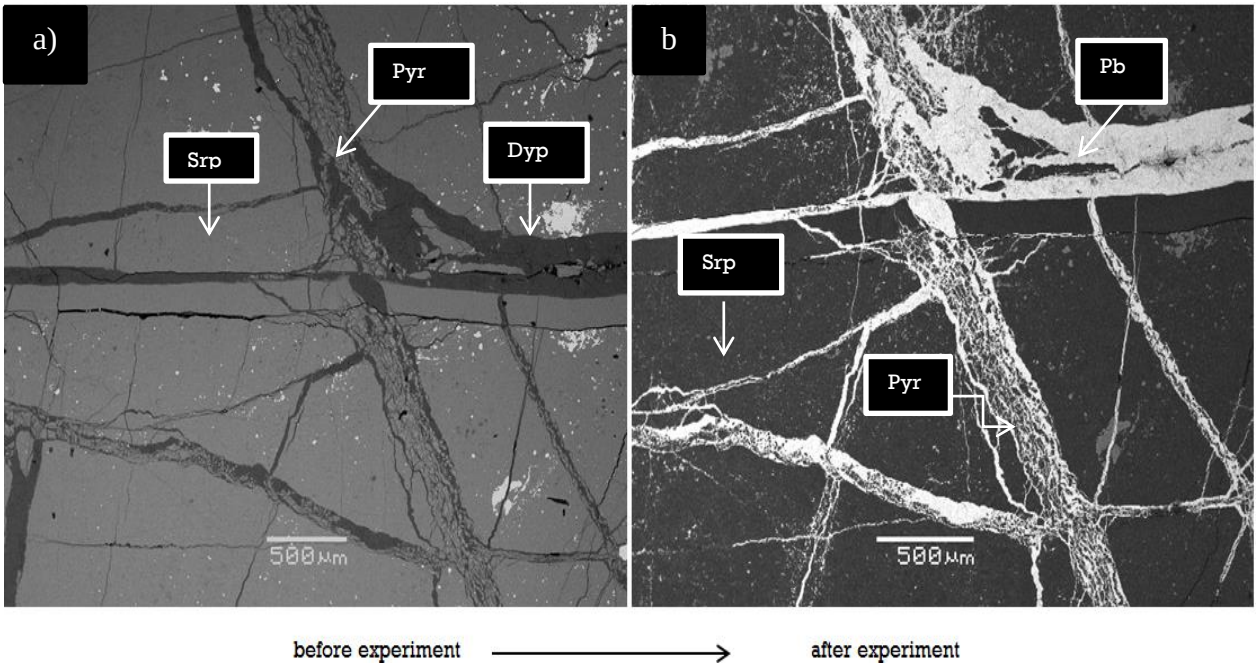


**Figure 5.15: Successive BSE Images of the Area A in chip Fer_412A: (a) before Experiment (b) after experiment**

It can be observed from figure 5.15 that the areas in the veins those were covered by dypingite before the experiment were more or less completely displaced by Pb during the experiment. However, pyroaurite and serpentine did not take part in reaction and were preserved during the experiment.

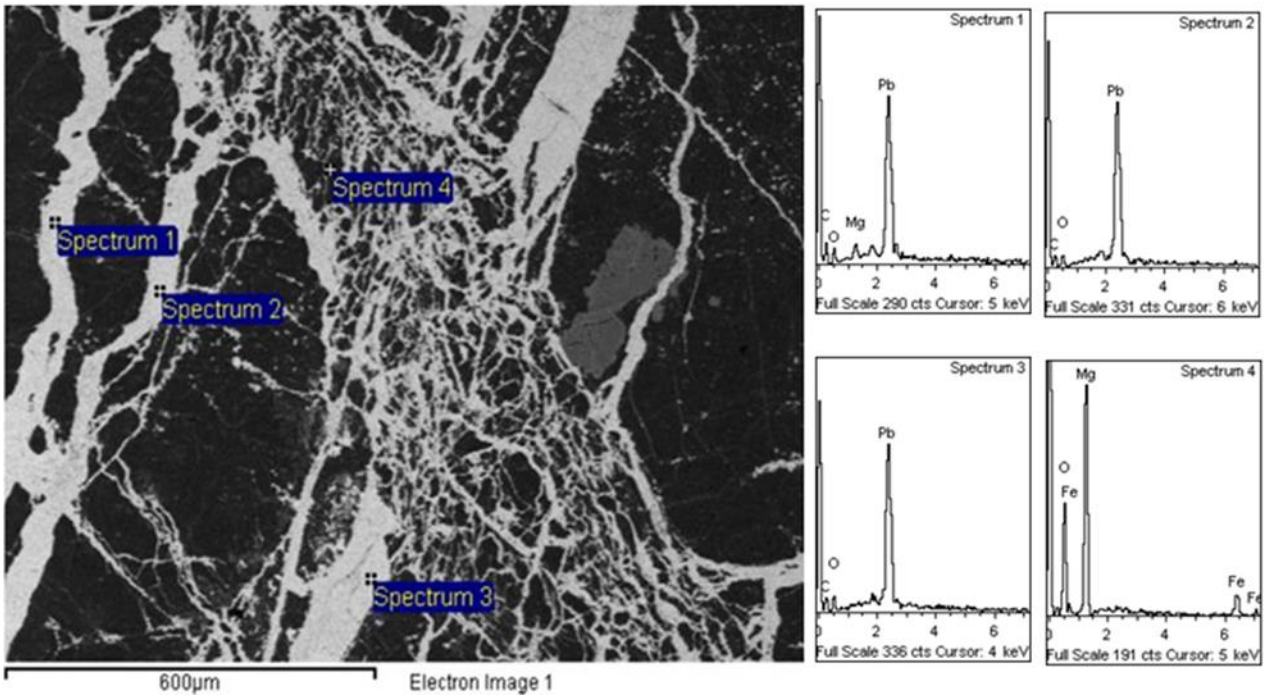


**Figure 5.16: Close up BSE image of Area A with EDS spectra displayed next to it.**

The close up BSE image of Area A with EDS spectra located next to it (figure 5.16). Spectra 1, 2 and 3 are showing good peaks of Pb in the vein with small peaks of C, Mg and O. The small peak of Mg in spectrum is most likely to be from the surroundings. The higher concentration of Pb in these areas is most likely showing the strong precipitation of Pb in these areas. Spectrum 4 is taken from the slightly darker parts in the vein, showing good peaks of Mg, Fe, C and O which shows that pyroaurite was completely preserved during the experiment

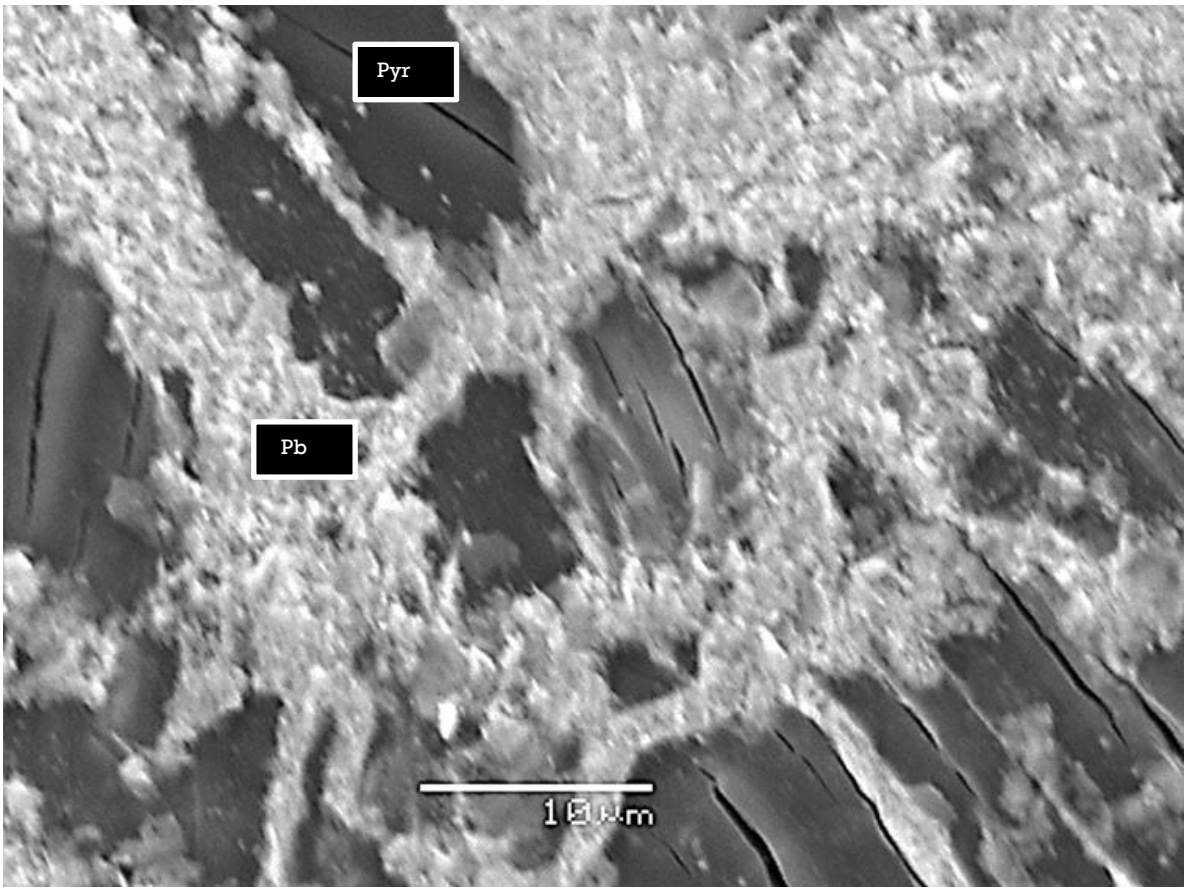


**Figure 5.17: Close up BSE image of an area located at Area A.**

The figure 5.17 is the close up BSE image of Area A, which is showing the altered parts along the fresh parts inside the vein. The fresh parts are representing the grains of mineral pyroaurite which were preserved during the experiment while altered parts are covered by the crystals of Pb precipitated on the areas which were covered by mineral dypingite before the experiment. The precipitation of Pb on dypingite on the surface of dypingite is most likely forming a new phase named as cerrusite ($PbCO_3$).

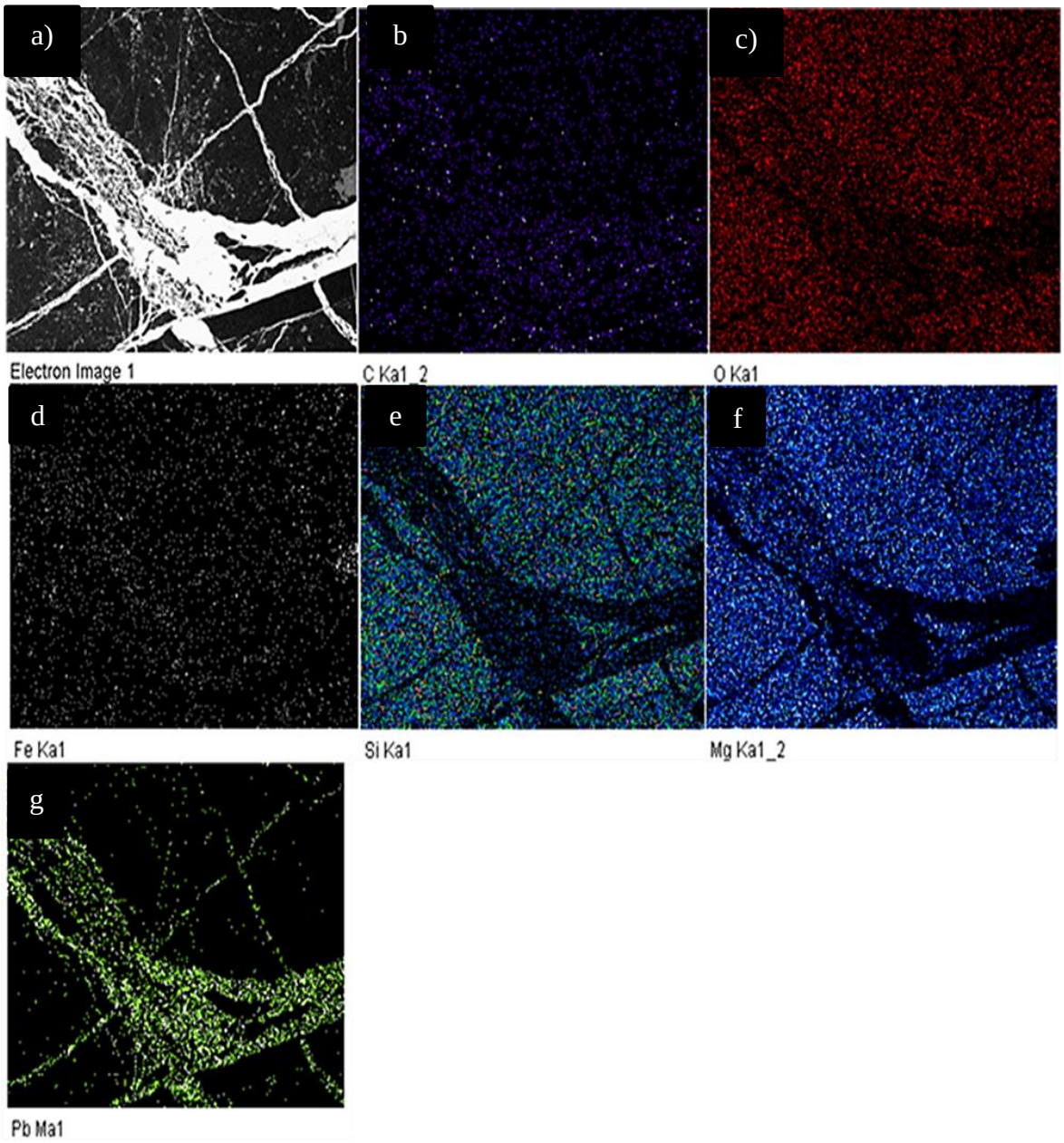


**Figure 5.18: Element maps of Area A. a) BSE image of the mapped area. b) Map of carbon. c) Map of oxygen. d) Map of iron. e) Map of silica. f) Map of magnesium. g) Map of lead.**

The figure 5.18 is showing the element maps of the area A. Image 5.18a is showing the area which was chosen for the element mapping. The concentration of carbon in image 5.18b shows relatively higher amount of carbon inside the vein in comparison with other parts in the area. The concentration of oxygen in image 5.18c is slightly lower inside the vein. The concentration of iron in image 5.18d is random in the vein which shows no difference. The concentration of Si in image 5.18e is higher in the areas with serpentine. The concentration of magnesium in image 5.18f is more or less nil in veins. The concentration of lead in image

5.18g is higher in the areas in the vein that were characterized as mineral dypingite before the experiment. It could be observed from element maps of Area A that the reaction between Pb and dypingite was very strong.

### 5.1.4 Reaction of Fer_412B with Cadmium chloride ($CdCl_2$)

The scanned image of the area that was chosen for detailed investigation by SEM is shown in appendix1.

**Area A**

Close up of area A is shown below in figure 5.20. The area was also chosen for elemental mapping.

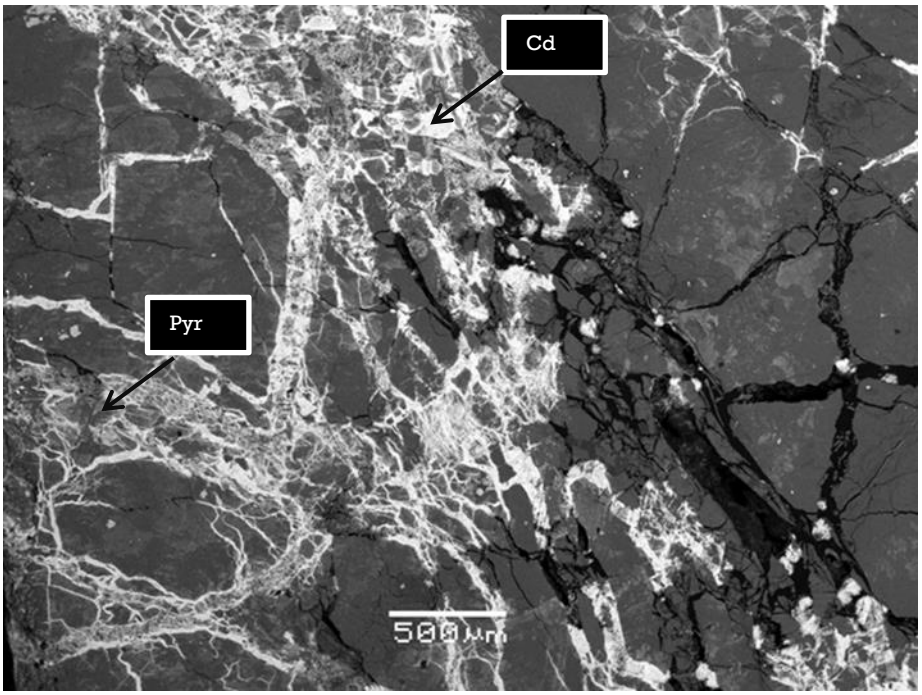


**Figure 5.19: Close up BSE image of area A.**

The close up BSE image shows the strong precipitation of Cd in areas which are surrounding the pyroaurite. These areas were characterized as mineral dypingite before the experiment (figure 5.19).

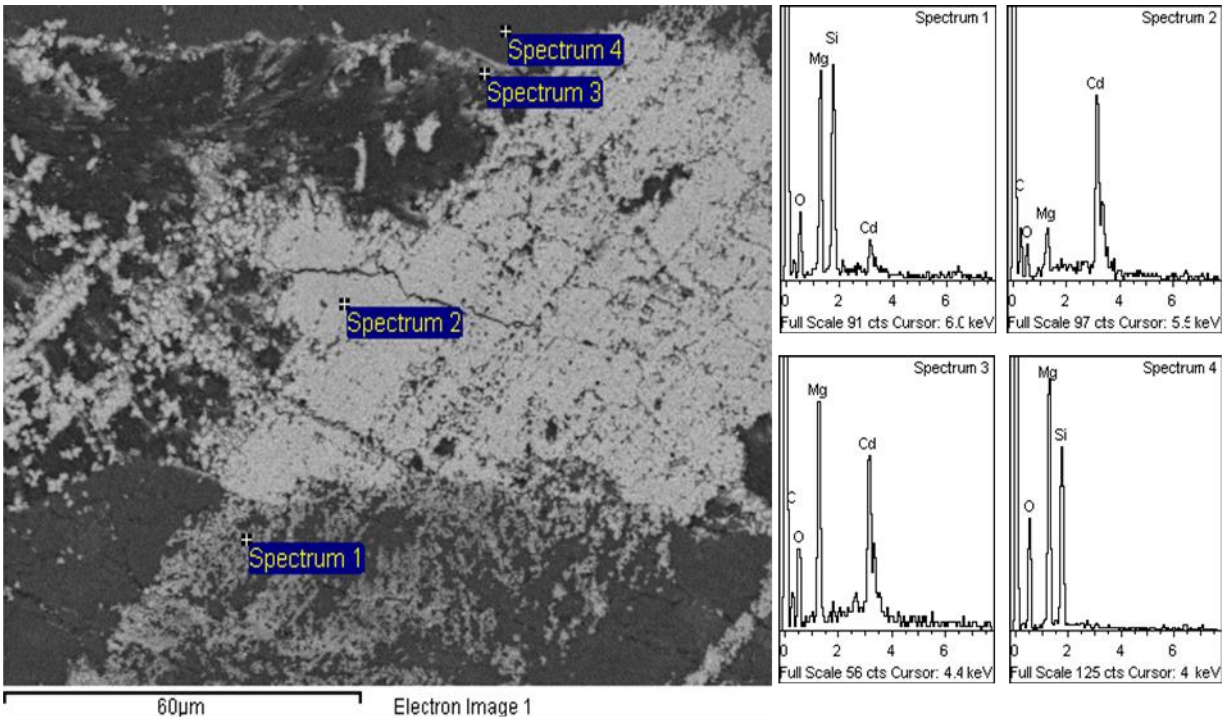


**Figure 5.20: BSE close up image of an area which is located at Area A with EDS spectra displayed next to it.**

The close up BSE image of Area A with EDS spectra located next to it (figure 5.20). Spectra 1 and 4 are showing good concentration of Mg, O and Si which is most serpentine outside the vein. The small peak of Cd in spectrum 1 is most likely from the surroundings effect. Spectrum 2 is showing good concentration of Cd with small concentrations of Mg which is most likely due to precipitation of Cd on dypingite. Spectrum 3 is showing good peak of Mg and Cd with slightly lower concentration of O which could due to the precipitation of a new phase otavite ($CdCO_3$) on dypingite.

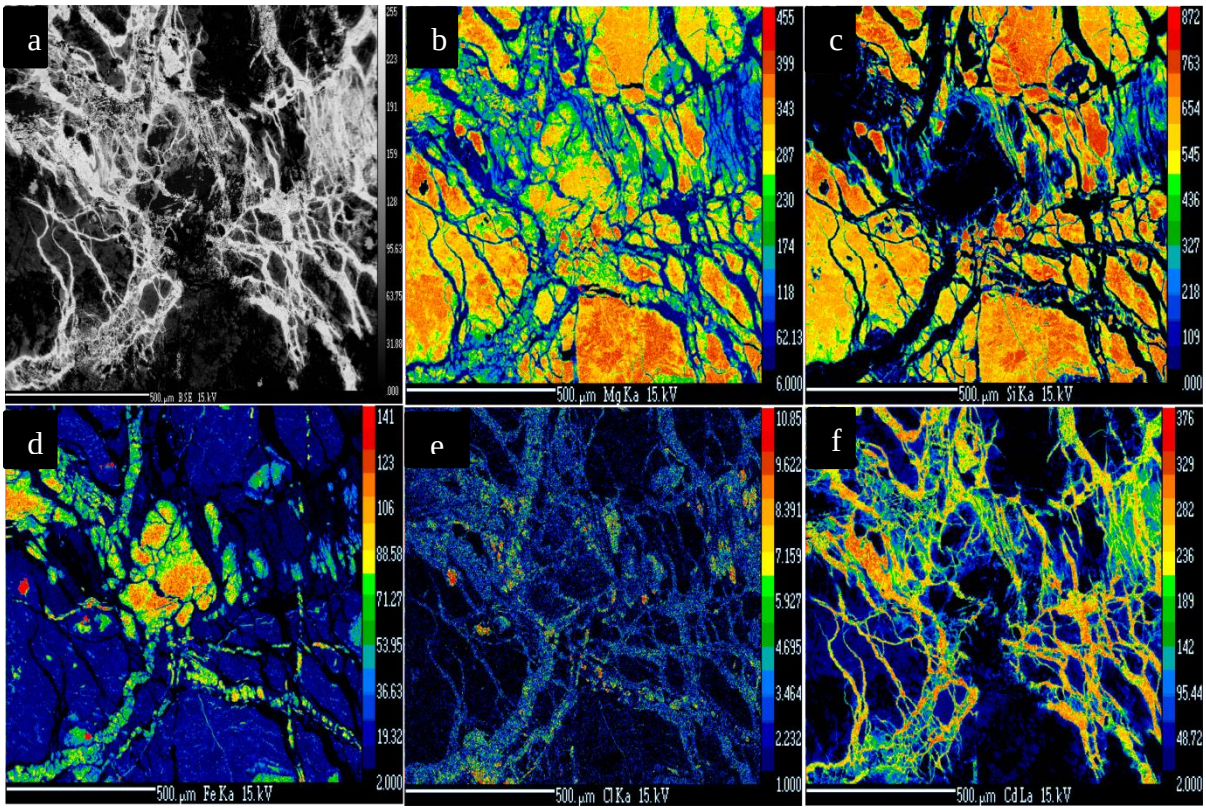


**Figure 5.21: Element maps of Area A by EMP. a) BSE image of the mapped area. b) Map of magnesium. c) Map of silica. d) Map of iron. e) Map of chloride. f) Map of cadmium.**

The figure 5.21 is showing the element maps of the Area A. Image 5.21a is showing the area which was chosen for elemental mapping. The concentration of magnesium and Silica can be seen in Image 5.21a and b, shows higher concentration of Mg and Si outside the fractures which is serpentine. It can be observed that there was no effect on serpentine during the experiment. The concentration of iron in image 5.21d is higher in the middle and the veins which depicts the presence of mineral pyroaurite. The concentration of chloride in image 5.21e shows reasonable amount of $Cl^-$ on the surface of mineral pyroaurite. It could be observed that there was no effect of $Cl^-$on the concentration of Fe and Mg, which indicates that the presence of $Cl^-$on the pyroaurite is most likely due to the anion exchange between $Cl^-$ and $CO_3^-$. The concentration of magnesium which can be seen in image 5.21f shows that the Cd is showing affinity to the areas in the fractures where we find a bit of magnesium which is most likely indicating the precipitation of otavite on the surface of mineral dypingite during the experiment.

### 5.1.5 Reaction of Fer_312 D with Copper sulphate ($CuSO_4$)

The scanned image of the area that was chosen for detailed investigation by SEM and EMP is shown in appendix 1. BSE close up images of area A before and after the experiment are shown below in figure 5.22.

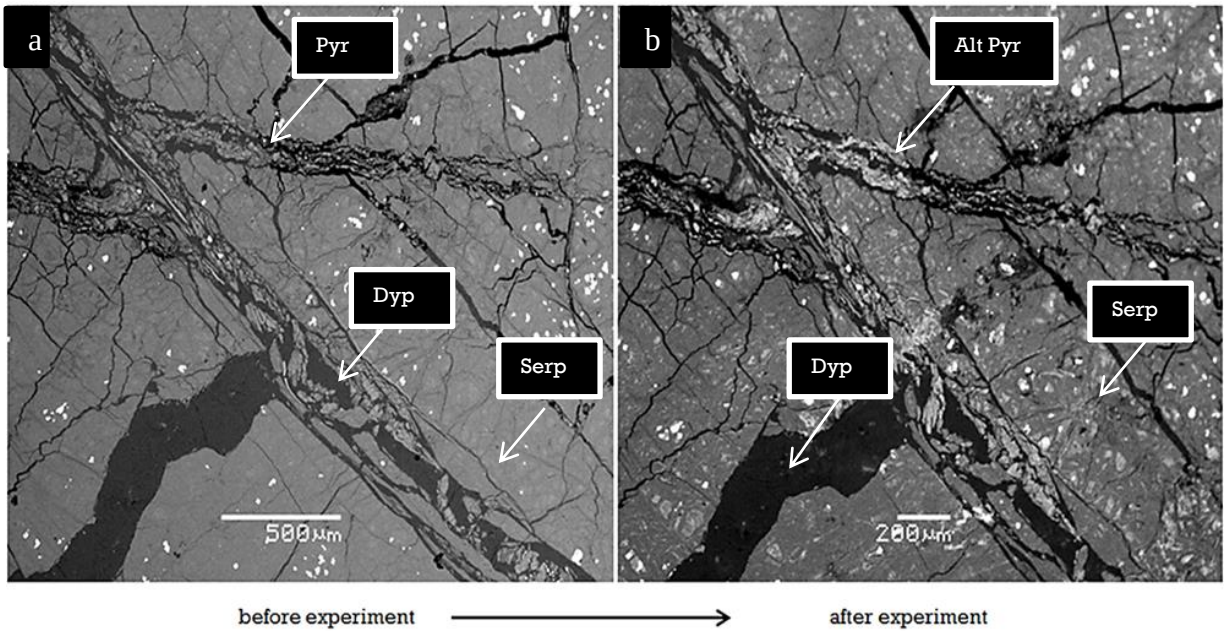


**Figure 5.22: Successive BSE Images of the Area A in chip Fer_312D: (a) before Experiment (b) after experiment**

It can be observed from the above image that there was not much change during the experiment and most of the parts were preserved during the experiment except some areas in the veins with mineral pyroaurite that reacted with Cu. However, the reaction in this case was not too strong.

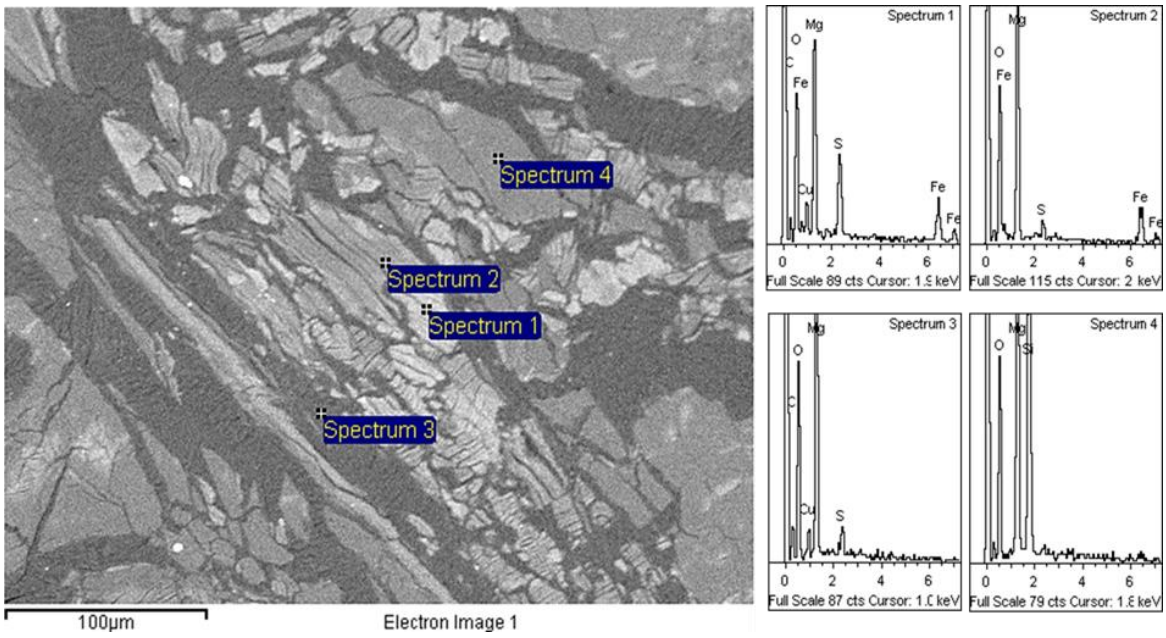


**Figure5.23: BSE close up image of an area located at Area A with EDS spectra displayed next to it.**

The close up BSE image of Area A with EDS spectra located next to it (figure 5.23). Spectrum 1 is showing good peaks of Mg, O, Fe, C with small peaks of Cu and S which most likely indicate the altered part of mineral pyroaurite. Spectrum 2 is showing good peaks of Mg, Fe and O with little peak of S which shows unaltered part of mineral pyroaurite. The small peak of S is from the altered part of mineral pyroaurite. Spectrum 3 is showing good peaks of Mg, O and C with small peaks of Cu and S which is showing that mineral dypingite is not showing affinity to Cu in this case. Spectrum 4 is showing good peaks of Mg, Si and O which is most likely to be serpentine.

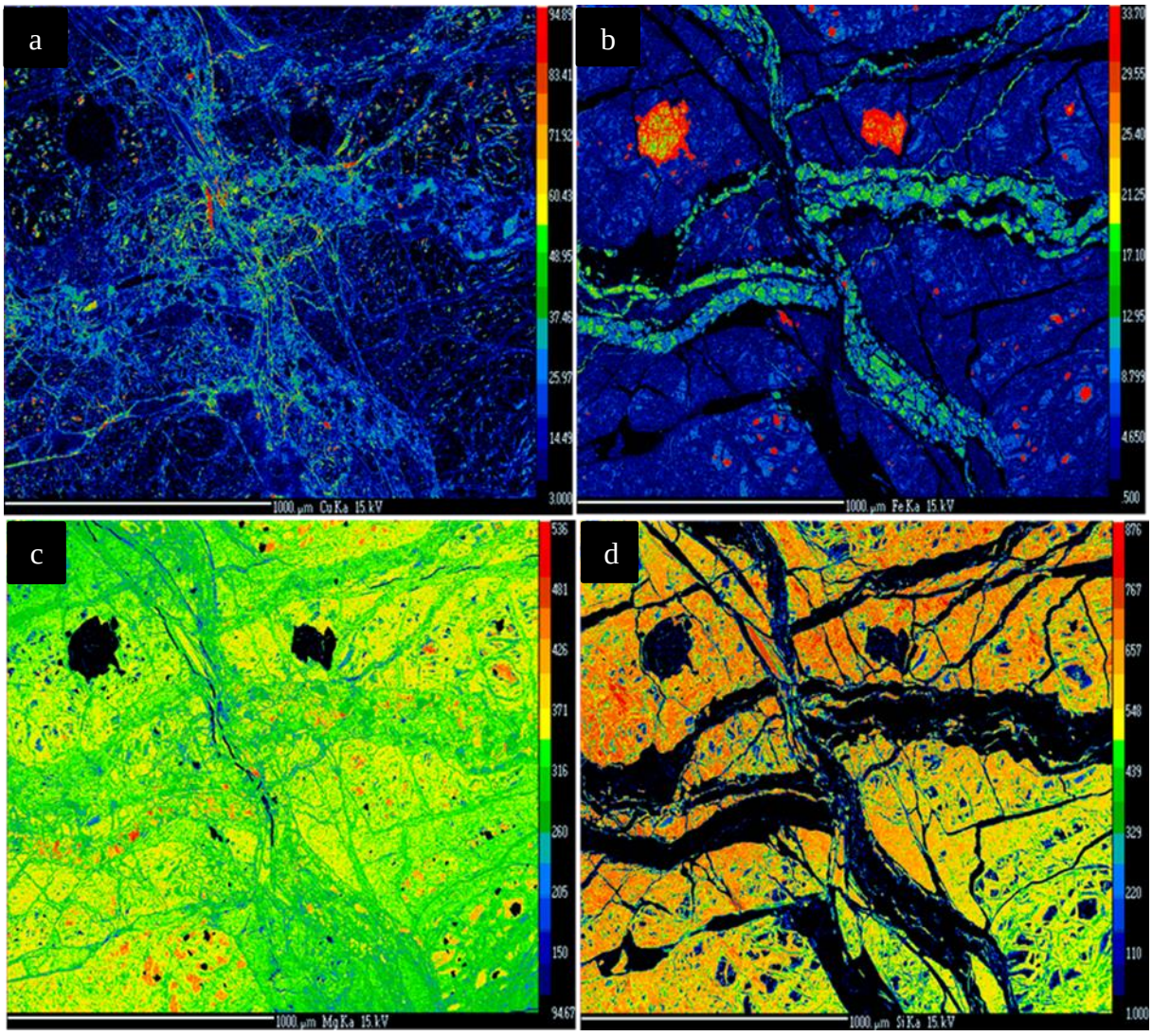


**Figure 5.24: Element maps of the Area A by EMP. a) Map of copper. b) Map of iron. c) Map of magnesium. d) Map of silica.**

The figure 5.24 is showing the element maps of Area A after the experiment. The concentration of Cu in image 5.24a shows considerable amount which is sitting on mineral pyroaurite in the area. The concentration of Fe which can be seen from image 5.24b shows that Fe is mostly present in the areas of the veins where we find mineral pyroaurite. It could be observed from the maps of Fe and Cu that the areas in the veins where we have higher concentration of Cu devoid of Fe. The concentration of Mg which can be seen from image 5.24c shows the considerable amount of Mg in the veins. The concentration of Si which can be seen from image 5.24d shows that Si is mostly outside the vein in the areas where we find mineral serpentine.

### 5.1.6 Reaction of Fer_312C with NaCl

The scanned image of the area chosen for detailed investigation by SEM is shown in appendix 1. The experiment of Fer_312C was performed by following the results from NaCl column experiment. Close up of area A is shown as below.

**Area A**

Close up images of Area A before and after the experiment are shown by the figure below

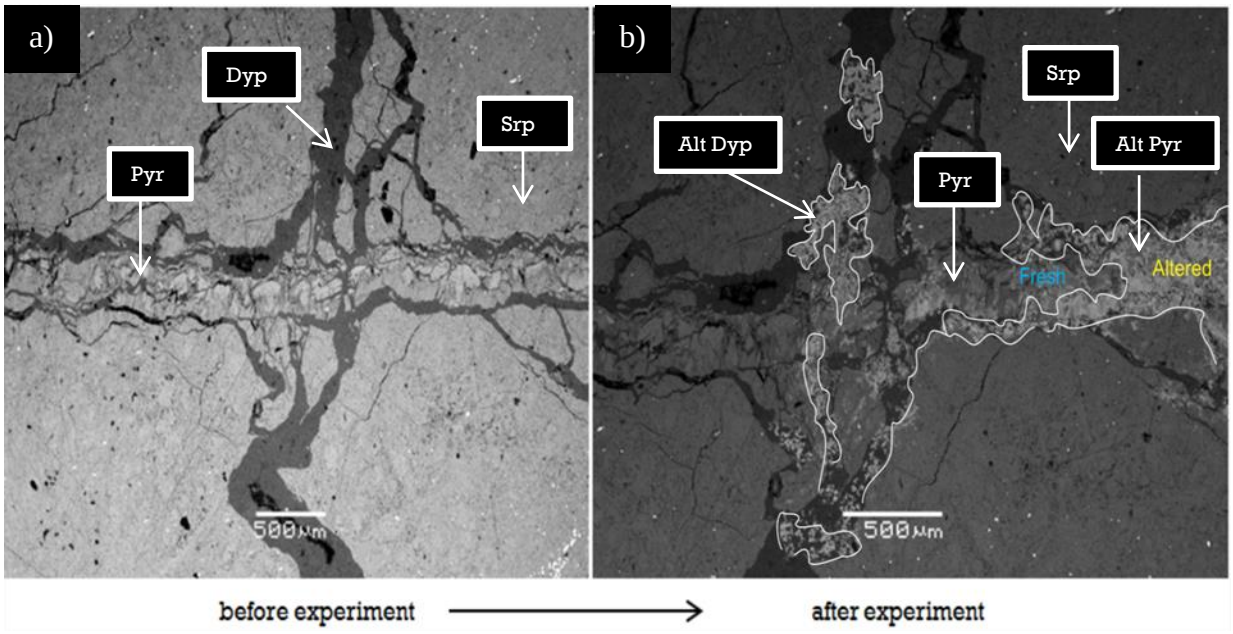


**Figure 5.25: Successive BSE Images of the Area A in chip Fer_312D: (a) before Experiment (b) after experiment**

The figure 5.25 shows that the vein with mostly dypingite cutting the vein with mostly pyroaurite from the middle. It can be observed that the vein was the most reactive part in the area and the surroundings with mostly serpentine has preserved itself during the experiment. It could be also observed that the NaCl was more reactive with the parts which were mostly comprised of mineral pyroaurite rather than dypingite which may be the result of anion exchange.

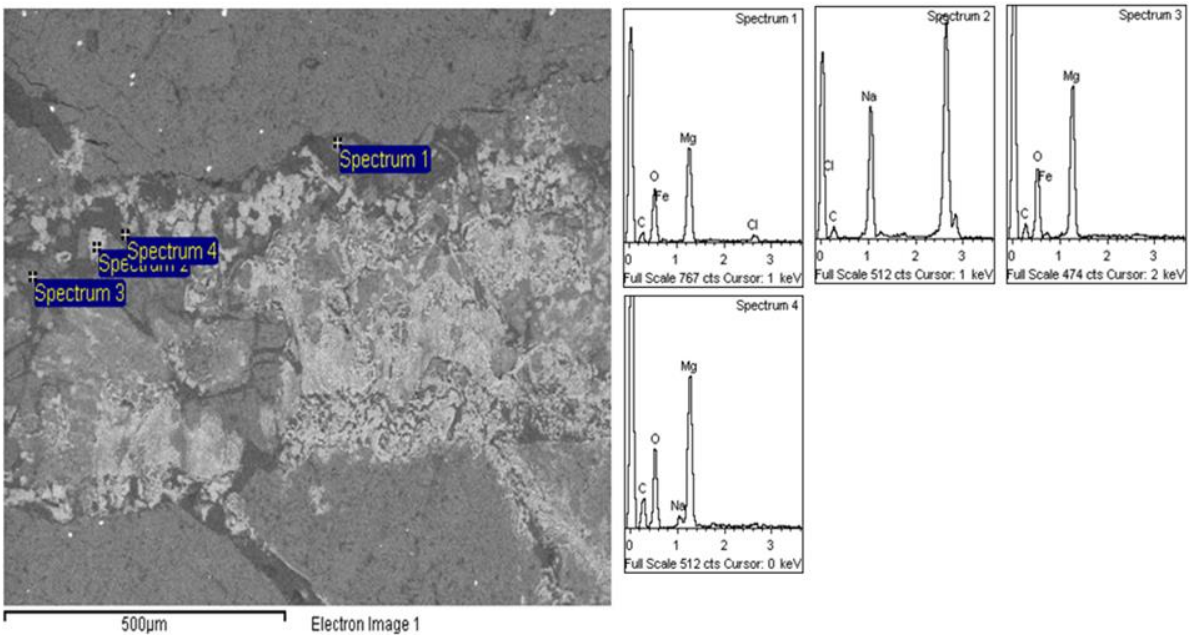


**Figure 5.26: Close up BSE image of an area located at Area A with EDS spectra displayed next to it.**

Spectrum 1 is showing peaks of Mg, O and Fe with a bit of Cl which is most likely to be altered pyroaurite. Spectrum 2 is indicating good concentrations of Na and Cl with a bit of C which is most likely to be pure crystal of NaCl. Spectrum 3 is showing peaks of Mg, Fe, O and C depicts pyroaurite which which was preserved during the experiment. Spectrum 4 is showing peaks of Mg, O and C with a bit of Na which is most likely to be altered dypingite.

**Mapping of the Area after experiment:**

Element maps of Area A are shown below in figure 5.28.

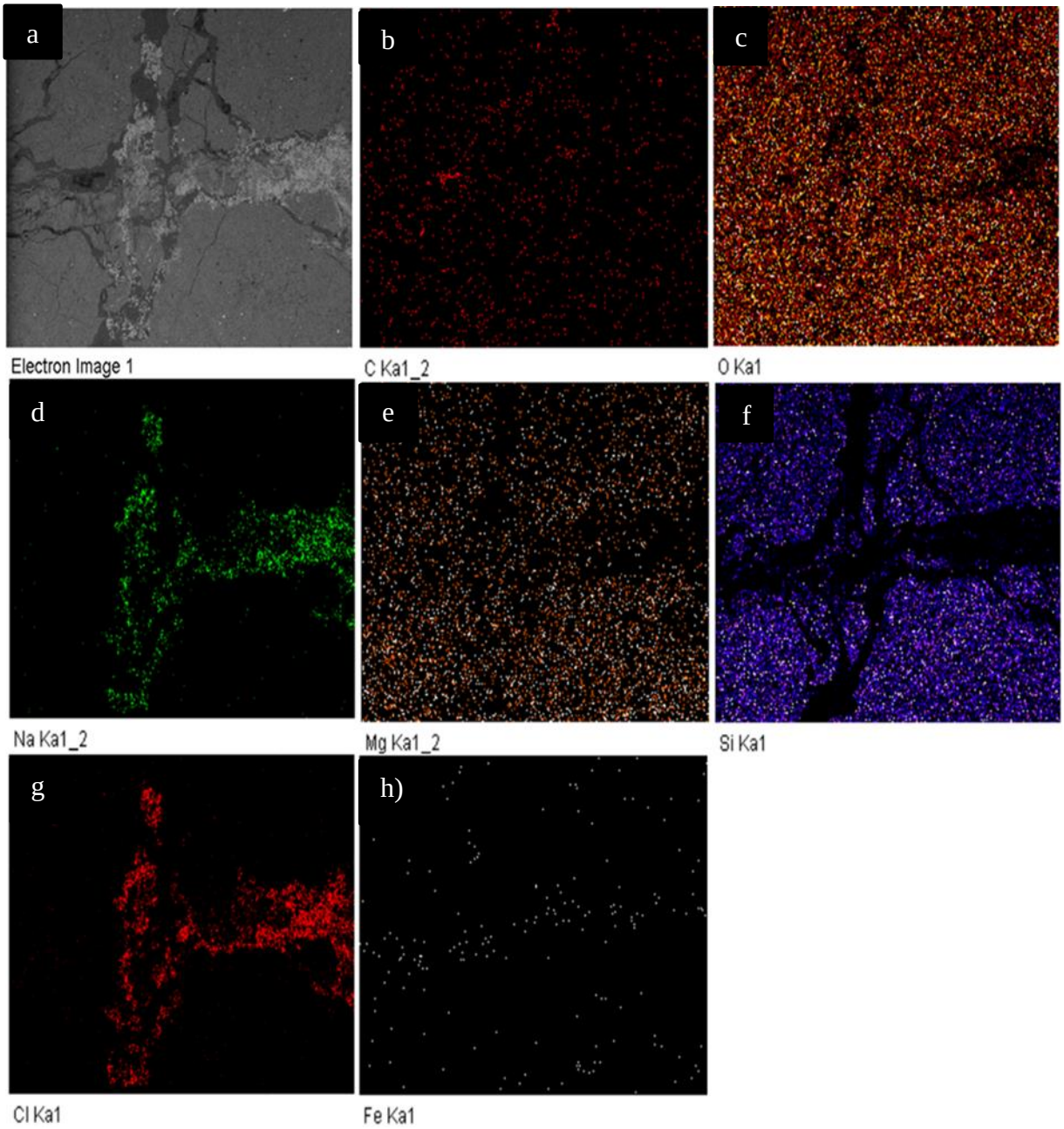


**Figure 5.27: Element maps of Area A after the experiment. Iron a) BSE image of the mapped area. b) Map of carbon. c) Map of oxygen. d) Map of sodium. e) Map of magnesium. f) Map of silica. g) Map of chloride. h) Map of iron.**

The figure 5.27 is showing the element maps of Area A after the experiment. Image 5.27a is showing the area which was chosen for the elemental mapping. The concentration of oxygen in image 5.27b is randomly distributed in the area and doesn't show a clear change in the area. However the concentration of oxygen in image 5.28b is slightly lower in the areas with

pyroaurite which are now covered by $Cl^-$ and Na (see also image 5.27d and g). This lower concentration of O implies that Cl is most likely replacing $CO_3^{2-}$ from the structure of mineral pyroaurite. The concentration of magesium, which can be seen from image 5.27e, shows the depletion of Mg from the areas situated in vein which were before characterized with pyroaurite and dypingite. The concentration of Si in image 5.27f shows that the serpentine was preserved during the reaction. The concentration of Fe, which can be seen from image 5.27h, shows that there has been decrease in the concentration of Fe in the vein which is most likely due to the anion exchange of pyroaurite.

### 5.1.7 XRD characterization of the reacted chip material

The reacted material from the $Cr(NO_3)_3$ solution experiment with Fer_312A was scratched off carefully to observe if any new possible phases have formed. It was observed that stichtite ($Mg_6Cr_2(OH)_{16}(CO_3)•4(H_2O)$) was formed during the reaction (figure 5.28). However this change in the phase is uncertain as stichtite may have been present before the experiment as stichtite is a common mineral in weathered dunites (Baidya, 1996).

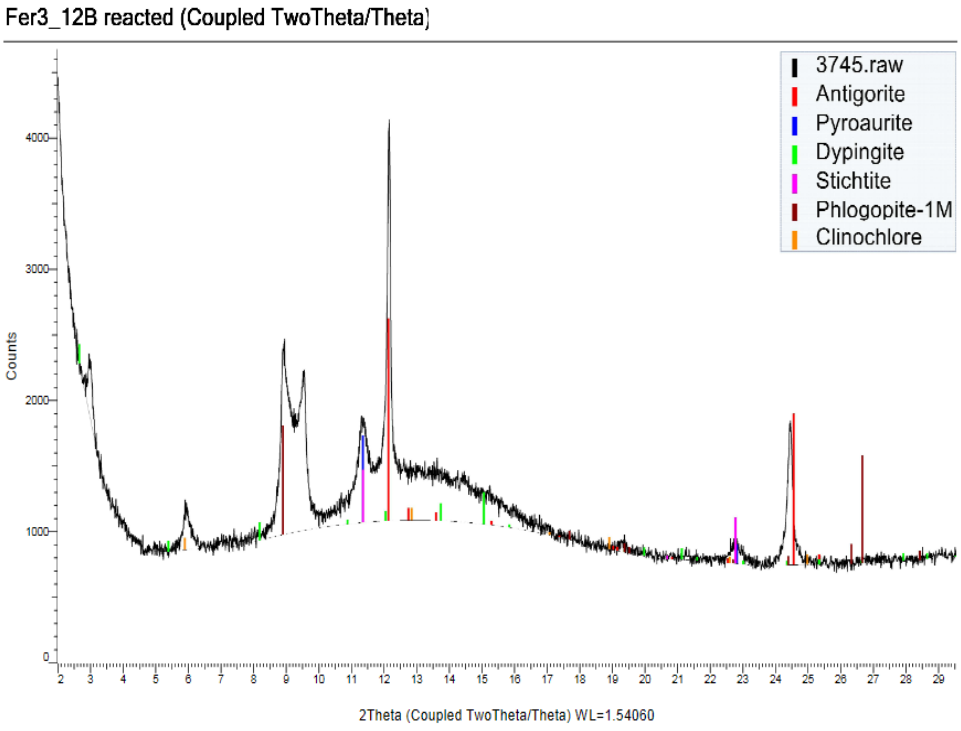


**Figure 5.28: XRD pattern of the reacted material from the veins in the sample Fer_312A.**

## 5.2 Column Experiments

### 5.2.1 Loading of Column with $CdCl_2$+NaCl Solution

The initial concentration of $Cl^-$ and Cd was 3mmol/l and 1mmol/l respectively. The outflow concentration of $Cl^-$ was below 0.1 mmol during the whole experiment and did not behave as a conservative tracer. The reason for this is the anion exchange between $Cl^-$ and $CO_3^{2-}$ in the pyroaurite (see section 6). Initially, concentration of Cd was zero until the first pore volume head past the column. Then it reached to more than 10 times of the initial concentration. At 1.3 pore volume there was sudden decrease in the concentration of Cd and it reached to zero again (figure 5.29). The possibilities that relate to this sudden increase in the concentration of Cd are elucidated thoroughly in general discussion (see section 6). The tabulated results can be found in appendix 2.1.

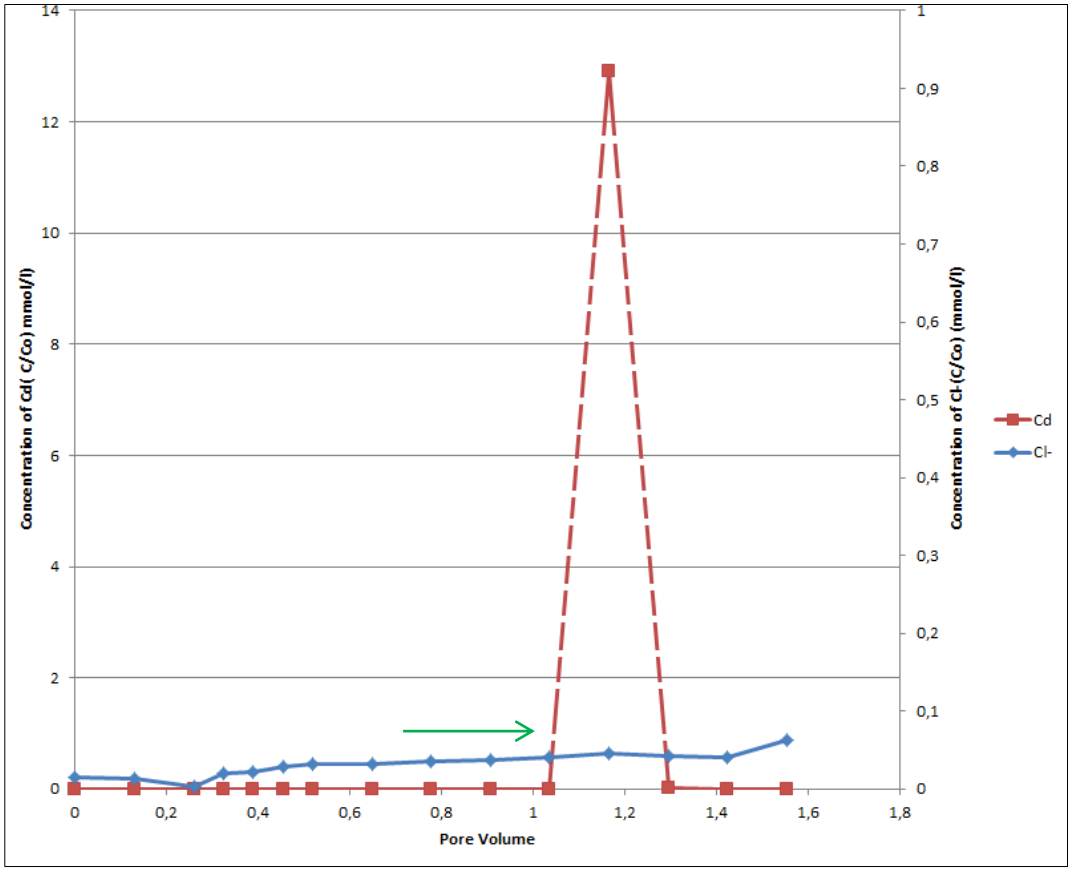


**Figure 5.29: Concentration of Cd and against pore volume. The green arrow in the plot is pointing out the concentration of Cd in the inlet solution.**

## 5.2.2 Loading of column with NaCl solution

The column was then treated with ultrahigh pure deionized water for 48 hours prior to the loading of column with NaCl solution. The concentration of $Cl^-$ in the inlet solution was 1 mole but figure 5.31 depicts its concentration as mmol. The concentration of $Cl^-$ before 1 pore volume shows the presence of $Cl^-$ even after running ultra-high pure deionized water through it which indicates release of $Cl^-$ from the structures of the minerals present in the column or from some remaining pore fluid from the former experiment. At the end of the experiment after 3.7 pore volumes $Cl^-$ couldn't reach to its inlet concentration which demonstrates the large $Cl^-$ scavenging of the column material (figure 5.30). The tabulated results can be found in Appendix 2.2.

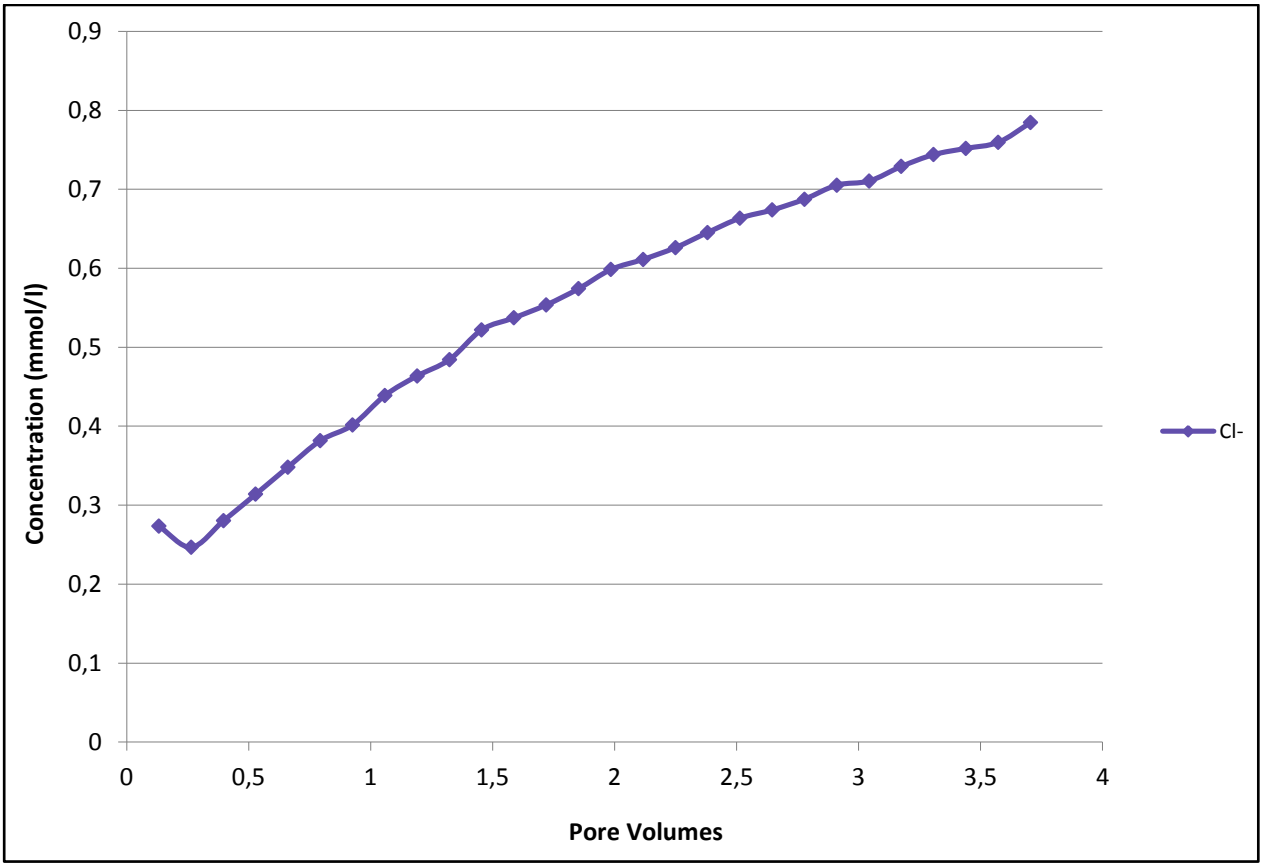


**Figure5.30: The change in concentration of $Cl^-$ in the column with respect to pore volume.**

### 5.2.3 XRD characterization of the reacted material from Column

The XRD analysis of the reacted column material showed no change in the final material (figure 5.31). The reason behind the small peaks of dypingite in the XRD patterns is that the structure of mineral dypingite has not been well defined yet.

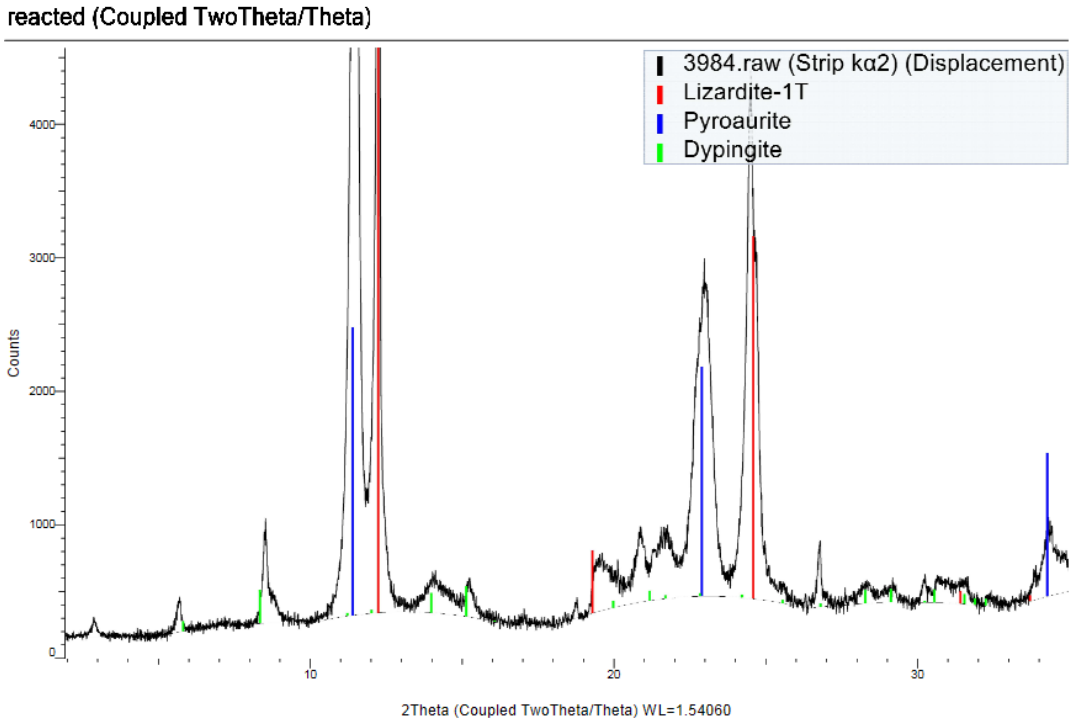


**Figure 5.31: XRD patterns of the reacted column material.**

### 5.2.4 Characterization of the reacted column material by SEM

The samples from the column material were chosen for SE imaging, BSE imaging and element mapping. The images of mineral pyroaurite and dypingite are shown below in figure 5.32.

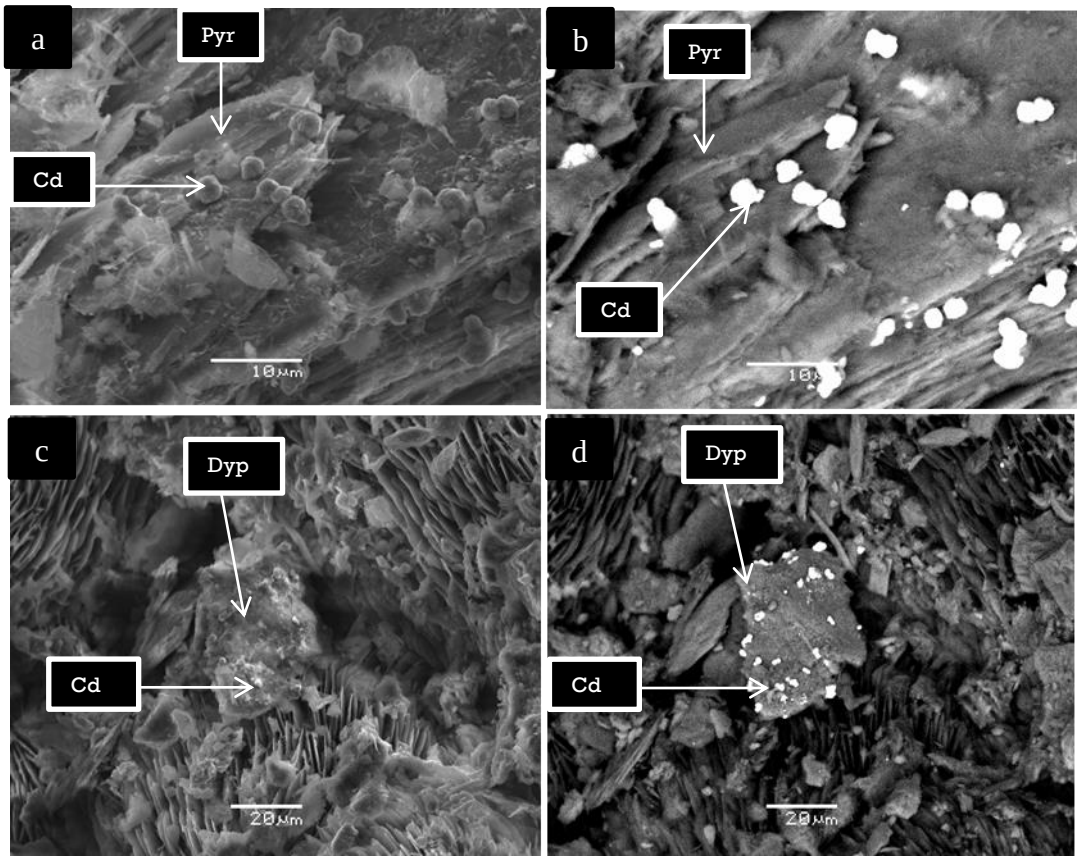


**Figure 5.32: SE and BSE images pyroaurite and dypingite. a). SE image of pyroaurite b) BSE image of pyrourite c)SE image of mineral dypingite d) BSE image of mineral dypingite.**

The figure 5.32 is showing SE and BSE images of the same areas in two different samples from the reacted column material. The spheres sitting on the mineral pyroaurite grain in SE image 5.32a can be seen as bright spots in BSE image 5.32b. These bright spots refer refer to Cd ions on the surface of pyroaurite. This area was also chosen for elemental mapping (see figure 5.33). The figure 5.23c and 5.23d are the SE and BSE images of the same areas in the sample, showing Cd ions sitting on mineral dypingite. The Cd seems to associate both with pyroaurite and dypingite.

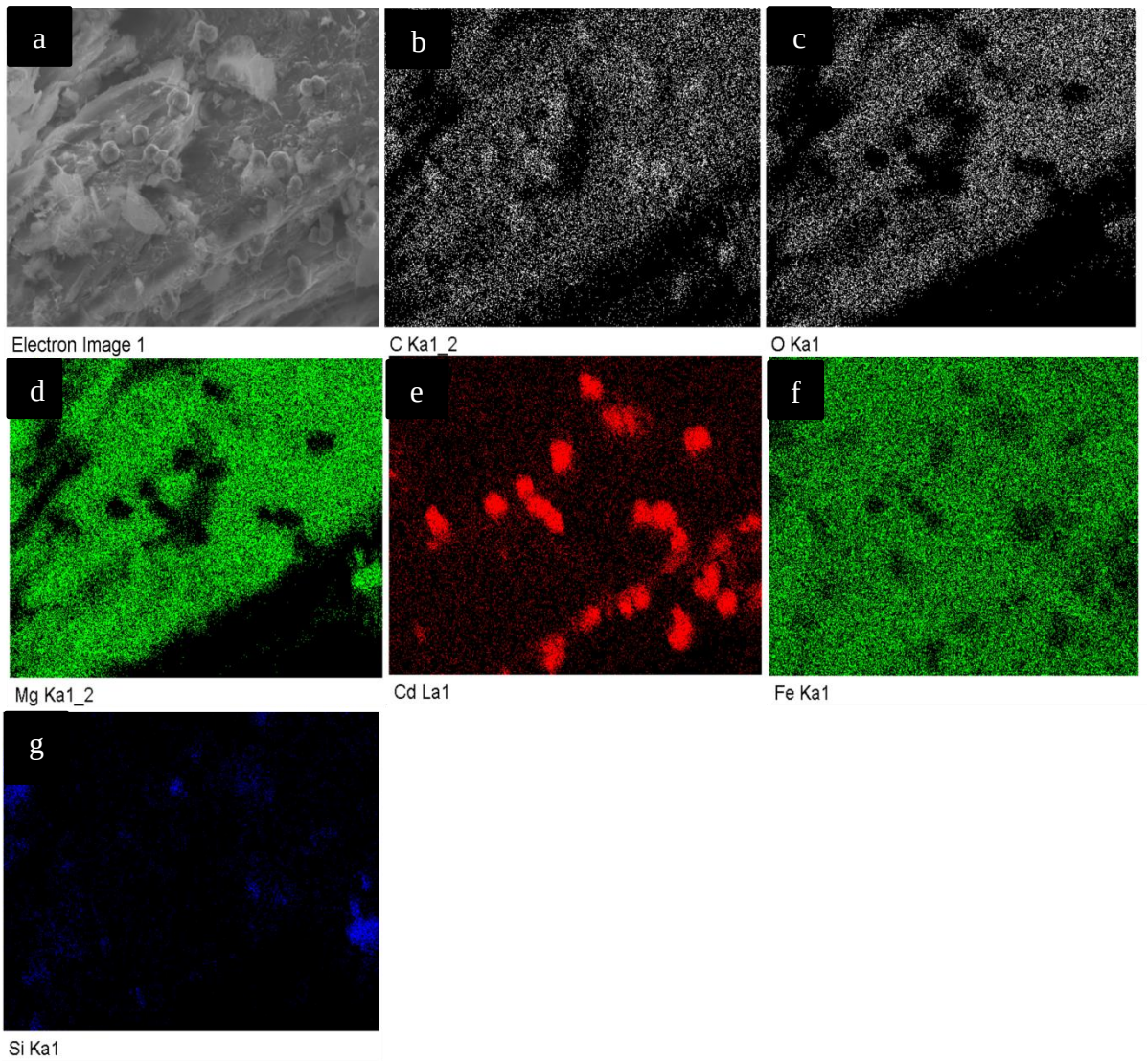


**Figure 5.33: Element maps of the same area shown in figure 5.32a and b. a) BSE image of the mapped area. b) Map of carbon. c) Map of oxygen. d) Map of magnesium. e) Map of cadmium. f) Map of iron. g) Map of silica.**

The figure 5.33 is showing the element maps of the same area which is shown by the figure 5.32. Image 5.32a is showing the area which was chosen for element mapping. The concentration of carbon, oxygen, magnesium, cadmium and iron can be seen on the image 5.33b, image 5.33c, image 5.33d and image 5.33e respectively. It can be observed that the areas that are covered by the Cd ions devoid of Mg, C, O and Fe. However, this replacement by Cd ions is very strong in case of Mg and O while Fe and O are still present in some areas where the Cd ions are sitting. The concentration of Si which can be seen on image 5.35f, shows the presence of Si mostly outside pyroaurite which shows that there is no serpentine impurity in the pyroaurite grain.

# 6. General Discussion

## 6.1 Chip experiments

During the chip experiments it was observed that most of the heavy metals like Pb, Cd, Cr were sorbed on the areas with mineral dypingite except Cu which was adsorbed on the surface of mineral pyroaurite. The results from chip experiments and column experiments are discussed in detail below.

**Chip Experiment with Cr**

Two chips, one coated with carbon were reacted with $CrNO_3$. The results showed that there was no effect of carbon coating on the reaction (see section 5.1.1 and 5.1.2). It was observed that Cr showed strong affinity to the parts with mineral dypingite and almost no reaction with pyroaurite and serpentine. The reaction between Cr and dypingite was incomplete as only the rims of the rose structure were totally coated. It is unclear if the incomplete reaction is due to a complete consumption of Cr from the fluid or the lack of reaction time (see figure 5.7). The sorption of Cr is still a quest as it cannot substitute Mg from the structure of mineral dypingite due to difference in their ionic radius. However, Cr can substitute Fe from the structure of mineral pyroaurite and it was also observed from the XRD patterns that a new phase of mineral stichtite was formed during the experiment (see figure 5.29). The formation of this new phase is possible as it is a common mineral in weathered dunites (Baidya, 1996).

**Chip Experiment with Pb**

The chip experiment with $PbNO_3$ showed a strong precipitation of Pb on dypingite (see section 5.1.3). The BSE images from the chip showed that the areas with mineral dypingite were completely altered during the reaction. However there was no effect of the reaction on mineral pyroaurite and serpentine as they remained completely unaltered during the experiment (see figure 5.16). The sorption of Pb on the surface of mineral dypingite is most likely due to the surface precipitation of Pb. Godelitsas, (2010) showed that Pb can be precipitated on the surface of minerals with substrate $CO_3^{2-}$ which can form a new phase in the form of cerussite ($PbCO_3$).

**Chip Experiment with Cd**

The chip experiment with $CdCl_2$ showed that Cd was efficiently sorbed in the areas of the chip where dypingite was exposed and there was no effect on the areas with pyroaurite and serpentine (see section 5.1.5). However, the reaction of Cd was not stronger than the reaction of Pb on dypingite. In case of Pb, Mg was strongly dissoluted while in case of Cd reaction there was still Mg on the surface of dypingite (see figure 5.21 and 5.17). Stipp et al., 1993 showed that cadmium can react with $CO_3^{2-}$ions which could result in a form of new phase known as Otavite ($CdCO_3$). The sorption of Cd on dypingite surface is most likely due to this surface precipitation of Cd.

**Chip Experiment with Cu**

The chip experiment with $CuSO_4$ solution showed different results from the chip experiments of Cr, Cd and Pb. It was observed that Cu was sorbed on the areas with mineral pyroaurite rather than mineral dypingite in this case (see section 5.1.5). However, the sorption of Cu on mineral pyroaurite was found only partly sorbed (see figure 5.24). The ionic radius of Cu and Fe is similar and it is most likely that Cu is substituting Fe from the structure of mineral pyroaurite in this case.

## 6.2 Comparison between the results of the reacted chip and reacted column material

The chip experiment with $CdCl_2$ solution and the reacted column material loaded with CdCl2+NaCl solution showed different results (see section 5.1.4 and section 5.2.4). It was observed from the BSE images of reacted column material that Cd was sorbed on both mineral pyroaurite and dypingite surfaces. However, in this case it was sorbed more efficiently on the surface of mineral pyroaurite (see figure 5.33). The reason behind this could be that pyroaurite is a more effective anion exchanger than dypingite and can deliver $CO_3^-$ easily. Godelitsas, 2010 showed that Cd is highly reactive with $CO_3^{2-}$ and can form surface precipitates in the form of $CdCO_3$. They also documented that the interaction of clays with dissolved heavy metals could lead to unusual phase transformations which results from the dissolution and afterwards the precipitation of a new metal-bearing phase. The adsorption of Cd on the surfaces of pyroaurite and dypingite in this case could be attributed to the reactivity of $CO_3^{2-}$ with Cd which has formed a new $CdCO_3$ separate phase in the form

of Otavite. However, the XRD data from initial and reacted column material doesn't support this hypothesis in this case (figure 6.1). Most probably the concentrations of otavite were so minute that XRD could not detect it.

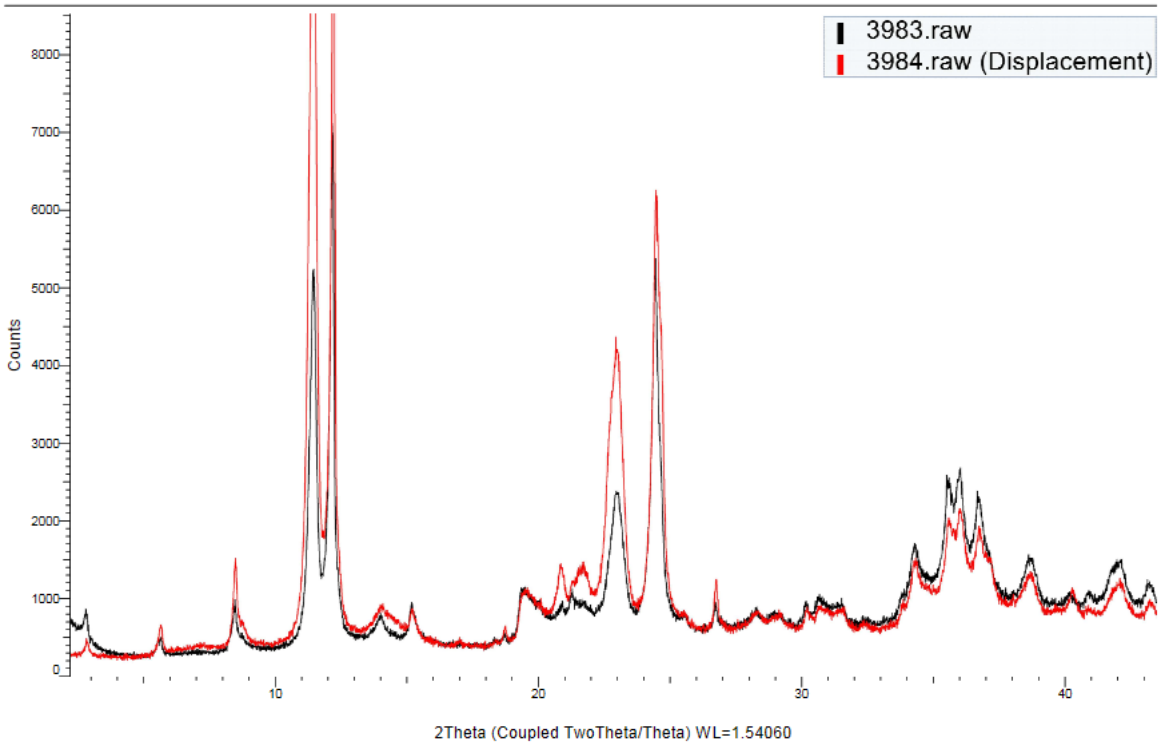


**Figure 6.1: XRD patterns of the initial and reacted column material. The black and white peaks are representing the compostion of initial and final material respectively.**

## 6.3 Column Studies

### Anion Exchange

The column experiment with the loading of $CdCl_2$+NaCl revealed that $Cl^-$ is not working as an ideal conservative tracer in this case. The retardation of $Cl^-$ in the column is most likely due to the anion exchange as $Cl^-$could replace $CO_3^{2-}$ in the structure of hydrotalcites which was also documented by Miyata, (1983). The anion exchange was also confirmed by the chip experiment with NaCl. The precipitation of $Cl^-$on the chip that was reacted with NaCl solution could be a drying off effect or salt precipitation but it is not likely that it would have crystallized there because the sample was washed 3 times with the Ultrahigh pure deionized

water prior to the SEM analysis (see section 5.1.6). The loading of the column with NaCl solution after the first showed that $Cl^-$ couldn't reach to its inlet concentration the column even after 3.5 pore volume (see section 5.2.2). The evidence of $Cl^-$ anion exchange was also found in the element maps of the chip that was reacted with $CdCl_2$ solution (see section 5.1.4).

**Cadmium Sorption in the Column**

The results from column experiments showed that after 1 pore volume we got a cadmium breakthrough. The cadmium front showed that the concentration of Cd reached to more than 10 times of the inlet concentration of Cd. However, after 1.3 volume the Cd was sorbed in the column until the end of the experiment. The sudden increase in concentration of Cd was most probably due to the precipitates that were forming during the experiment and got out through the column. It is possible that the initial cadmium carbonates or otavites were so fine grained that they pressed out of the column with pore water. (see section 5.2.1 and 5.2.4).

**Drinking water limit of cadmium**

The maximal admissible concentration of cadmium is documented as 5 ppb (Appelo, 2006). The column experiments in this study have shown satisfactory results if we ignore the error from the experiments. The plot from the column experiment with $CdCl_2$+NaCl has been redrawn in the logarithmic scale in order to compare the results with drinking water limit of Cd in ppb (figure 6.2). The tabulated results conversions into ppb could be find in appendix 2.4.

The figure 6.2 is showing the concentrations of Cd and $Cl^-$ in ppb. The drinking water limit of Cd in water is shown by the green arrow in the plot and the black arrow is pointing out the error during the experiment. In order to test if our material could act as efficient good sorbent to meet water drinking water standards, experiments should be carried out with lower concentrations of heavy metals.

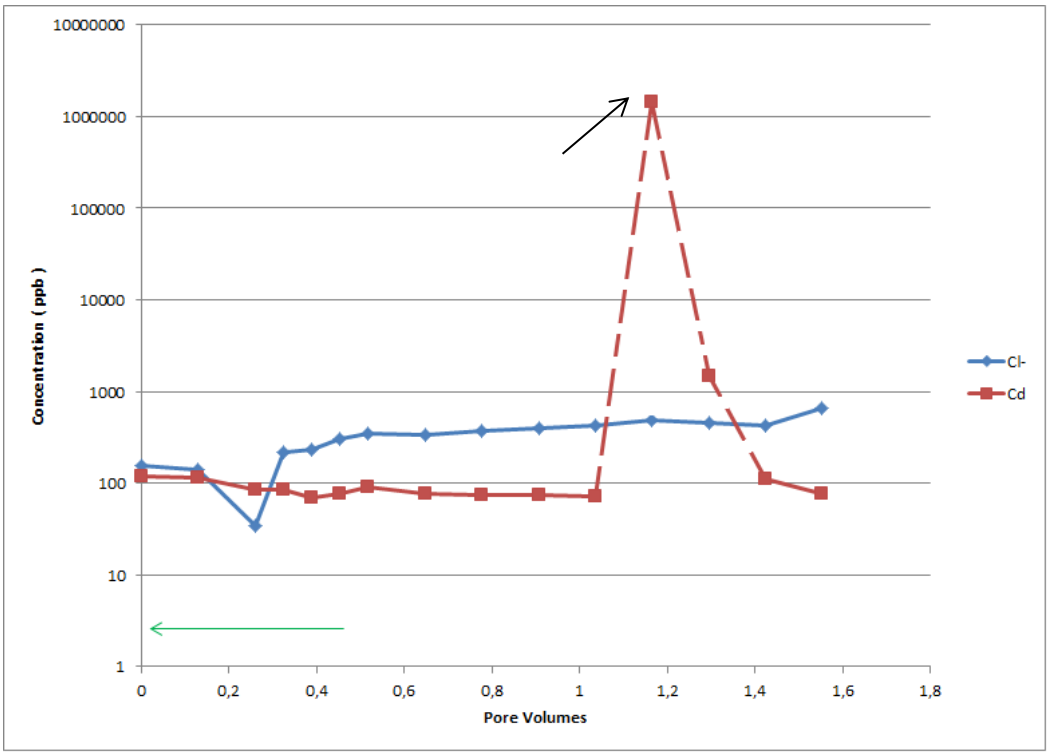


**Figure 6.2: showing the relative concentrations of Cd in ppb. The initial concentration of Cd in the inlet solution was about 112000 ppb.**

# 7. Conclusion

The study was designed to determine the potential of naturally weathered dunites as adsorbents for heavy metals. The main goal of the study was to determine if this weathered material could be used to remove heavy metals from the contaminated water. This was done by reacting the chips with heavy metal solutions and performing column experiments. One of the significant findings to emerge from this study is that Pb, Cd and Cr were sorbed on the surface of mineral dypingite during the course of chip experiments. However, Cu did not show any affinity to mineral dypingite and was sorbed on the surface of mineral pyroaurite. The SEM-BSE images along with EDS showed that Pb and Cd formed new surface precipitates on the dypingite in form of new carbonate phases. These new carbonate phases by the precipitation of Pb and Cd were identified as cerrusite and otavite respectively. The reaction of Cr was not as strong as Pb and Cd with mineral dypingite and it was not trapped as a new carbonate system. The sorption of Cu on the surface of mineral dypingite is most likely due to the substitution of Fe in the structure.

The SEM-X-ray element mapping, SEI and BSEI of the reacted column material revealed that Cd was precipitated both on mineral pyroaurite and dypingite which was different from the results of chip experiments where Cd was found only precipitated on the surface of mineral dypingite. The most obvious finding from column experiments was $Cl^-$ did not work as an ideal conservative tracer and was retarded due to the anion exchange. This anion exchange was confirmed by the chip experiment with NaCl. The column experiment with $CdCl_2$+NaCl solution showed that overall the Cd was sorbing in the column very efficiently if we ignore the error during the experiment. The precipitation of Cd in the column therefore suggests that weathered dunites have good potential for sorbing heavy metals like Cd from contaminated water.

### 7.1.1 Recommendations for further research work

This research has thrown up many questions in need of further investigation such as:

The structure of mineral dypingite is not well known and a better understanding of its structure may throw a light on the finding in this work. A comparison of synthetic and natural dypingite with respect to heavy metal sorption may be another important research avenue.

Chloride in case of weathered dunites could not be used as an ideal conservative tracer so any other tracer like tritium should be tested in case of column experiments.

Desorption studies of the column material should be studied so that we could know the efficiency of this material as an adsorbent.

The actual reaction mechanisms are hard to differentiate through SEM/EMP so AFM and surface chemical methods could be used for advanced studies.

To test if our material could work as an efficient sorbent to meet water drinking limit, experiments should be carried out with lower concentrations of heavy metals.

# 8. References


Adamson, A. (1990). *Physical chemistry of surfaces.* Newyork: Wiley.

Allman, R. (1968). The crystal structure of pyroaurite. *Acta Cryst.*, 972-977.

Amphlett, C.B., Mcdonald, L.A & Redman, M.J 1958. Synthetic inorganic ion-exchange materials—I zirconium phosphate. *Journal of Inorganic and Nuclear Chemistry,* 6**,** 220-235.

Bhatnagar, Amit, A. M. (2005, Septemeber 7). Conventional and Non Conventional adsorbents for removal of pollutants from water. *Indian Journal of Chemical Technology*, ss. 203-217.

Beinlich, A. & Austrheim, H.2012. In situ sequestration of atmospheric CO2 at low temperature and surface cracking of serpentinized peridotite in mine shafts. *Chemical Geology,* 332–333**,** 32-44.

Babel, S. & Kurniawan, T.A. 2003. Low-cost adsorbents for heavy metals uptake from contaminated water: a review. *Journal of Hazardous Materials,* 97**,** 219-243.C.A.J Appelo, D. (2006). *Geochemistry, groundwater and pollution second editon.* Crc press.

Dabrowski, A. (2001, may). Adsorption-From theory to practice. *Advances in colloid and interface surface*, ss. 135-224.

DIONEX Corporation. (2005). ICS-1000 Ion Chromatography System.

Faust, S.D., Aly, 1987. *Adsorption processes for water treatment*. Boston [u.a.], Butterworths.

Godelitsas, A.a. (2010). Dissolution, sorption/(re)precipitation, formation of solid solutions and crystal growth phenomena on mineral surfaces: implications for the removal of toxic netaks from the environment. *Notes in Mineralogy*, 289-324.

Hanaa, M. S. (2000, September). Heavy metals in drinking water and their environmental impact on human health. *ICEHM2000*, ss. 542-556.

Hyperphysics, 2014. Figure, Bragg's law calculation. Available at: http://hyperphysics.phy-astr.gsu.edu/hbase/quantum/bragg.html (Accessed on 12/05/2014)

Jayakumar R, M. D. (2010). Biomedical applications of chitin and chitosan based nanomaterials-A short review. *Cabohydrate Polymers*, ss. 227-232.

Kao, G. B.-c. (1984). Structural and IR Relations Among Brucite-like divalent metal hydroxides. *Physics and Chemistry of minerals*, 187-191.

Katlego Setshedi, J. R. (2011, January 02). Removal of Pb(II) from aqueous solution using hydrotalcite-like nanostructured material. *Internaional Journal of the Physical sciences* , ss. 64-72.

Koretsky, C. (2000). The significance of surface complexation reactions in hydrologic systems: A geochemist's perspective. *J. Hydrol*. 230, 127–171.

Meghdad Pirsaheb, T. K. (2013). Measurement of Heavy Metals Concentration in Drinking Water from Source to Consumption Site in Kermanshah - Iran. *World Applied Sciences Journal 21*, ss. 416-423.

Mehmet Emin Argun, S. D. (2007, June 8). A new approach to modification of natural adsorbent for heavy metal adsorption. *Bioresource technology*, ss. 2516-2527.

Mellini, G. C. (2004). The Modulated crystal structure of antigorite : The m=17 polysome. *American Mineralogist*, ss. 147-158.

Meyn M., Beneke K. & Lagaly G. Anion-exchange reactions of layered double hydroxides. *Inorg. Chem*. 29, 5201-5207

Mills, S.J., Christy, A.G., Genin, J.-M.R., Kameda, T., Colombo, F. (2012): Nomenclature of the hydrotalcite supergroup: natural layered double hydroxides. *Mineralogical Magazine*, 76, 1289-1336.

Mindat.org. Description of Feragen Chromium Mines, Røros, Sør-Trøndelag, Norway. Available at: http://www.mindat.org/loc-34980.html (Accessed on 03/04/2014)

Miyata, S. (1983). Anion-exchange properties of hydrotalcite-like compounds. *Clay and Clay minerals*, 305-311.

Moore, A. H. (1980). Petrology, mineralogy and origin of the feragen ultramafic body, Sør-Trøndelag, Norway. *Norsk Geologisk Tidsskrift 60*, 249-257.

Omar E. Abdel Salama, N. A. (2011, January 14). A study of the removal characteristics of heavy metals from wastewater by low-cost adsorbents. *Journal of advanced research*, ss. 297-303.

Pronczuk J, B. M.-N. (2011). Children's environmental health in developing countries. *Encyclopedia Environ. Health*, ss. 601-610.

Raade, g. (1970). Dypingite, A new Hydrous basic carbonate of magnesium, from norway. *The american mineralogist*, ss. 1457-1465.

Seida., Y. (2001, july). Rapid removal of dilute lead from water by Pyroaurite-like compound. *water research*, ss. 2341-2346.

Sposito, G. (1989). *The Chemistry of soils.* newyork: Oxford Univeristy press.

Stipp, S. L; Hochella, M. F., Parks, G. A., Leckie, J. O. (1992). Cd2+ uptake by calcite, solid-state diffusion, and the formation of solid-solution: Interface processes observed with near-surface sensitive techniques (XPS, LEED, and AES). *Geochim. Cosmochim. Acta*. doi:10.1016/0016-7037(92)90321-9

Taylor, H. (1969). Segregation and Cation-ordering in sjogrenite and pyroaurite. *Mineralogical Magazine*, ss. 338-343.

Taylor, J.-R. a. (1971). Crystal structure of Coalingite. *Mineralogical magazine*, 286-294.

Vodela, J. J. (1997). Drinking water contaminants . *Poult. Science*, ss. 1474-1492.

# Appendices

## Appendix 1

# Fer_312A

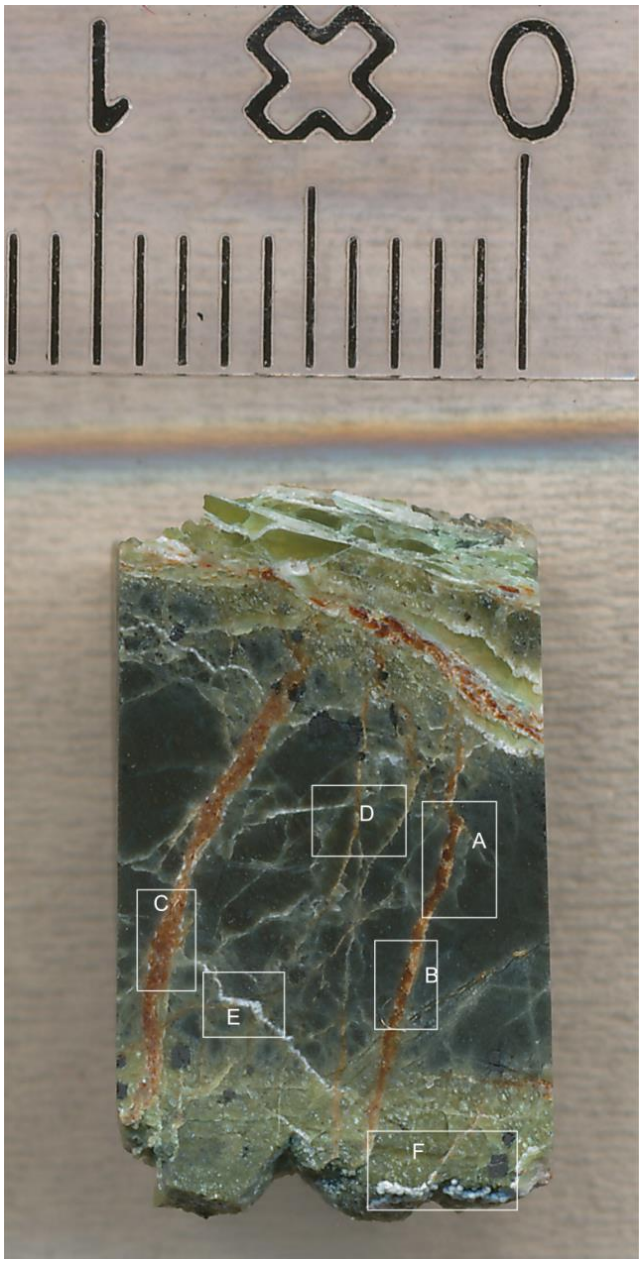


| Area | Page numbers |
|---|---|
| Area A | 19, 34 |
| Area B | 21, 36 |
| Area E | 39 |
| Area F | 42 |

# Fer_312B

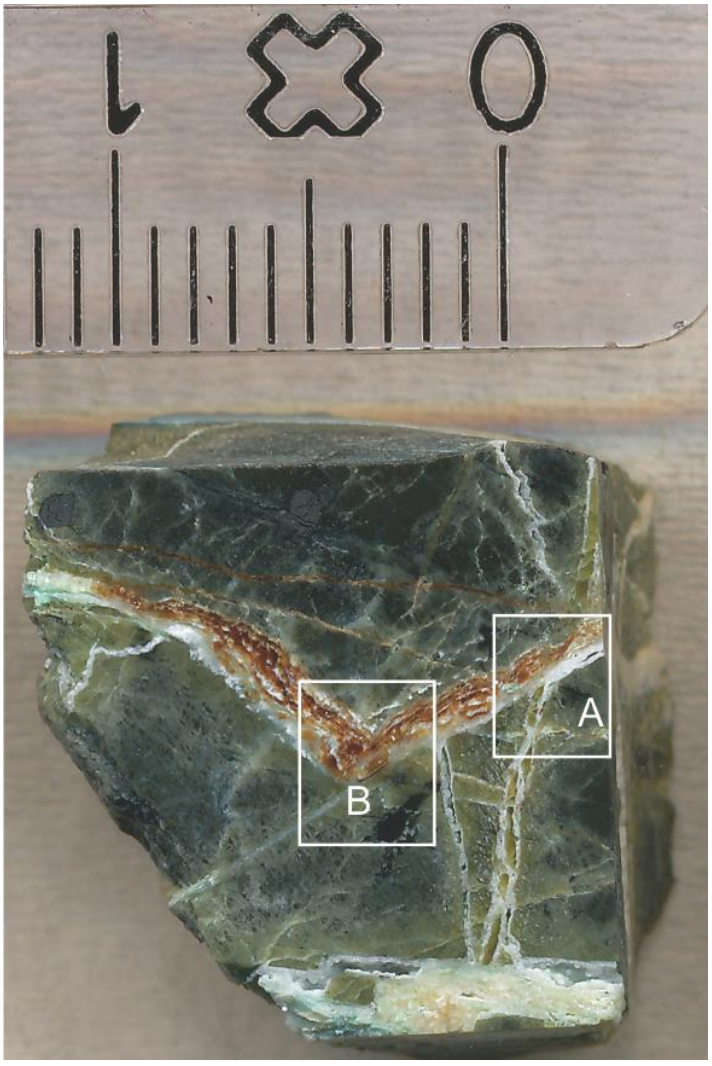


| Area | Page numbers |
|---|---|
| Area A | 24, 43 |
| Area B | 26, 46 |

# Fer_312C

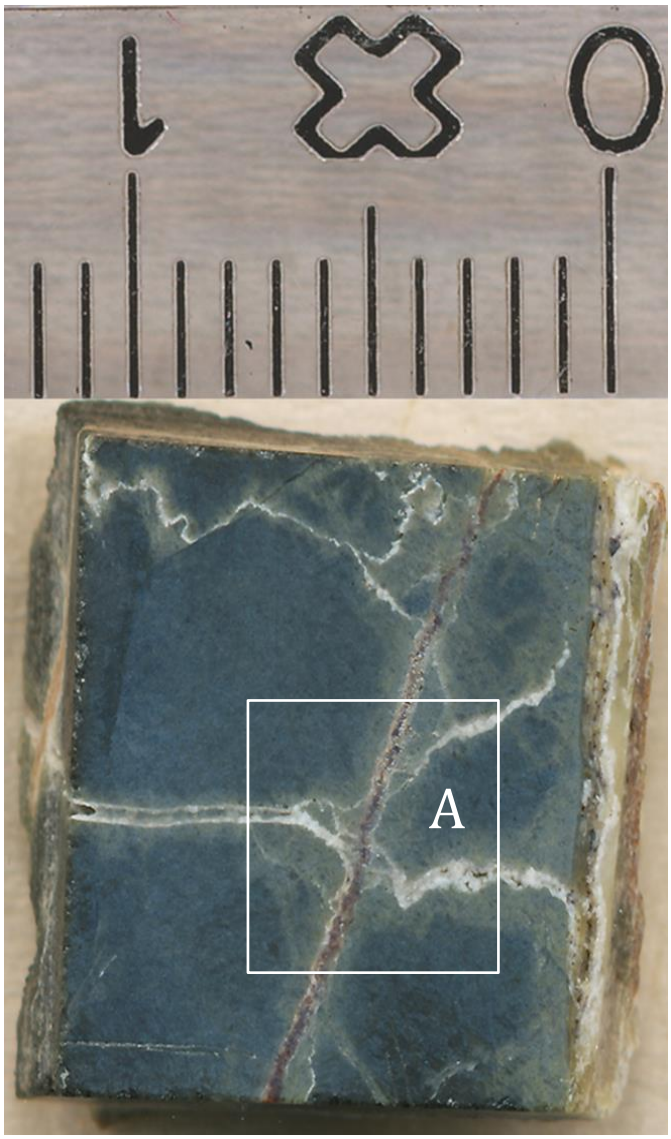


| Area | Page Number |
|---|---|
| Area A | 58 |

# Fer_312 D

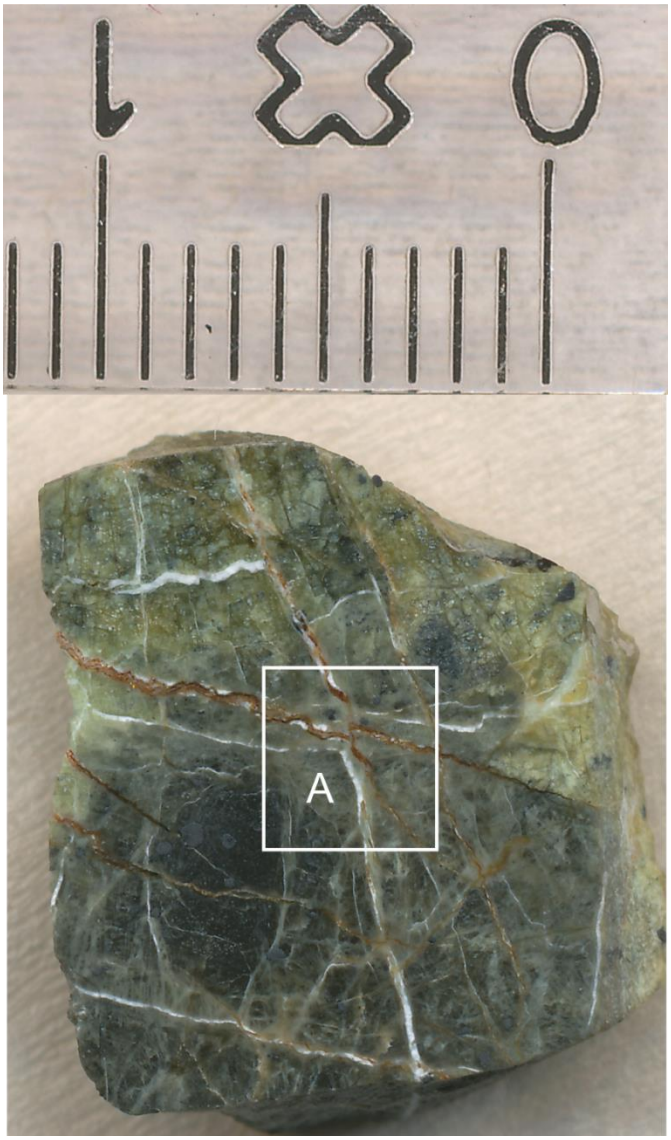


| Area | Page number |
|---|---|
| Area A | 55 |

# Fer_412 A

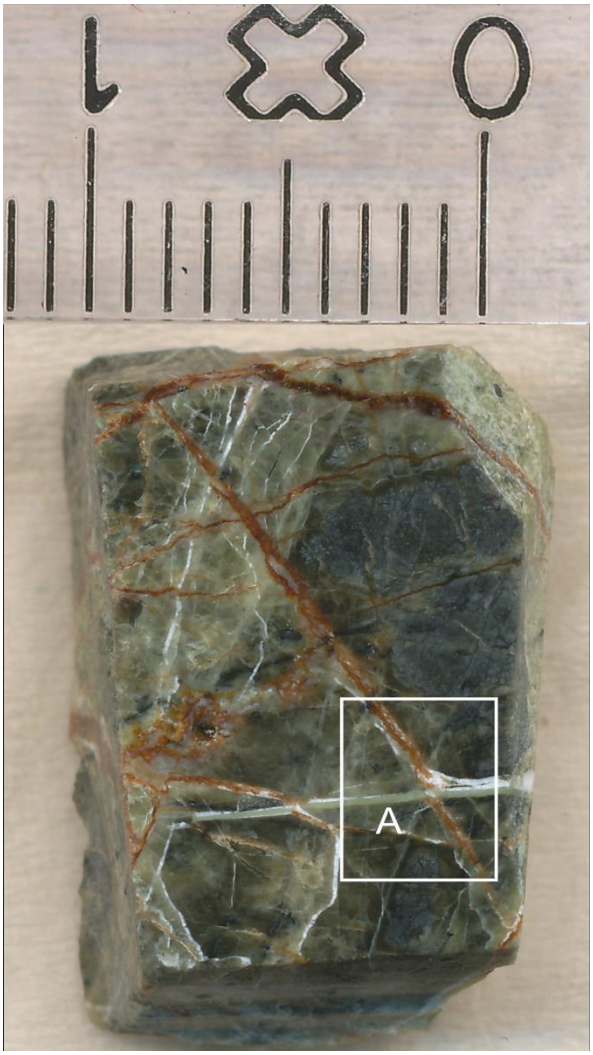


| Area | Page number |
|---|---|
| Area A | 48 |

# Fer_412 B


| Area | Page number |
|---|---|
| Area A | 52 |

# Appendix 2

## Appendix 2.1

**Porosity= 0.47%**

**Inflow rate= 0.45 ml/min**

**One pore Volume= 75.57*0.46=34.76**

| Pore volumes | Volume (ml) | Time | Cl mmol/l | | Cd mmol/l | | Cl C/Co | C/Co Cd |
|---|---|---|---|---|---|---|---|---|
| 0 | 0 | 0 | 0,043465 | | 0,001055 | | 0,014488 | 0,001055 |
| 0,129451 | 4,5 | 10 | 0,039116 | | 0,001039 | | 0,013039 | 0,001039 |
| 0,258902 | 9 | 20 | 0,00961 | | 0,000754 | | 0,003203 | 0,000754 |
| 0,323627 | 11,25 | 25 | 0,06101 | | 0,00077 | | 0,020337 | 0,00077 |
| 0,388353 | 13,5 | 30 | 0,066197 | | 0,000624 | | 0,022066 | 0,000624 |
| 0,453078 | 15,75 | 35 | 0,085701 | | 0,000697 | | 0,028567 | 0,000697 |
| 0,517804 | 18 | 40 | 0,097114 | | 0,000804 | | 0,032371 | 0,000804 |
| 0,647255 | 22,5 | 50 | 0,096358 | | 0,000682 | | 0,032119 | 0,000682 |
| 0,776706 | 27 | 60 | 0,104798 | | 0,000667 | | 0,034933 | 0,000667 |
| 0,906157 | 31,5 | 70 | 0,113419 | | 0,000663 | | 0,037806 | 0,000663 |
| 1,035608 | 36 | 80 | 0,121498 | | 0,000642 | | 0,040499 | 0,000642 |
| 1,165059 | 40,5 | 90 | 0,137383 | | 12,9069 | | 0,045794 | 12,9069 |
| 1,29451 | 45 | 100 | 0,12811 | | 0,013367 | | 0,042703 | 0,013367 |
| 1,423961 | 49,5 | 110 | 0,121672 | | 0,000981 | | 0,040557 | 0,000981 |
| 1,553411 | 54 | 120 | 0,188928 | | 0,000687 | | 0,062976 | 0,000687 |

# Appendix 2.2

**Porosity= 0.47%**

**Inflow rate= 0.26 ml/min**

**One pore Volume= 75.57*0.26=20**

| | Time | Conc Cl ppm | Conc Cl mmol/l | volume | pore volume | |
|---|---|---|---|---|---|---|
| | 10 | 9,688581 | 0,27338 | 2,7 | 0,076018 | |
| | 20 | 8,744656 | 0,246745 | 5,4 | 0,152036 | |
| | 30 | 9,931143 | 0,280224 | 8,1 | 0,228054 | |
| | 40 | 11,12449 | 0,313897 | 10,8 | 0,304072 | |
| | 50 | 12,34219 | 0,348256 | 13,5 | 0,38009 | |
| | 60 | 13,53051 | 0,381786 | 16,2 | 0,456108 | |
| | 70 | 14,23069 | 0,401543 | 18,9 | 0,532126 | |
| | 80 | 15,5552 | 0,438916 | 21,6 | 0,608144 | |
| | 90 | 16,43233 | 0,463666 | 24,3 | 0,684162 | |
| | 100 | 17,16324 | 0,48429 | 27 | 0,76018 | |
| | 110 | 18,50148 | 0,522051 | 29,7 | 0,836198 | |
| | 120 | 19,0397 | 0,537238 | 32,4 | 0,912216 | |
| | 130 | 19,62049 | 0,553626 | 35,1 | 0,988234 | |
| | 140 | 20,34759 | 0,574142 | 37,8 | 1,064252 | |
| | 150 | 21,20745 | 0,598404 | 40,5 | 1,14027 | |
| | 160 | 21,66293 | 0,611257 | 43,2 | 1,216288 | |
| | 170 | 22,1903 | 0,626137 | 45,9 | 1,292306 | |
| | 180 | 22,87169 | 0,645364 | 48,6 | 1,368324 | |
| | 190 | 23,51354 | 0,663475 | 51,3 | 1,444342 | |
| | 200 | 23,88265 | 0,67389 | 54 | 1,52036 | |
| | 210 | 24,36529 | 0,687508 | 56,7 | 1,596378 | |
| | 220 | 24,99625 | 0,705312 | 59,4 | 1,672396 | |
| | 230 | 25,17876 | 0,710462 | 62,1 | 1,748414 | |
| | 240 | 25,83608 | 0,729009 | 64,8 | 1,824432 | |
| | 250 | 26,36551 | 0,743948 | 67,5 | 1,90045 | |
| | 260 | 26,64476 | 0,751827 | 70,2 | 1,976468 | |
| | 270 | 26,91601 | 0,759481 | 72,9 | 2,052486 | |
| | 280 | 27,80184 | 0,784476 | 75,6 | 2,128504 | |

# Appendix 2.3

| Cl/ppm | Cd/ppm | Cl/ppb | Cd/ppb | time | volume | Porevolume | |
|---|---|---|---|---|---|---|---|
| 1,54 | 0,1182 | 154,0825 | 118,2 | 0 | 0 | 0 | |
| 1,39 | 0,1164 | 138,6656 | 116,4 | 10 | 4,5 | 0,129451 | |
| 0,34 | 0,0845 | 34,06878 | 84,5 | 20 | 9 | 0,258902 | |
| 2,16 | 0,0862 | 216,2792 | 86,2 | 25 | 11,25 | 0,323627 | |
| 2,35 | 0,0699 | 234,6676 | 69,9 | 30 | 13,5 | 0,388353 | |
| 3,04 | 0,0781 | 303,8114 | 78,1 | 35 | 15,75 | 0,453078 | |
| 3,44 | 0,0901 | 344,269 | 90,1 | 40 | 18 | 0,517804 | |
| 3,42 | 0,0764 | 341,5892 | 76,4 | 50 | 22,5 | 0,647255 | |
| 3,72 | 0,0747 | 371,5088 | 74,7 | 60 | 27 | 0,776706 | |
| 4,02 | 0,0743 | 402,0702 | 74,3 | 70 | 31,5 | 0,906157 | |
| 4,31 | 0,0719 | 430,7116 | 71,9 | 80 | 36 | 1,035608 | |
| 4,87 | 1445,573 | 487,0214 | 1445573 | 90 | 40,5 | 1,165059 | |
| 4,54 | 1,4971 | 454,149 | 1497,1 | 100 | 45 | 1,29451 | |
| 4,31 | 0,1099 | 431,3286 | 109,9 | 110 | 49,5 | 1,423961 | |
| 6,70 | 0,0769 | 669,7511 | 76,9 | 120 | 54 | 1,553411 | |